
UNIVESITY OF THESSALY
SCHOOL OF ENGINEERING
DEPARTMENT OF MECHANICAL ENGINEERING

# Experimental Study of Jet Flows in Quiescent and Turbulent Ambient Conditions

By
**Petrolekas Dimitrios**

Submitted in partial fulfilment of the requirements for the diploma of Mechanical Engineering
**VOLOS 2022**

# Certified by the members of the Thesis Committee:

| | |
|---|---|
| First examiner | Dr. Georgios Charalampous |
| [Supervisor] | Assistant Professor, Department of Mechanical Engineering, |
| | University of Thessaly |
| Second examiner | Dr. Anastasios Stamatellos |
| | Professor, Department of Mechanical Engineering, |
| | University of Thessaly |
| Third examiner | Dr. Nikolaos Pelekasis |
| | Professor, Department of Mechanical Engineering, |
| | University of Thessaly |

# Abstract

The main aim of this Thesis is to study the concentration field of an axisymmetric jet in quiescent and turbulent ambient environments with the aid of the flow visualization method. Five types of ambient turbulence are examined. The most prominent is the homogeneous and isotropic turbulence (HIT), while the other four have different directions of anisotropy in the area where the experimental investigation occurs. In the case of homogeneous and isotropic turbulence, the mean flow is created with a random jet array, and it is considered negligible. For better comprehension of the jet's properties, its behavior in the different turbulent backgrounds is compared with the one in quiescent environment.

The flow visualization method was performed by means of a conventional laser module to visualize the jet flow and simultaneously quantify the jet concentration in the cross-sections of the jet. The jet flows were created using a conventional air compressor, which supplied the air throughout the whole procedure. This air flow was infused with smoke and accordingly emitted from the jet's orifice, where the flow visualization takes place. The jet concentration is measured for jet discharge flows with Reynolds numbers of 1400 to 9800 in the near-field region. These flows correspond to laminar, transitional and turbulent flow regimes. The behavior of the flow was captured on a camera, where 200 pictures represented each measurement. The pictures acquired by the experimental equipment were post-processed and the jet concentration was determined for the jet flow for each case of ambient environment.

The results are depicted in radial concentration profiles, centerline concentration profiles and contour plots of concentration. These diagrams are important for the interpretation of the jet's interaction with each case of ambient environment. They indicate that the ambient turbulence has a greater effect on the jet's flow when the flow is laminar or transitional ($\mathrm{Re} = 1400 - 2800$) and a lesser effect when the flow is turbulent ($\mathrm{Re} = 4200 - 9800$), in the near-field region investigated. This is explained with the momentum of the jet flow and the momentum of the external turbulence. Laminar or transitional jet flows have a low momentum, resulting in the flow being more susceptible to disruptions caused by the turbulence in the surrounding environment. Turbulent flows have high momentum, and they cannot be significantly affected by the external turbulence.

# Περίληψη

Ο κύριος στόχος της παρούσας διπλωματικής εργασίας είναι να μελετήσει το πεδίο συγκέντρωσης ενός αξονοσυμμετρικού πίδακα σε ήρεμο και τυρβώδες περιβάλλον με τη βοήθεια της μεθόδου απεικόνισης ροής. Στη μελέτη αυτή εξετάζονται πέντε τύποι περιβάλλουσας τύρβης. Η πιο εμφανής είναι η ομοιογενής και ισότροπη τύρβη, ενώ οι άλλες τέσσερεις έχουν διαφορετικές κατευθύνσεις ανισοτροπίας στον χώρο που πραγματοποιείται η πειραματική διαδικασία. Στην περίπτωση ομοιογενούς και ισότροπου στροβιλισμού, η μέση ροή δημιουργείται με τυχαία διάταξη πίδακα και θεωρείται αμελητέα. Για την καλύτερη κατανόηση των ιδιοτήτων του πίδακα, η συμπεριφορά του στα διαφορετικά τυρβώδη υπόβαθρα συγκρίνεται με εκείνη σε ηρεμία.

Για τη λειτουργία της μεθόδου απεικόνισης ροής, χρησιμοποιείται μια συμβατική μονάδα λέιζερ για να οπτικοποιηθεί η ροή του πίδακα και ταυτόχρονα να ποσοτικοποιηθούν οι συγκεντρώσεις του πίδακα σε όλη την περιοχή της ροής. Για να δημιουργηθεί η ροή πίδακα, χρησιμοποιείται ένας συμβατικός αεροσυμπιεστής που παρέχει αέρα καθ'όλη τη διάρκεια της διαδικασίας. Η ροή αέρα εγχέεται με καπνό και στη συνέχεια εκπέμπεται από το στόμιο του πίδακα, όπου λαμβάνει χώρα η οπτικοποίηση της ροής. Η συγκέντρωση του πίδακα μετράται για ροές πίδακα με αριθμούς Reynolds από 1400 έως 9800 στην περιοχή κοντινού πεδίου. Οι ροές αυτές αντιστοιχούν σε στρωτή, μεταβατική και τυρβώδη ροή. Η συμπεριφορά της ροής σε κάθε περιβάλλον καταγράφηκε σε μια κάμερα, όπου 200 φωτογραφίες αντιπροσώπευαν κάθε μέτρηση. Οι εικόνες που αποκτήθηκαν από τον πειραματικό εξοπλισμό υποβλήθηκαν σε μεταγενέστερη επεξεργασία και έτσι προσδιορίστηκε η συγκέντρωση του πίδακα σε ολόκληρο το πεδίο ροής του πίδακα για κάθε περίπτωση εξωτερικού περιβάλλοντος.

Τα αποτελέσματα απεικονίζονται σε διαγράμματα στα οποία παρουσιάζεται η μεταβολή της συγκέντρωσης κατά την ακτινική και την αξονική διεύθυνση της ροής καθώς και σε διαγράμματα με ισοϋψείς καμπύλες συγκέντρωσης. Τα διαγράμματα αυτά είναι σημαντικά προκειμένου να γίνουν αντιληπτές οι διαφορές στην ένταση του πίδακα σε σχέση με την καθεμία περίπτωση του εξωτερικού περιβάλλοντος. Τα διαγράμματα υποδεικνύουν ότι η περιβάλλουσα τύρβη έχει μεγαλύτερη επίδραση στη ροή του πίδακα όταν η ροή είναι στρωτή ή μεταβατική ($\mathrm{Re} = 1400 - 2800$), και μικρότερη όταν η ροή είναι τυρβώδης ($\mathrm{Re} = 4200 - 9800$), στην περιοχή κοντινού πεδίου που εξετάστηκε. Αυτό εξηγείται με την ορμή της ροής του πίδακα και την ορμή της εξωτερικής τύρβης. Οι στρωτές ή οι μεταβατικές ροές πίδακα έχουν χαμηλή ορμή, με αποτέλεσμα η ροή να είναι πιο επιρρεπής σε διαταραχές που προκαλούνται από την περιβάλλουσα τύρβη. Οι τυρβώδεις ροές έχουν υψηλή ορμή και δεν μπορούν να επηρεαστούν σημαντικά από την εξωτερική τύρβη.

# Acknowledgements

The current project could not have been completed without the support of many. Initially, I would like to express my sincere gratitude to my academic supervisor Prof. Georgios Charalampous, for providing me the necessary means to complete this project. Next, I would like to thank the technicians in the Department who helped with the construction of the experimental setup and to overcome the technical problems that occurred during the experiments.

I would also like to thank all my friends that were close to me and supported me in order to overcome all difficulties that ensued with the writing of this thesis. Furthermore, I would like to specifically thank my friends called Fillipos Katsimalis, Dimitrios Tsogias and Dimitrios Sdrolias that were there for me throughout my whole academic journey and always supported me.

Finally, I would like to thank my family for their constant support and trust they had in me. Their continuous encouragement and useful advises, helped me improve myself and strive for the better.

# Table of Contents

# List of Figures

# List of Tables

# Nomenclature

| | | |
|---|---|---|
| $D_0$ | Diameter of the jet orifice/nozzle | $L$ |
| $r_0$ | Radius of the jet orifice/nozzle | $L$ |
| $U$ | Average velocity of the jet flow at the orifice | $LT^{-1}$ |
| $Q$ | Volumetric flow rate of the jet flow | $L^3T^{-1}$ |
| $c_0$ | Average concentration of the jet at the orifice | $ML^{-3}$ |
| $X$ | Axial-downstream distance of the jet flow measured from the virtual source | $L$ |
| $x$ | Axial-downstream distance of the flow measured from the orifice | $L$ |
| $x/r_0$ | Axial-downstream distance of the jet flow measured from the orifice divided with the radius of the orifice | - |
| $x/D_0$ | Axial-downstream distance of the jet flow measured from the orifice divided with the Diameter of the orifice | - |
| $r$ | Radial (crosswise) distance of the jet flow | $L$ |
| $r/r_0$ | Radial distance of the jet flow divided with the orifice radius | - |
| $R(x)$ | Radius of the jet flow for each value of $x$ | $L$ |
| $u(x,r)$ | Cross section average velocity profile of the jet flow | $LT^{-1}$ |
| $c(x,r)$ | Average contaminant's concentration profile of the jet flow | $ML^{-3}$ |
| $u_{max}(x)$ | Maximum speed of the jet flow at the centerline for each value of $x$ | $LT^{-1}$ |
| $c_{max}(x)$ | The peak jet concentration along the centerline for each value of $x$ | $ML^{-3}$ |
| Re | Reynolds number | - |
| $v$ | Kinematic viscosity of the fluid | $L^2T$ |

# 1. Introduction

Turbulence is a very complex phenomenon by its nature. Most of turbulent flows are hard to study and be fully comprehended. The first light that was shed in the phenomenon of turbulence was with the aid of the Navier-Stokes equation but the whole concept of turbulence remained still vague (Thomas, 1972). The breakthrough in the study of turbulence was made in 1941 when Kolmogorov presented his three hypotheses, which revolutionised the study of turbulence and are still used to this day. However, turbulence is still part of continuous and demanding scientific research due its theoretical significance and practical importance. Turbulent flows are encountered in several engineering applications of industrial and environmental interest, including turbulent jets which are particularly important since they are used in processes such as combustion, mixing and pollution control.

One way to study turbulence is to develop theoretical mathematical models based on experimental data obtained on idealized turbulent flows. The homogeneous and isotropic turbulence (HIT) is such a model. Experimentally, the HIT field can be simulated by oscillating grids, wind tunnels and space distributed actuators. The latter method is the most recent one and involves the use of synthetic jets. In this work the experimental study of jets is performed by means of the flow visualization method. The concentration field of the jet flow is investigated in quiescent environment and different turbulent fields generated by synthetic jets.

This Thesis consists of the following Parts: (1) Introduction, which includes a theoretical review (2) Methods, which includes a detailed description of the experimental setup (3) Results and Discussion, which includes the detailed presentation and discussion of the radial profiles, centerline profiles and contour plots of concentration (4) Conclusions and (5) References.

## 1.1 Basic Theory

### 1.1.1 Turbulent flows

Turbulence is a very complex fluid motion, which is characterized by chaotic changes in the velocity of the flow and pressure. Turbulent flows are present in many circumstances even though the observer may not even observe them. They can be seen on many occasions, created by nature such as the water flow in rivers and waterfalls, and man-made like the flows created by the smoke from chimneys in the environment, the flows in pumps and compressors, the flows around automobiles, airplanes etc. Examples of turbulent flows are the smoke rising from a cigarette, which for the first centimetres is

laminar and after the increase of the flow velocity becomes turbulent and the external flow over airplanes, as displayed in the following pictures.

a) 

b) 


**Figure 1-1:** Examples of turbulent flow: a) Smoke's flow transition b) An airplane's wake

The common attribute of turbulent flows is that the flow becomes unstable, irregular, precarious and the motion of every eddy is unpredictable. These characteristics indicate that the flow is actually turbulent (Pope, 2002). The main property of turbulent flows is that they have an enhanced ability to transfer momentum, energy, and various types of fluid particles. This is very effective in case of mixing processes due to the enhanced mixing rates. Typical example of such improvement is the minimization of the impact of a pollutant stream, when it is ejected from the chimneys to the atmosphere (Alnahhal, 2010).

### 1.1.2 Navier-Stokes

In the field of fluid mechanics, the Navier-Stokes equations are used to describe the fluid flows. These equations represent the Newton's second law of motion for fluids. The former states that the sum of the forces applied to a body is equal to the acceleration times the mass of the body. The Navier-Stokes equations were first introduced in the 19$^{th}$ century by the Irish physicist Sir George Gabriel Stokes and the French physicist and engineer Claude-Louis Marie Henri Navier. The equations are part of the differential equations with boundary conditions family with the assumption of atmospheric turbulence and they are expressed as follows:

$$\partial_t \vec{u} + (\vec{u} \cdot \vec{\nabla})\vec{u} = -\frac{1}{\rho}\vec{\nabla}p + v\Delta\vec{u}$$

$$\vec{\nabla} \cdot \vec{u} = 0$$

where $\vec{u}$ is the velocity of the flow, $p$ the static pressure, $v$ the kinematic viscosity, $\rho$ the density and $\Delta\vec{u} = \nabla^2\vec{u}$. The second equation is called the continuity equation. The main advantage of the Navier-Stokes equations is that they can be used for all flows and hold true even for extremely unpredictable flows when the Reynolds number is very high. However, the solutions given by the equations are very scarce due to the term $(\vec{u} \cdot \vec{\nabla})$, which adds non-linearity to the equations (Obligado et al., 2013).

### 1.1.3 The Reynolds number

A criterion to define the transition from laminar to turbulent flow is the Reynolds number. The Reynolds number can be defined as the ratio of inertial forces over viscous forces within a moving fluid. The relationship representing the Reynolds number is:

$$\mathrm{Re} = \frac{UL}{v}$$

, where $L$ is the characteristic dimension (usually length), $U$ the velocity of the flow and $v$ the kinematic viscosity. The typical example is when the flow transitions from laminar to turbulent around the value of $Re = 5 \times 10^5$, in the case of boundary layer flow over a flat plate. For pipe flow, experimental tests have shown that for $Re$ values lower than 2300 ($Re_D < 2300$) the flow is laminar, while for $Re$ values greater than 2900 ($Re_D > 2900$) the flow is turbulent; $Re$ values in between 2300-2900 indicate transition from laminar to turbulent flow (Holman, 2002).

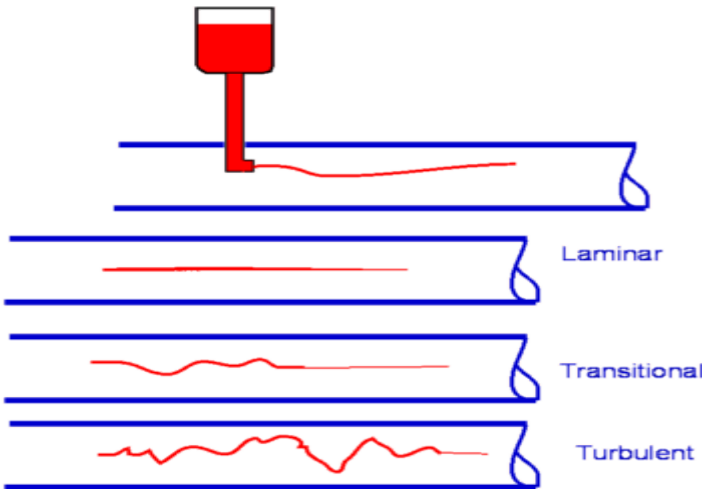


**Figure 1-2:** The Reynolds experiment (University of Sydney, 2005)

### 1.1.4 Free shear flows

An important category of fluid flows are the free shear flows. The free shear flows are consisted of all the fluid flows which are free to develop without any effects from solid boundaries. Furthermore, these flows can be considered without boundaries and include also flows originated through contact with solid surfaces (Bernard & Wallace,2002). There are four types of free shear flows. The first type is the plane jet, where the fluid leaves the orifice to a greater area due to the excess of the jet's velocity compared to ambient fluid's. The second type is the mixing layer, where the fluid layers flow at different velocities and they are brought together. The third type is the wake, in which the flow usually develops downstream of a streamlined body. During this type of flow turbulence is formed around the body, which is filled in the wake region, thus a decrease of momentum of the mean velocity behind the body in comparison with the outside region is observed (Bernard and Wallace, 2002). The fourth type is the boundary layer flow, where the fluid flows on a plate and forms a boundary layer. Here it is assumed that the velocity distribution on the plate is zero due to the flow's steadily increase away from the plate and additionally due to the no-slip condition, which indicates that the first layer on the flat plate will get a velocity with a zero value (Douglas et al. 1995). Figure 1-3 demonstrates the four types of free shear flows:

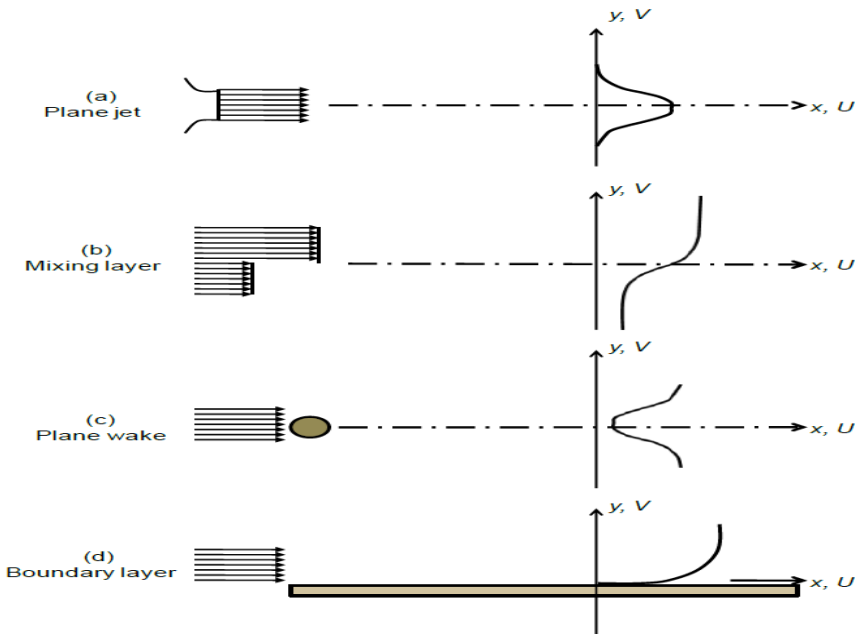


**Figure 1-3**: Depictions of two-dimensional flows (Alnahhal, 2010)

### 1.1.5 Unpredictability and randomness of turbulent flows

The most common feature of the turbulent flows is that their fluid velocity fields vary at a large scale and irregularly in both time and space. For instance, if we assume $U(t)$ a variable, a component of velocity is

random when it does not have a unique value at a fixed time and space. In other words, if an experiment is repeated under a specific set of conditions (boundary, initial, etc.) and the values of velocity $U(t)$ have a great deviation between them in every repetition, then $U(t)$ is a random variable. As far as turbulence is concerned, we have some predictability in time due to the exponential growth of disturbances in boundary or initial conditions with time, although there is no deterministic prediction of the flow's evolution. Therefore, one could say that the predictions become less reliable the further one goes into the future. (Lorenz, 1963)

#### 1.1.5.1 Statistical parameters

As it was previously mentioned, the Navier-Stokes equation allows to determine the velocity at a specified time and position for laminar flows. On the other hand, when studying turbulent flows, one should seek to find the probability of deterministic events due to the heavy dependence of the Navier-Stokes equation on the initial and boundary conditions. The former occurs because of the non-linearity and results in random solutions (Vassilicos, 2015). On the contrary, many turbulent flows reach a statistically stationary state and, thus it is possible to use some useful tools provided from the scientific field of statistics, for the characterization of random variables associated with turbulence.

#### 1.1.5.2 Mean values

The most recognisable statistical parameter is the mean velocity, which is usually expressed as $\overline{U}$. This parameter stands for the probability-weighted average of all possible values of $\overline{U}(t)$ for a time period of $T$. It is calculated by the following equation:

$$\overline{U} = \frac{1}{T}\int_0^T U(t)dt$$

In the scientific field of statistics another parameter of great importance is the standard deviation, which is commonly denoted as $\sigma_u$. The standard deviation is calculated through variance ${\sigma_u}^2$, in other words the mean-square fluctuations. Variance is calculated by the following equation:

$${\sigma_u}^2 = \frac{1}{T}\int_0^T u^2 dt$$

where $u$ are the fluctuations and are defined as $u = U(t) - U$. Therefore, the standard deviation is calculated by:

$$\sigma_u = \sqrt{{\sigma_u}^2}$$

The parameter of $U$ stands for the average distance the values are from the mean.

### 1.1.6 Kolmogorov hypotheses

As it was previously mentioned, the three hypotheses introduced by the Russian mathematician, Andrey N. Kolmogorov played a crucial role in the study of turbulence. Although before analyzing further the three hypothesis, one ought to know some information about energy dissipation and energy cascade.

#### 1.1.6.1 Energy dissipation

Energy dissipation is the conversion of the fluid's mechanical energy to heat, something caused from the fluid's viscosity. This phenomenon has a strong presence in the case of turbulence due to the high viscosity created by the turbulent motion. One way to measure the amount of energy transferred is the mean dissipation rate $\varepsilon$. The following equation defines the mean dissipation rate (Hinze, 1975)

$$\varepsilon = v\left\langle\left(\frac{\partial u_i}{\partial x_j}+\frac{\partial u_j}{\partial x_i}\right)\frac{\partial u_j}{\partial x_i}\right\rangle$$

where $u$ are the velocity fluctuations of the flow, $v$ the kinematic viscosity and the indexes of $i$ and $j$ represent the velocities in the directions of the three axes $x, y$ and $z$.

#### 1.1.6.2 Energy cascade

The first concept of energy cascade was introduced by the British scientist Lewis Fry Richardson in 1922. Energy cascade indicates that turbulence can be composed of different sized eddies. An eddy is considered to be a turbulent motion which is localized in a region of specified size. These eddies have a size $l$, a characteristic velocity $u(l)$ and timescale $\tau(l) = l/u(l)$. Additionally, a large eddy occupied region can contain smaller eddies. Large size eddies are those with lengthscale of $l_0$ and characteristic velocity of $u_0$ comparable to the flow's lengthscales, which are $L$ and $U(t)$ respectively. According to Richardson, eddies of large size are unstable and break up easily, resulting their energy to be transferred to smaller eddies. Smaller eddies following the same pattern break up and transfer their energy to even smaller eddies. Thus, this continuous energy transfer from bigger to smaller eddies is called energy cascade and it continues until the eddy is stable, which means that the Reynolds number ($Re = u(l)l/v$) is sufficiently small. The former theory is of great importance since it places the dissipation in the end of energy cascade sequence. (Pope, 2000)

#### 1.1.6.3 1st Kolmogorov hypothesis

The first hypothesis is associated with the isotropy of the small-scale motions. It is also called Kolmogorov's hypothesis of local isotropy and goes as follows:

*At sufficiently high Reynolds number, the small-scale turbulent motions ($l \ll l_0$) are statistically isotropic.*

The former indicates that eddies with small-scale turbulent motion can be assumed as isotropic since the directional biases of the large scales are lost in the chaotic motion as energy is transferred to smaller eddies.

#### 1.1.6.4 2nd Kolmogorov hypothesis

The second hypothesis is linked with the fact that the directional and geometrical information of the eddies gets lost as the energy passes down the cascade, resulting in universal statistics of small-scale motions, which are similar for every high Reynolds number turbulent flow. It is also called Kolmogorov's first similarity hypothesis and goes as follows:

*In every turbulent flow at sufficiently high Reynolds number, the statistics of the small-scale ($l < l_{EI}$) motions have a universal form that is uniquely determined by $v$ and $\varepsilon$.*

where $l_{EI}$ is a lengthscale that demarches the large anisotropic eddies and the small isotropic eddies and is calculated by $l_{EI} \approx (1/6)l_0$, where $v$ is the kinematic viscosity and $\varepsilon$ is the dissipation (energy transfer) rate.

#### 1.1.6.5 3rd Kolmogorov hypothesis

The third and last hypothesis is based on the fact that the Reynolds number of the intermediate scales (scales between small and large) are relatively large and are not affected by the viscosity $v$. It is also called the second similarity hypothesis and goes as follows:

*In every turbulent flow at sufficiently high Reynolds number, the statistics of the motions of scale $l$ in the range $l_0 \gg l \gg \eta$ have a universal form that is uniquely determined by $\varepsilon$ independent of $v$.*

Where $\eta$ is the Kolmogorov length scale and is defined as $\eta = (v^3/\varepsilon)^{1/4}$.

## 1.2 Experimental simulations of turbulence

### 1.2.1 Homogeneous and isotropic turbulence

One way to study the turbulent flows is to develop theories while working on simpler turbulent flows, one of which is the homogeneous and isotropic turbulence. Homogeneous isotropic turbulence is in general terms an idealized version of realistic turbulence with the proper modifications made, so as to be used in analytical studies (Taylor, 1935). The term 'homogenous' indicates that the statistical properties are invariant under arbitrary translations of the coordinate axes and the term 'isotropic' indicates that for a full rotation group, the statistical properties are invariant. This includes reflections and rotations of the

coordinate axis (Monin & Yaglom, 2013). The homogenous and isotropic turbulence can be assumed for many types of turbulent flows, such as flows associated with combustion, droplet vaporization, inertial particle clustering etc and will be the main theory that is going to be used for the analysis of the results of this work.

Most of the methods for creating homogenous turbulent flows can be divided into two categories, those producing spatially decaying turbulence at a mean velocity and those generating stationary turbulence in closed space (box or tank) with zero mean velocity (Goepfert, 2010). In the case of the spatially decaying turbulence, all the experiments associated with grids in wind tunnels fall in. Furthermore, the range of the turbulent Reynolds numbers and the turbulence fluctuations are small when working at typical laboratory-scale wind tunnel velocities. In the case of stationary turbulence, the use of an oscillating grid is mostly preferred, in order to keep the fluctuations of the turbulence at a small size (an order of 0.1 m/s) and simultaneously achieve a good degree of isotropy without the long-time length in takes to develop.

This section provides information for the facilities that are used to originate homogeneous & isotropic turbulence. For most of the experimental studies associated with HIT, the primary options are oscillating grids, wind tunnels and space distributed actuators.

### 1.2.2 Oscillating grids

Oscillating grids are rather bulky, are equipped with mechanically moving parts and homogeneity and isotropy can be achieved on planes parallel to the grids. They typically consist of a planar grid with uniform mesh spacing M, positioned horizontally inside a water-filled container, oscillating vertically with frequency f and stroke S. The oscillatory motion produced from the grid's mechanical part creates stationary turbulence that spatially decays in the grid-normal direction. However, in planes parallel to the grid the turbulence can be assumed to be homogenous with the mean-flow velocity components of a small magnitude comparing to the flow's fluctuations. In more general terms, oscillating-grids are used to study a large variety of problems mainly associated with turbulent entrainment across a density interface due to their approximation of a 'zero-mean-shear' turbulent flow (McCorquodale, 2018). Figure 1-4 depicts a typical oscillating grid. In order to better comprehend the use of an oscillating grid, Figure 1-5 and Table 1 depict the experimental setup and its conditions from the experiment involving oscillating grids conducted by Cheng and Law (2001).

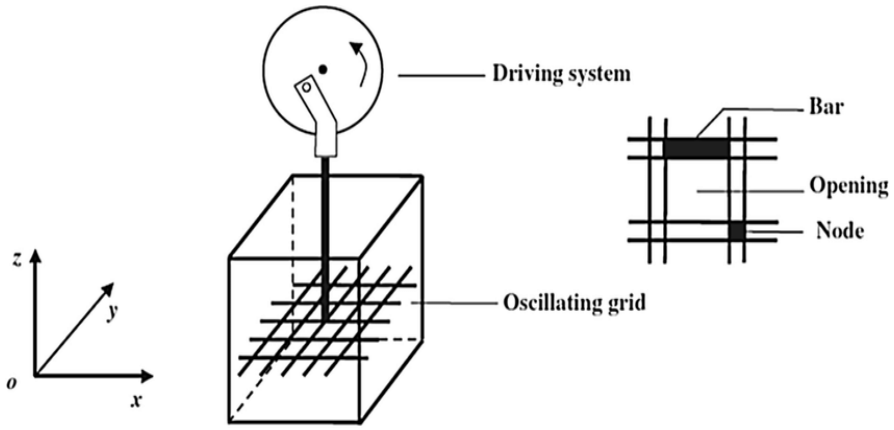


**Figure 1-4:** A typical oscillating grid (Luo et al. 2021)

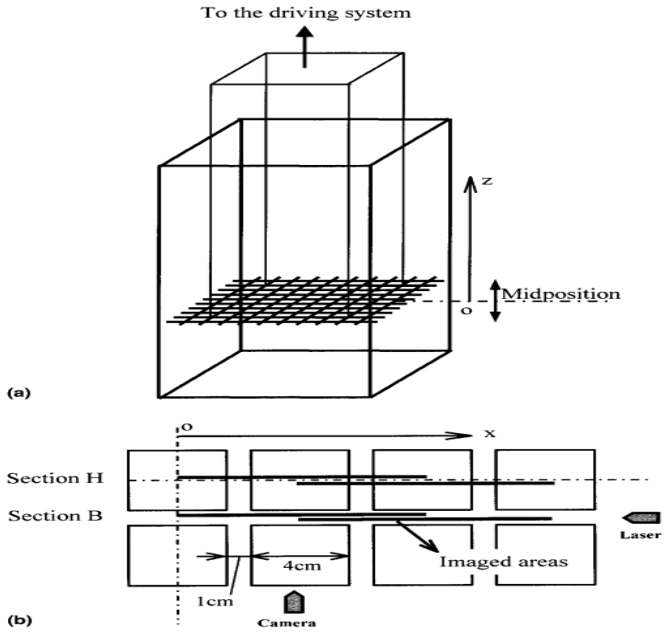


**Figure 1-5:** Cheng & Law's (2001) experimental setup: (a) Water tank, (b) Plan view of imaged locations

**Table 1:** Cheng and Law's experimental conditions (2001)

| Tank dimensions | | | Grid Description | | Operating Values | |
|---|---|---|---|---|---|---|
| Length (cm) | Width (cm) | Height (cm) | Mesh size M (cm) | Bar section (cm x cm) | Oscillating frequency f (Hz) | Stroke S (cm) |
| 50 | 50 | 100 | 5 | 1 x 1 | 1-4 | 4 |

Note: $M$ stands for the mesh size, $f$ is the oscillation frequency, $S$ the stroke, $H$ the inner box height and $Re$ the grid's Reynolds number.

### 1.2.3 Wind tunnels

The wind tunnel is basically a tube through which an artificial wind with known conditions is blown. Most of the wind tunnels consist of the test section where the measurements are taken, the settling chamber , whose purpose is to assure the flow arrives to the test section with a uniform profile of velocity, the fans and motors to propel the air flow, the air filters to avoid unwanted particles that can disrupt the measurements, the guide vanes and the turbulence generator element (grids).The main aim of a wind tunnel is to provide information about some parameters of wind such as pressure or velocity in a specific position (Muniz and Riera, 2017). Table 2 depicts some turbulence characteristics from some typical wind tunnel experiments conducted by Hideharu (1991) and Comte-Bellot & Corrsin (1966) and (1971).

**Table 2:**Typical measurements in wind tunnel experiments

| | $U_0$ (m/s) | $M$ (mm) | $X/M$ | $Re_M$ $(10^3)$ | $u'/U_0$ (%) | $u'/v'$ |
|---|---|---|---|---|---|---|
| Hideharu (1991) | 5 | 46.7 | 50 | 15.6 | 16.4 | 1.22 |
| Comte-Bellot and Corrsin (1966, 1971) | 10 | 50.8 | 42 | 34 | 2.22 | 1 |

Note: $U_0$ is the mean velocity, $M$ the mesh size of the grid, $X$ the variable of the $X$-direction, $Re_M$ the mesh Reynolds number, $u'$ the longitudinal component of the turbulence velocity fluctuations, $v'$ the lateral component of the turbulence velocity fluctuations.

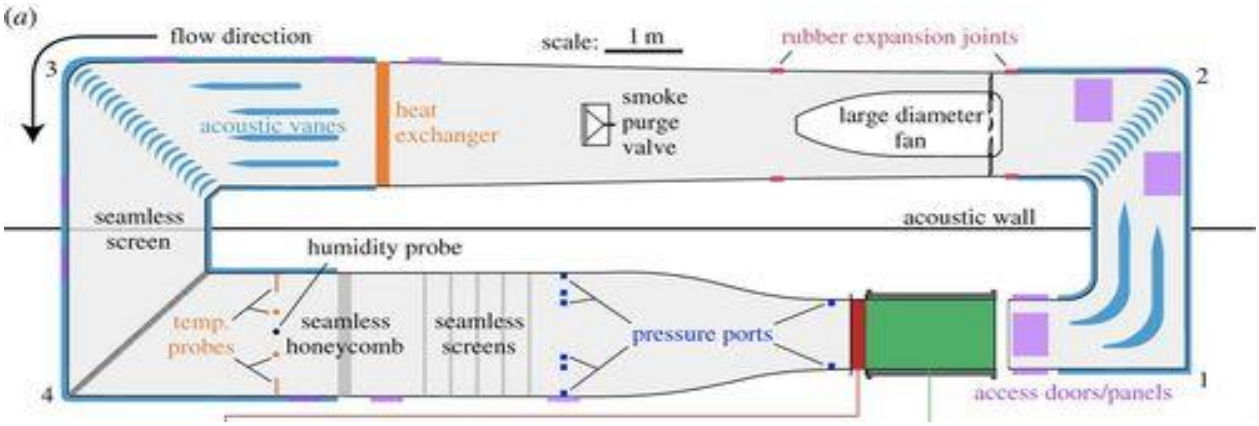


**Figure 1-6:**Wind tunnel scheme (Quinn et al. 2017)

### 1.2.4 Space distributed actuators

This method is the most recent in comparison with the previous ones. In order to better comprehend this method, some information about the function of synthetic jets must be noted. A synthetic jet is generally formed by the back-and-forth movement of a flow through a small opening. In other words, a synthetic

jet is created from the periodic ejection and suction of a fluid from a nozzle, in contrast with a conventional jet in which the stream of a fluid mixes with the ambient fluid, thus requiring an external source of fluid. The term 'synthetic jet' was originally introduced by Ari Glezer in his early work on synthetic jets in the late 80s and early 90s. More recently, Variano and Cowen (2008) created a planar array of randomly actuated synthetic jets placed on the bottom of a tank. The previous configuration can create turbulence with a satisfactory level of two-dimensional homogeneity and isotropy over a large region and a large Reynolds number, something that can be adapted for the study of turbulence at boundaries.

Some alternative methods were introduced due to requirement of high efficiency mixing devices for the study of premixed combustion. Some of which are the systems introduced by Birouk et al. (1996), that use fans in the corners of a cubic box, all pointed towards the center of the cubic box. Additionally, a similar method with the previous one is the one introduced by Hwang and Eaton (2004), which is simpler and can provide high velocity fluctuations with high Reynolds numbers and simultaneously spatial homogeneity. It consists of a cubic chamber with solid walls and eight loudspeakers instead of fans, used by Birouk et al., each placed at each corner of the cube, and all pointed towards the center. The loudspeakers are functioning as synthetic jets because their membranes push air out of a plenum through an orifice, thus creating powerful turbulence in the center of the cube. Table 3 depicts some flow statistics derived from experiments done from Birouk et al. (1996) and Hwang and Eaton (2004), assuming homogeneous and isotropic turbulence.

**Table 3:** Typical measurements of space distributed actuators

| | Birouk et al. (1996) | Hwang and Eaton (2004) |
|---|---|---|
| Medium: | Air | Air |
| $u_{1,\mathrm{RMS}}$ (m/s) | 0.95 | 0.87 |
| $u_{2,\mathrm{RMS}}$ (m/s) | 1 | 0.84 |
| $u_{1,\mathrm{RMS}}$ / $u_{2,\mathrm{RMS}}$ | 0.95 | 1.03 |
| $U_1$(m/s) | 0.1 | 0.019 |
| $U_2$(m/s) | -0.075 | -0.088 |
| $U_1$ / $u_{1,\mathrm{RMS}}$ | 0.11 | 0.022 |
| $U_2$ / $u_{2,\mathrm{RMS}}$ | -0.075 | -0.1 |
| $\varepsilon$ $(m^2/s^3)$ | 82 | 11 |
| $Re$ | 110 | 220 |
| $\eta$ (mm) | 0.08 | 0.13 |

Note: The table shows (from top to bottom): rms velocities, isotropy ratio, mean velocities, mean velocity to rms velocity ratios, dissipation rate, Reynolds number, Kolmogorov lenghtscale.

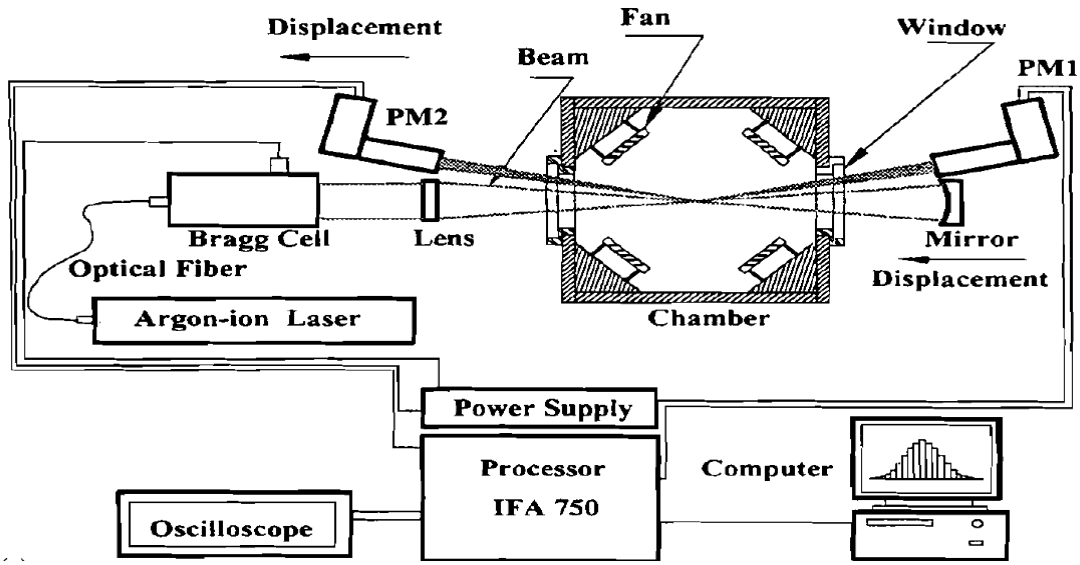


**Figure 1-7:** Experimental setup of Birouk et al. (1996)

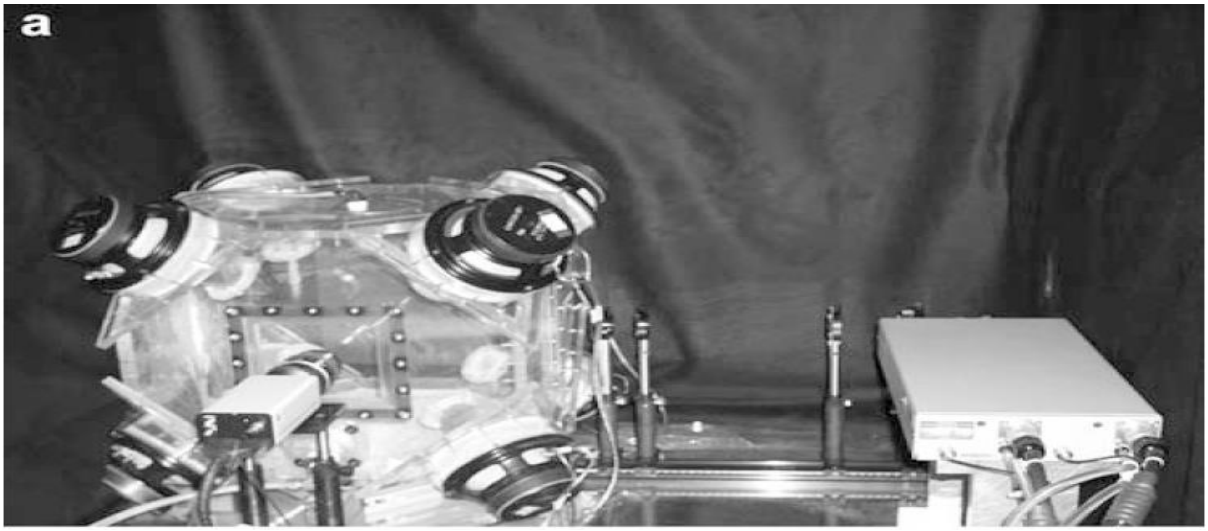


**Figure 1-8:** Experimental setup of Hwang and Eaton (2004)

## 1.3 Jets

A simple definition of a jet is that it is the flow generated by a continuous source of momentum. In other words, a jet can be created when a moving fluid enters a calm body of the same fluid. Typical examples are the discharge of a fluid in the environment through a narrow pipe or the emptying of a river in a lake. In such cases, a velocity shear is created between the jet and the ambient fluid, thus creating turbulence and mixing. In turbulent jets due to the instabilities of the shear layers, created by the fluid's turbulent flow, eddies are formed which move randomly and are responsible for the exchange of matter (such as

constituents), heat and momentum with the ambient fluid (Abramovich, 1963). Most of the studies concerning turbulent jets are very demanding because of the high dependence of the jet's properties with the geometry of the flow stream and simultaneously with all kinds of forces acting on the fluid. (Cushman-Rosin, 2019)

Round and plane jets are simple forms of jet flows since their mean flow can be described by two spatial variables. The recent studies on jets show the same interest in both jet flows, comparing to earlier years where research was more focused on plane jets, probably due to the improved measurement techniques and signal processing analysis, as pointed out by Abdel-Rahman (2010). Regarding the round free jet, this flow can be characterized by three different regions: (a) the near-field region, usually situated at distances $x \leq 6D$, wherein the flow characteristics are similar to those at the exit of the nozzle and the potential core of the flow is included; (b) the intermediate-field region, usually situated at distances $6D < x < 30D$; (c) the far-field, usually situated at distances $x \geq 30D$, wherein the flow is fully developed. The intermediate-field region along with the near-field region, comprise the development portion of the jet. This region finds a lot of interest in practical applications of jets due to the substantial influence of mass, momentum and heat transfer associated with the upstream conditions (Abdel-Rahman et al. 1996). The research work on jet flows can be divided into (a) the work focused on the initial conditions of the jet flow (i.e., the flow development region) and (b) the work focused on the fully developed (or self-similar) region of the flow (Abdel-Rahman, 2010).

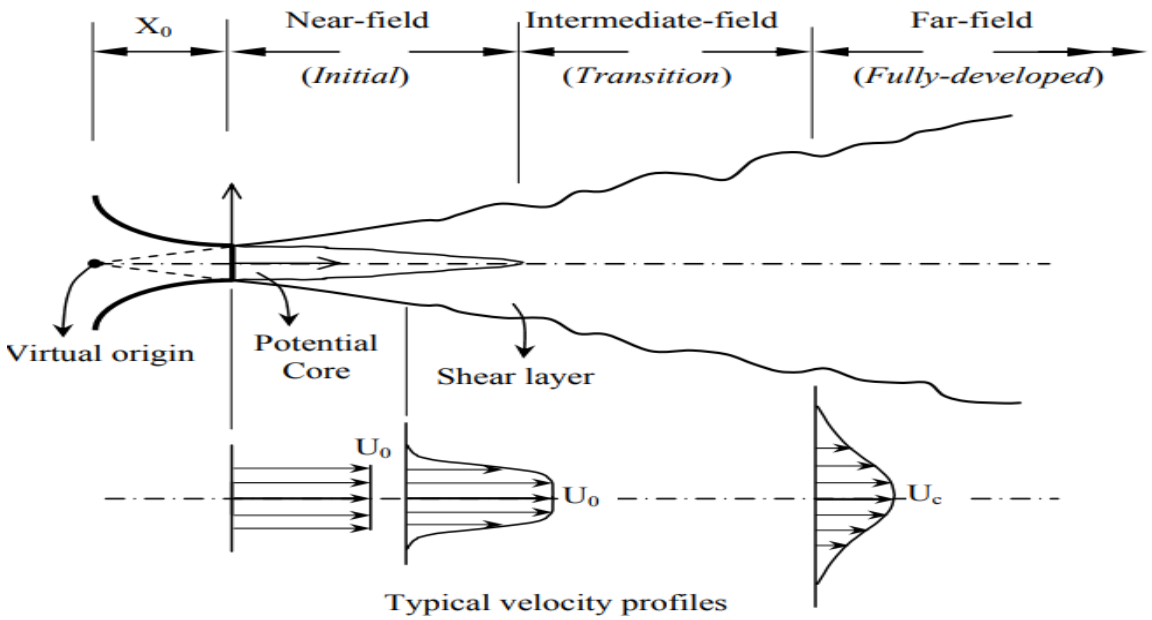


**Figure 1-9:** A schematic of the free turbulent jet's flow development (Rahman, 2010)

### 1.3.1 Flow profile

Experimental studies associated with jets penetrating a tranquil fluid of the same density, indicate that the turbulence produced by the jet forms an envelope of a nearly conical shape, as depicted in Figure 1-10 (Cushman-Roison, 2019). The opening angle of the flow is always the same, regardless of the properties of the fluid and the specifics of release. The angle which is used universally is 11.8°. Therefore, when counting from one side to another, this sums up to about 24°. Therefore, the relationship between the radius R of the jet and the downstream distance $x$ is given by:

$$R(X) = \tan(11.8^{\circ})\, X \cong \frac{1}{5} X$$

According to the previous function, it is easy to see that for the value of $X = 0$, the radius is zero. Since the initial jet radius is not zero but equal to half the exit diameter *D*, the downstream distance x required to be measured not from the orifice (jet's exit) but from a distance 5*D*/2 into the conduit. This point is named the 'virtual source'. The following image depicts a schematic of the flow with all the previously noted properties shown.

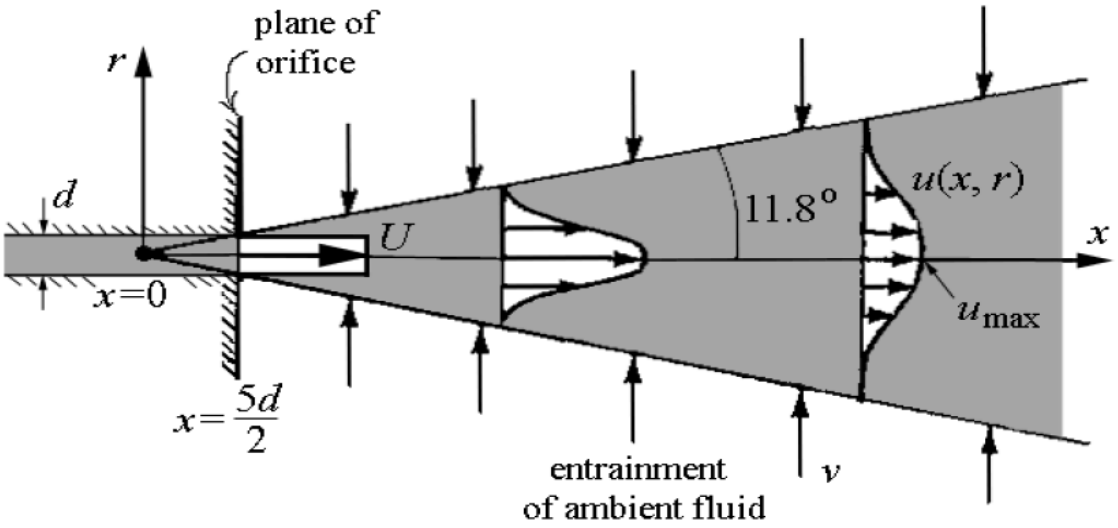


**Figure 1-10:** Schematic depiction of the flow's profile, coming from a jet penetrating a quiescent fluid (Cushman-Roison, 2019)

### 1.3.2 Velocity

Experimental studies on turbulent jets show that the velocity in the jet follows a law of similarity, which means that all cross-sections appear indistinguishable, apart from a stretching factor and the profile of velocity across the jet takes a Gaussian shape. Thus, the equation for the velocity can be written as:

$$u(X,r) = u_{max}\, exp\left(-\frac{r^2}{2\sigma^2}\right)$$

where $r$ is the cross-jet radial distance from the centerline, σ the standard deviation associated with the spread of the profile at the centerline, $u_{max}(X)$ the maximum speed at the centerline and $X$ the downstream distance (from the virtual source). It can be assumed that 4$\sigma$ = 2R since, based on statistics, 4$\sigma$ is the width of the distribution that encompasses 95% of the area under the bell curve (Gaussian shape). Therefore, the previous equation can be altered to the following one:

$$u(X,r) = u_{max} exp\left(-\frac{50r^2}{X^2}\right)$$

### 1.3.3 Momentum

In these cases of turbulent jets entering a quiescent environment, the momentum flux in the jet's cross section is assumed to be constant downstream due to the absence of external forces that can disrupt the flow. From a mathematical point of view the flux equals the momentum per unit volume $\rho u$ times the velocity, therefore the statement that the momentum is constant downstream can be written as:

$$\int_0^\infty \rho u^2\, 2\pi r dr = \rho U^2 \frac{\pi D^2}{4}$$

where, $\rho$ is the fluid density, $D$ the orifice diameter, $u$ the fluid velocity and $U$ the average velocity at the orifice. Combing the previous two equations after the calculation of the integral, the following relationship is deduced:

$$u_{max} = \frac{5D}{X} U$$

This relationship indicates that when the distance from the virtual source is increasing, the velocity along the centerline of the jet is decreasing inversely.

### 1.3.4 Volumetric flux Q

An important flow characteristic is that the flow's volumetric flux Q is not constant along the jet due to the entrainment of the calm surrounding fluid. The volumetric flux $Q$ is calculated according to the following equation (Cushman-Roison, 2019):

$$Q = \int_0^\infty u 2\pi r dr = \frac{\pi}{50} u_{max} X^2 = \frac{\pi}{10} DUX$$

that is, the volumetric flux Q increases linearly with the downstream distance. Accordingly, the increment rate of the volumetric flux, referred to as entrainment rate $E$, is constant:

$$E = \frac{dQ}{dX} = \frac{\pi DU}{10}$$

A new term can be introduced which is called the entrainment velocity. This is the radial velocity $v$ that carries the entrainment. From the principle of volume conservation along the $dx$ direction of the jet, one gets:

$$dQ = v\, dA$$

where $dA = 2\pi RdX$ the lateral area of this section of the jet and $v$ the transverse (radial) velocity that carries the entrainment. If one substitutes the relationship $dA = 2\pi RdX$ and $R = X/5$ (the radius of the jet in terms of the downstream distance $X$) in the previous equation, one gets:

$$\frac{dQ}{dX} = 2\pi Rv = \frac{2\pi Xv}{5}$$

If one equates the above expression for $dQ/dX$ with the one that it was previously obtained, the following relationship is deduced:

$$v = \frac{UD}{4X} = \frac{u_{max}}{20}$$

### 1.3.5 Interaction with the ambient fluid

In most of the experimental studies associated with jets, the jet contains a contaminant while the surrounding fluid does not. This method allows for a better visualization of the jet flow and a better understanding of the jet's behavior with the ambient fluid. In order for this method to be used correctly, a very useful tool is the Reynolds number. With its assistance, one is able to know the properties of each type of flow and better comprehend its reaction with the surrounding fluid.

In accordance with the review of Abdel-Rahman (2010), recent investigations on round jets indicate that when the Reynolds number is increased from 20000 and beyond, the entrainment in the jet remains constant (Rahman, 2010). Also, the radial spread of the mean velocity field and the decay of the mean centerline velocity in the downstream direction are independent of the Reynolds number, when this is greater than a few thousand at the exit of the jet. Furthermore, a laminar jet, called ''laminar dissipated jet'', is obtained when the Reynolds number is lower than 30. For Reynolds numbers greater than 500, the jet has at start a laminar length which later becomes turbulent. The laminar length decreases with the

increase of the Reynolds number. Although, for Reynolds numbers higher than 2000, the jet's flow becomes turbulent very near the jet's exit. (Abdel-Rahman, 2010)

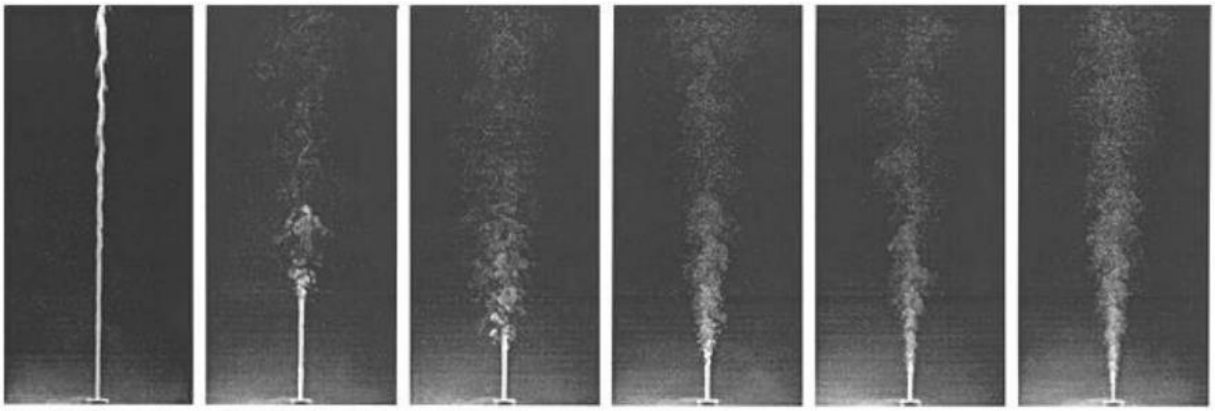


**Figure 1-11:** The increasing Reynolds effect on the jet's flow (Rahman, 2010)

Studies conducted by Obot et.al (1984), have shown that for the Reynolds number values of 13000 and 22000 the entrainment for each nozzle studied is independent of the exit Reynolds number. This agrees with another study by Ricou et.al (1961), which shows that the rate of entrainment decreases with the Reynolds number up to the value of Re=10000, beyond that the entrainment coefficient takes a constant value. Furthermore, it is observed that the Reynolds number has an impact on the decay of the centerline velocity and the radial spread of the velocity field, both of which increase as the Reynolds number decreases. More specifically, Rajaratnam and Flint-Peterson (1989) studied the variation of the spread rate of circular jets with Reynolds number. The study resulted that the spread rate continuously decreases with the Reynolds number and reaches an asymptotic value of 0.16 at the value of Re= 10000. In another study by Abdel-Rahman et al. (1996), the effect of the Reynolds number at the exit of the jet was investigated experimentally using an LDA system. They noticed that the centerline mean velocity of the jet is decaying faster as the exit Reynolds number is decreasing. This may be caused by the enhanced mixing and interaction of the jet's fluid with the ambient environment due to the structure of vortex, which moves more violently and rapidly as the Reynolds number decreases. Finally, Albertson et al. (1950) has created some analytical expressions for the mean flow characteristics. For Reynolds numbers varying from 2.2 x $10^4$ to 5.3 x $10^4$, they reported a velocity decay constant of 6.2 along the jet axis for the jet developing region.

### 1.3.6 Contaminant's concentration

In experimental studies, it is important to determine the concentration of the contaminant in the jet flow and its behavior with the ambient fluid. Thus, the development of mathematical formulas is necessary. One may assume that the concentration has a Gaussian profile, as the velocity, which can be written as:

$$c(X,r) = c_{max}\, exp\left(-\frac{r^2}{2\sigma^2}\right) = c_{max}\, exp\left(-\frac{50r^2}{X^2}\right)$$

where $c_{max}(X)$ is the peak concentration along the centerline, which depends on the value of the downstream distance $x$, i.e., $c_{max}(X) = c(X,0)$. The requirement for the conservation of the total amount of contaminant transferred by the jet, while assuming that the surrounding fluid is contaminant free, is the following:

$$\int_0^\infty cu2\pi r dr = c_o U \frac{\pi D^2}{4}$$

where $c_o$ stands for the average concentration at the exit of the jet (orifice). If one calculates the integral, the following relationship is obtained:

$$c_{max} = \frac{5D}{X} c_o$$

This relationship indicates that the centerline concentration varies along the jet. This is due to the dilution of the jet's contaminant from the ambient fluid. In other words, the concentration of the contaminant diminishes, as the downstream distance increases.

Interestingly, the above equation indicates that the maximum concentration at the orifice ($X = X_0 = 5D/2$) is related to the maximum concentration at a distance $1D$ from the orifice ($X_1 = X_0 + D$) and, more generally, at a distance $nD$ from the orifice ($X_n = X_0 + nD$), in accordance with:

$$5\frac{C(X_0,0)}{C_0} = 7\frac{C(X_1,0)}{C_o} = 9\frac{C(X_2,0)}{C_o} = 11\frac{C(X_3,0)}{C_o} = \cdots = (5+2n)\frac{C(X_n,0)}{C_o} = 10$$

# 2. Methods

## 2.1 Flow visualization

The method that was used to visualise the outgoing air flow from the jet, is called flow visualization. Flow visualization is an optical method to obtain instantaneous concentration measurements and related fluid properties. In simpler terms, flow visualization is the process of making the physics of fluid flows visible. For the flow to become visible, tracer particles are added. The tracer particle material has a great variety and its selection and concentration in the fluid greatly depends on the type and fluid of the flow. When the fluid of the flow being studied is air, the most common trace materials are smoke and oil mist due to their small particle size of less than 1μm (Lewis, 2003).

Figure 2-1 depicts a simple schematic of the flow visualization method. During this method, it can be assumed that the tracer material used was smoke. After the tracer material being released, it is swept with the flow, resulting in the flow structure becoming more observable. However, in order to examine the properties of the flow, these tracer particles should be illuminated for better exposure. The illumination of the tracer particles is done via laser beam pointed directly on the flow as depicted in Figure 2-1. The exposure of each particle is recorded in a separate frame. The illuminated tracer particles are recorded with the aid of a camera to capture their density inside the flow. After that, the density of the tracer particles inside the flow is used to identify the properties of the flow that is being studied with the aid of a computer as seen in Figure 2-1.

In general terms flow visualisation is a commonly used method because it is capable to measure an entire two-dimensional section of the flow field simultaneously, it allows data processing due to the generation of large numbers of image pairs, which with the help of a personal computer can be analysed and provide a large quantity of information. However, it should be pointed out, that flow visualization is not able to measure the components along the z-axis, which sometimes can disrupt the other measurements due to the introduction of an interference in the data measured from the x and y components. This problem can be resolved by adding another camera pointed at the y-z axis. Therefore, the use of two cameras allows to measure all three concentration components.

After taking the images needed for the study of the flow, the processing of the images taken by the camera was done with the help of computer software that provided the necessary information needed to understand the properties and behavior of the flow.

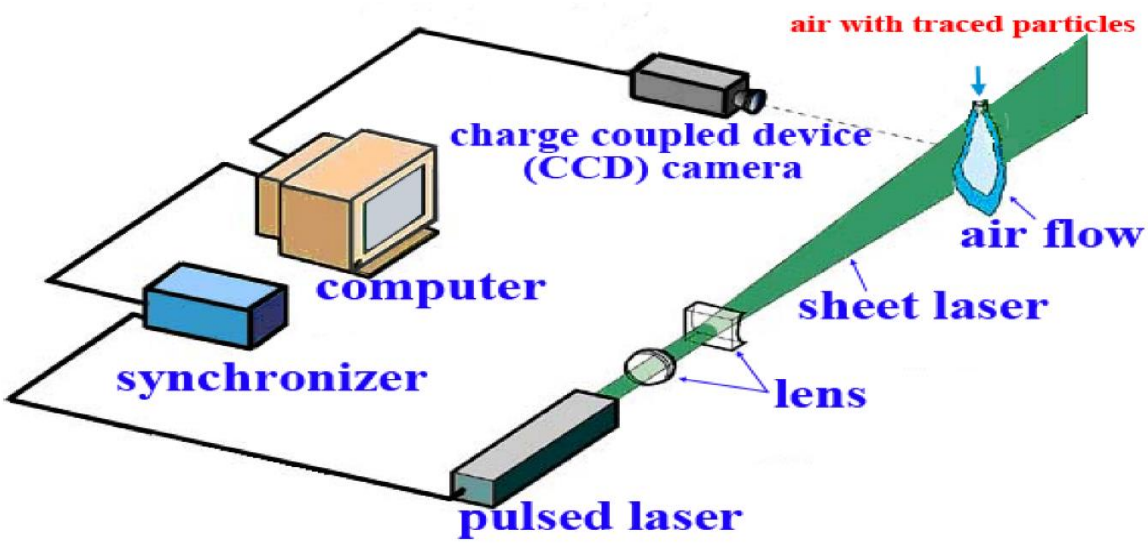


**Figure 2-1:** A simple schematic of a flow visualization method (Xie et al. 2020)

## 2.2 Experimental setup

### 2.2.1 Overview

The experimental setup was designed with the aim to implement properly the flow visualization method. The setup consisted of the following parts:

- An air compressor
- An air rotameter
- A smoke generator
- A mixing tank
- An Arduino control system
- The jet
- A laser beam
- A turbulence chamber with eight loudspeakers (synthetic jets)
- An audio amplifier
- A camera
- The laboratory's computer

The experimental setup is presented schematically in Figure 2-2. The air flow 'generated' from the air compressor reaches the air rotameter, where the volumetric flowrate is adjusted to the required value. The air flow is then fed to the mixing tank, where it is infused with the smoke coming from the smoke

generator. Then, the combined air-smoke flow reaches the jet's exit. The laser beam, adjusted with expanding lens, is directly pointed at the jet's exit to have a better visual of the flow. In this way, one can get with the aid of the laboratory's camera, placed across the jet, good quality pictures. To acquire the photos, the camera was controlled from the laboratory's computer and was set to take 200 pictures per measurement. These pictures were displayed in the laboratory's computer and then analyzed with the assistance of computer software. Finally, the loudspeakers located in the vertices of corners of the cube are the means for creating turbulence during some of the experiments. Each component of the setup will be analyzed in the following sections. Figure 2-3 presents the experimental setup from the frontal view.

During the course of the experimental work, a wide range of flow conditions was investigated, by performing measurements for seven different volumetric jet flow rates in various turbulent states. The different volumetric flow rates employed were 10, 20, 30, 40, 50, 60, 70 l/min, which correspond to Reynolds numbers 1400, 2800, 4200, 5600, 7000, 8300 and 9800, respectively, as presented in Table 4. The turbulent states examined were the following:

1. No turbulence (Quiescent environment),
2. Turbulence generated from all loudspeakers (simulating HIT),
3. Turbulence generated from the loudspeakers on the right side of the support structure (loudspeakers 3468)
4. Turbulence generated from the loudspeakers on the left side of the support structure (loudspeakers 1257)
5. Turbulence generated from the loudspeakers on the upper side of the support structure (loudspeakers 5678)
6. Turbulence generated from the loudspeakers on the bottom side of the support structure (loudspeakers 1234)

In Table 4 the environmental conditions where the experiments took place and simultaneously the properties of the flow for each case are depicted. Finally, Table 5 depicts which loudspeakers operated to create each case of turbulent environment.

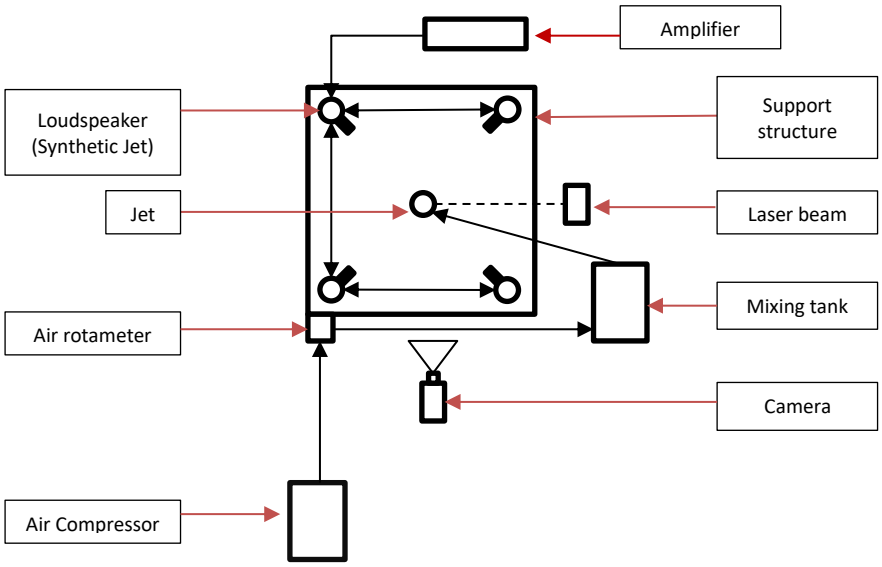


**Figure 2-2:** A simple schematic depicting the experimental arrangement

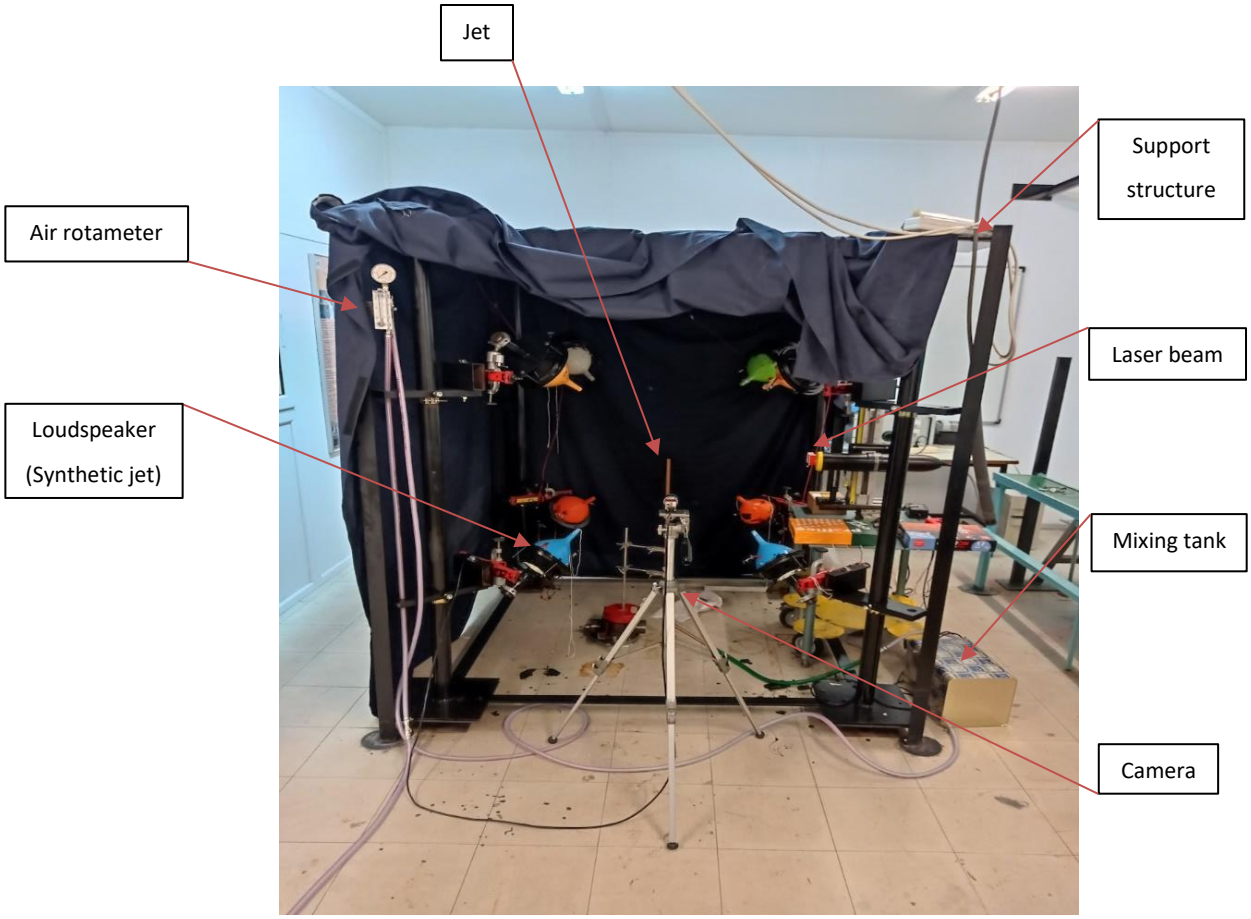


**Figure 2-3:** A general view of the experimental setup

**Table 4:** The conditions at which the experimental equipment operated

| **Medium** | **Air** | **Air** | **Air** | **Air** | **Air** | **Air** | **Air** |
|---|---|---|---|---|---|---|---|
| **Volumetric flow rate Q (l/min)** | 10 | 20 | 30 | 40 | 50 | 60 | 70 |
| **Atmospheric Pressure (atm)** | 1 | 1 | 1 | 1 | 1 | 1 | 1 |
| **Temperature Ambient (℃)** | 20 | 20 | 20 | 20 | 20 | 20 | 20 |
| **Air Density ($kg/m^3$)** | 1.2047 | 1.2047 | 1.2047 | 1.2047 | 1.2047 | 1.2047 | 1.2047 |
| **Air Viscosity (kg/m*s)** | $1.82*10^{-5}$ | $1.82*10^{-5}$ | $1.82*10^{-5}$ | $1.82*10^{-5}$ | $1.82*10^{-5}$ | $1.82*10^{-5}$ | $1.82*10^{-5}$ |
| **Mean Velocity (m/s)** | 2.12 | 4.24 | 6.37 | 8.49 | 10.61 | 12.73 | 14.85 |
| **Reynolds number** | 1400 | 2810 | 4210 | 5620 | 7020 | 8430 | 9830 |
| **Rounded Re** | 1400 | 2800 | 4200 | 5600 | 7000 | 8400 | 9800 |

**Table 5:** Loudspeaker's operational status

| **Loudspeakers:** | 1 | 2 | 3 | 4 | 5 | 6 | 7 | 8 |
|---|---|---|---|---|---|---|---|---|
| **Ambient conditions:** | | | | | | | | |
| Quiescent ambient | | | | | | | | |
| Homogeneous and isotropic turbulence | On | On | On | On | On | On | On | On |
| Anisotropic turbulence (Right) | | | On | On | | On | | On |
| Anisotropic turbulence (Left) | On | On | | | On | | On | |
| Anisotropic turbulence (Upper) | | | | | On | On | On | On |
| Anisotropic turbulence (Bottom) | On | On | On | On | | | | |

### 2.2.2 Support Structure

For the foundation of the experimental setup, a cubic metal frame with dimensions 1.80 x 1.80 x 1.80 m was used as a support structure. This structure was made in a way that aims in minimizing the optical obstructions that can occur to the flow visualization equipment and associated procedures. Due to the lack of solid walls, the structure allows the smoke flow visualization without any window reflections. Furthermore, it minimizes the acoustic resonances and standing waves, thus, making the random phasing in the power supply unnecessary. In the following image, one can clearly see the support structure (the

black cubic metal frame), where most of the equipment needed for the experiment is located. In Figure 2-4 an early stage of the support structure is depicted.

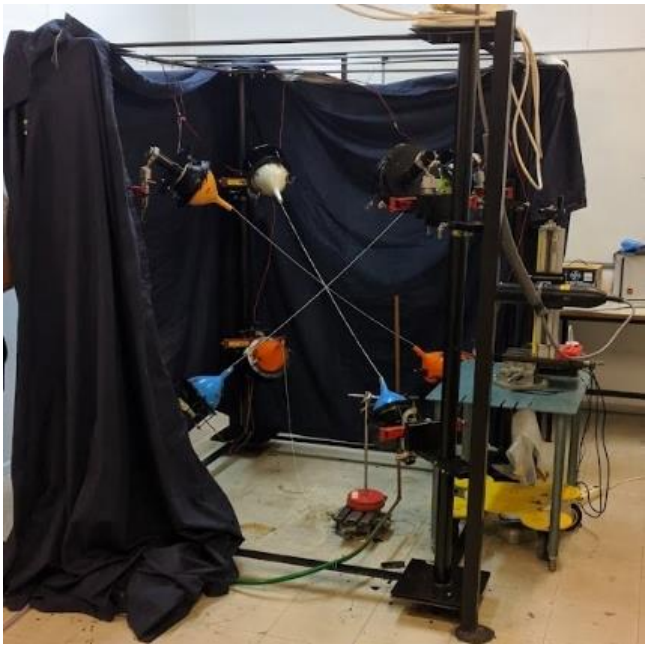

**Figure 2-4:** The support structure in an early stage

### 2.2.3 Loudspeakers and amplifier

In this setup, eight loudspeakers were placed in the tips of the universal joints located at the edges of the cubic metal frame that was previously presented. For the loudspeakers to align properly, the joints were supplied with adjustable rods where the loudspeakers were mounted and could slide up and down, as it can be seen in the Figure 2-5. All the loudspeakers were pointed to the centre of the cube where the flow exits the jet.

In this experimental procedure, the synthetic jets all consisted of loudspeakers, in front of which, ejector tubes (perforated plates) were mounted on each of the eight corners of the support structure respectively; they were all pointing towards the center of the system. The main purpose of this arrangement was to increase the mass flowrate of the system and homogenize the momentum flux simultaneously. In other words, an almost accurate homogenous and isotropic turbulent field could be created, which allowed the study of the behavior of the flow infused with plume at different conditions.

The loudspeakers were powered by an amplifier with a maximum power of 6.25 W/loudspeaker. The current experiment's amplifier was a D&J AMM-2000 2-Channel mosfet amplifier, operated at 50 watts; the amplifier is depicted in Figure 2-6. During this experiment, the amplifier transmitted to the

loudspeakers sinusoidal signals with the frequency (*f*) of 40 Hz. This frequency could be altered from the amplifier's control system, which provided a range of sinusoidal signals frequency values. The amplifier's control system is depicted in Figure 2-7. In order to meet the operational requirements of the amplifier, a car battery operating at 12 V (voltage) and approximately 4.17 A (current) was used. Additionally, plastic type funnels with a diameter of 200 mm (ending to a nozzle of 14 mm) were used to cap the loudspeakers. These provided a better control of the air flow coming from the loudspeakers and, a better accuracy of where the air flow is ejected. Accordingly, with the help of the funnels, the turbulence in the centre of the cube was increased.

**Figure 2-5:** The loudspeaker with the funnel attached


**Figure 2-6:** The amplifier transmitting the loudspeakers with sinusoidal signals


**Figure 2-7:** The amplifier's control system

### 2.2.4 Air compressor

During the experiments, a conventional air compressor which was powered up by electricity was used. The compressor was an LD2501 model manufactured by AIR-PHOON. The air compressor's power was 2.5 HP, compressed the air at 116 PSI, had a maximum air flow of 120 L/Min, a total volume of 24 L and required 250 V for it to operate. The purpose of the air compressor was to supply air to the jet. As it can be seen in Figure 2-8, the compressed air is fed to the jet via a purple hose. The air compressor operated until the required air pressure was met, after that, it stopped and operated again when the value of the air pressure dropped.

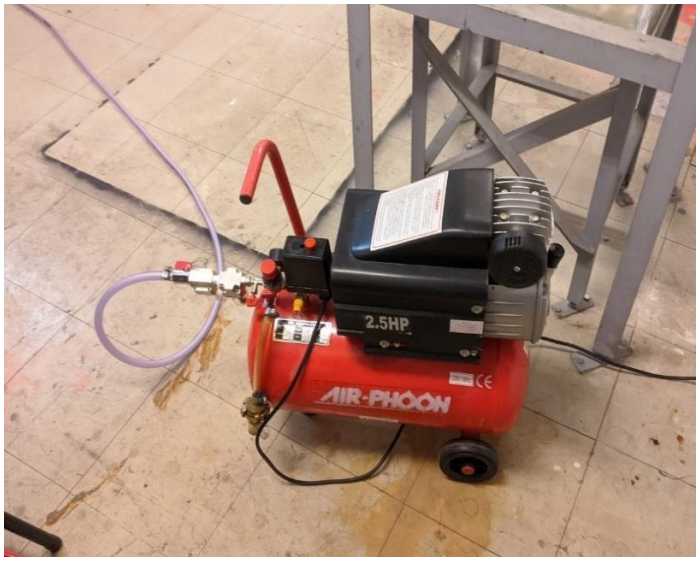


**Figure 2-8:** The air compressor providing the experimental arrangement with constant supply of air

### 2.2.5 Air rotameter

The air rotameter is a device that controls the volumetric flowrate of the air that passes through the mixing tank and ends up to the jet. With its assistance, it was possible to perform experiments with different conditions i.e., different air flowrates at the jet exit. The connections for the supply of air from the air compressor to the air rotameter, the mixing tank and finally the jet, were made using reinforced hose. As Figure 2-9 depicts, the air rotameter uses 'Liters per minute' as volume flow measurement unit and as for the pressure has both a 'bar' and a 'psi' unit measurement scale. Finally, it allows the selection of different volumetric flow rates from 10 l/min to 90 l/min.

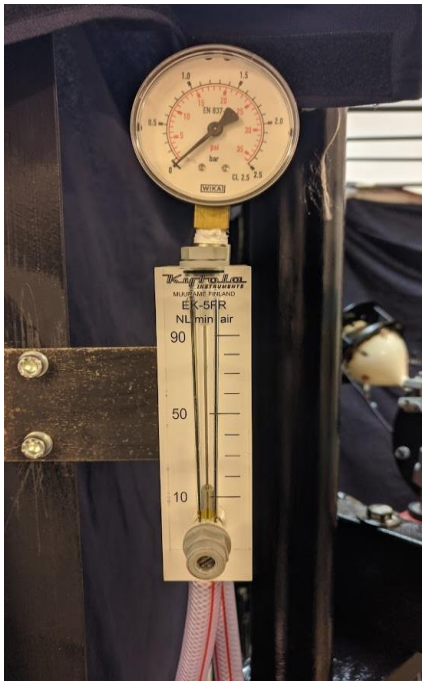


**Figure 2-9:** The air rotameter

### 2.2.6 Mixing tank and smoke generator

The smoke generator is a device that creates a plume using smoke liquid and electric current. During the experiment a **PRO**SOUND 400W compact remote controlled smoke generator with 0.25 L fluid tank (235 mm x 140 mm x 162 mm dimensions), 230 V input power AC, 2000 g weight and a power of 400 W was used. This smoke generator was very useful because it allowed an output of 2500 cubic feet per minute (cfm). In Figure 2-10 the smoke generator can be seen.

In order to create a sufficient mixing tank, a conventional metal container that had the required volume for the smoke generator to fit in, was used. The can had four holes, two of them were drilled in the machinery department of the University and the other two were in the original container. During the

experimental procedure, the original holes were used, one for the incoming air flow, and the other one for the exiting combined air-smoke flow, while the drilled holes were used, one for the power supply cable, and the other one for the connectivity with the Arduino cable. In Figure 2-11 the conventional can (mixing tank) where the smoke generator is located, is depicted. In order for the mixing tank to be operatable, the following actions were made. Firstly, two holes were opened via drilling in the bottom of the container, so the cables can fit in. The drilling of the holes was done very carefully to ensure the minimum space possible between the cable and the hole, so there are no leaks of smoke from the container. Afterwards the smoke generator was placed inside the container, then, the cables inside the two holes were fitted and accordingly the container was closed tightly. Finally, the smoke generator was tested to see if there are any leaks in the container and if the plume is well-combined with the air flow.

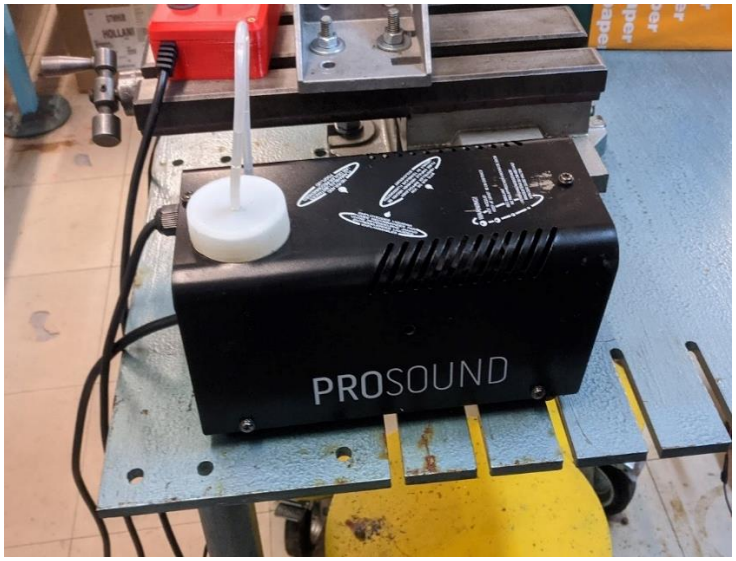


**Figure 2-10:** The smoke generator used to create the plume

**Figure 2-11:** The mixing tank where the smoke generator is placed during the experimental process

### 2.2.7 Arduino microcontroller

During the course of the experiments, an ARDUINO UNO REV3 microcontroller (circuit board) was used. The purpose of this device was to activate the smoke generator and control the frequency of the smoke ejected from the smoke generator. The device could act as a digital pulse generator. The Arduino microcontroller was connected to the smoke generator via the cable that came through a drilled hole in the mixing tank (can). The device was set to eject the smoke every ten seconds. This time value was selected because it allowed to have a better visualization of the outgoing combined air-smoke flow from the jet due to the often renewal of the smoke inside the control volume.

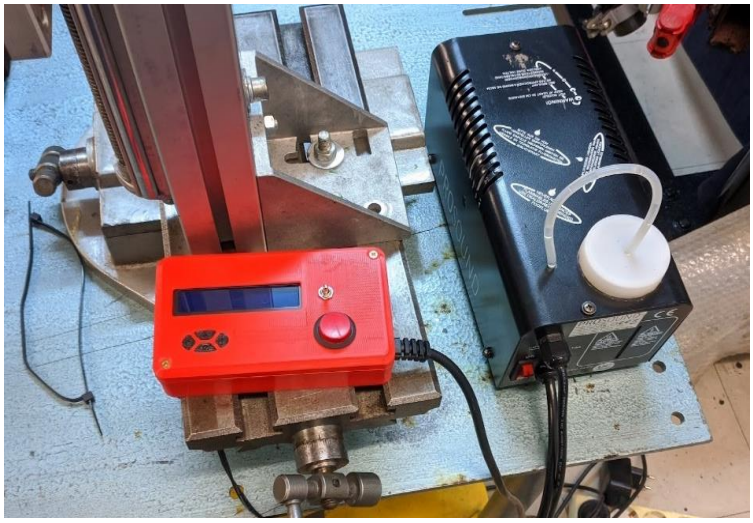

**Figure 2-12:** The Arduino microcontroller-LCD Keypad system connected with the smoke generator

### 2.2.8 The laser beam

The laser beam used was a THORLABS laser module. The model was the CPS532 collimated laser-Diode-Pumped DPSS laser module, which featured wavelengths from 531 nm to 533 nm and provided a total power of 4.5 mW. Furthermore, it has a beam divergence of 5 mrad and operated with 250 mA current and 5 VDC Voltage. It was made of aluminium and had a diameter of 11 mm and length of 72.8 mm. The laser was mounted on a mounting kit, specially designed for this laser module, to have a better stability and visualisation of its beam. Furthermore, in front of the laser a cylindrical lens was placed, in order for the beam to be directly pointed to the flow. The laser's main purpose was to project a green light at the exiting air-smoke flow to have a superior visualization of the flow.

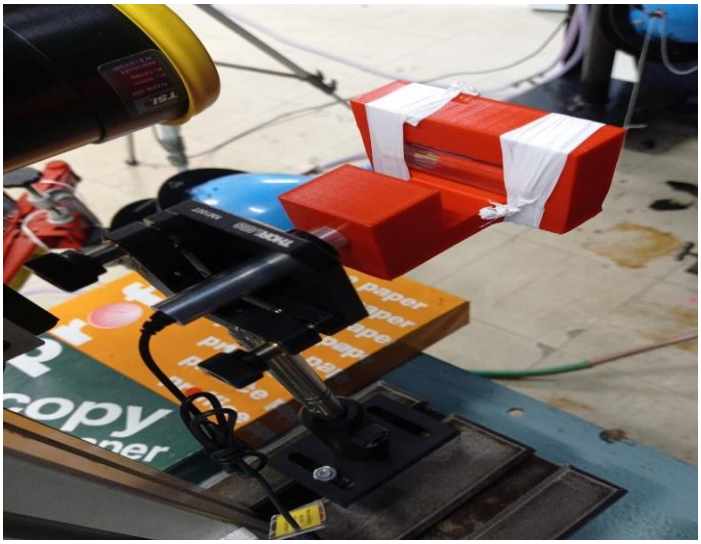


**Figure 2-13:** The laser with the cylindrical lens

### 2.2.9 The camera and the camera software

The camera used in the experiments was a MAKO U-503B, which was suitable for taking a consecutive series of pictures. The camera had a resolution of 2592 (H) x 1944 (V) pixels, pixel size of 2.2µm x 2.2µm and, image buffer (RAM) of 128 Mbyte and, maximum frame rate of 14 fps at full resolution. The camera was placed at the top of a tripod, which was located opposite the jet. The tripod allowed to precisely adjust the height of the camera, to ensure that the camera is exactly at the same height as the exit of the jet. The program used for controlling the camera was Vimba Viewer and it was installed in the laboratory's computer. The program helped with the adjustment of the camera settings, the frequency by which the photos were taken and the properties of the photos, such as, the offset X and Y, the height, and the width. For this experiment the values of 100000 µs for the exposure, 600 for offset Y, 1064 for offset X, 1024 for height and 768 for width, were set. Finally, Mono8 was used as pixel format and acquired 200 photos for each measurement.

**Figure 2-14:** The camera used for image acquisition

## 2.3 Image Processing

After completing the experimental part of the work, the images acquired from the laboratory's camera had to be processed in order for the data that the images provide to be available for interpretation. For this procedure to be completed, the laboratory's software was used. By means of this computer software, the analysis of the images and the construction of the diagrams needed for the current study was made possible. At the start of the process, every set of pictures was loaded to the software and with its assistance, the mean and standard deviation pictures were created for each set of pictures. After that, the mean picture was loaded in the software and used to create the plots needed for the current study. Some mean and standard deviation pictures are presented in the following section.

# 3. Results and Discussion

In this part of the Thesis, the experimental results will be presented, analysed, and discussed. The main interest is to study the interaction of the jet flow with the ambient fluid (air), by examining the tracer's concentration distribution for different jet flow rates in different ambient environments. The main aim is to understand the effect of the external turbulence on the jet development. The experiments were conducted in quiescent and different turbulent environments (Section 2.2), as follows:

- Quiescent ambient environment: The loudspeakers were not in operation.
- Homogeneous and Isotropic Turbulence (HIT): All the eight loudspeakers located in the eight corners of the support structure were in operation and, acting as synthetic jets, they generated the turbulence in the surrounding air. This arrangement is considered to simulate a HIT environment.
- Anisotropic turbulence generated from the right-side loudspeakers, where the mean direction of the external turbulence is perpendicular to the direction of the flow.
- Anisotropic turbulence generated from the left-side loudspeakers, where the mean direction of the external turbulence is perpendicular to the direction of the flow.
- Anisotropic turbulence generated from the upper-side loudspeakers, where the mean direction of the external turbulence is opposite to the direction of the jet flow.
- Anisotropic turbulence generated from the bottom-side loudspeakers, where the mean direction of the external turbulence is the same with the direction of the jet flow.

The experiments were performed by employing different jet flow rates, in each of the above ambient environments, as described in the experimental Part of the Thesis (Section 2.2). The discharge rate of the jet was varied in the range of 10 to 70 l/min, which correspond to Reynolds numbers of 1400 and 9800, respectively. Based on the Reynolds number and relevant literature (see Section 1.3), the discharge flow with Re = 1400 ($Q$ = 10 l/min) is a laminar flow, the discharge flow with Re = 2800 ($Q$ = 20 l/min) is a transitional flow, and the discharge flows with Re = 4200 -9800 (Q = 30 -70 l/min) are turbulent flows.

This part of the Thesis consists of the following sections: (a) Mean and standard deviation pictures, which constitute the basis for the subsequent analysis; (b) Radial profiles of mean concentration, whereby the concentration distribution of the plume in the radial direction is visualized; (c) Centreline profiles of mean concentration, which show the concentration distribution of the plume in the axial-downstream direction; (d) Contour plots of mean concentration, whereby the geometry of the flow and the concentration of the jet along and across the flow could be determined; this Section includes contours in quiescent environment for determining the jet's angle.

## 3.1 Mean and standard deviation pictures

The image processing methodology includes the creation of the mean and standard deviation pictures, which provide the basis for the subsequent analysis. This Subsection presents and discusses the image data obtained for a jet discharge flowrate of 10 l/min ($\mathrm{Re} = 1400$) at all the six ambient conditions under study. The analysis of the data for this (laminar) jet flow is indicative of the analysis performed for the image data obtained with the other jet flows examined (Q = 20-70 l/min, $\mathrm{Re} = 2800 - 9800$).

### 3.1.1 Mean pictures

The main concept of the mean picture is to represent a set of pictures acquired by the camera. Thus, each set of pictures for every measurement is depicted in a mean picture. The brightness of the mean pictures stands for the smoke's concentration in the jet flow and the surrounding fluid. In other words, a bright pixel represents a point where the smoke concentration is high, and a black pixel represents a point of low to zero concentration.

Figure 3-1a depicts an image of the jet being ejected into quiescent environment at a volumetric flowrate of 10 l/min and $\mathrm{Re} = 1400$, which means that the discharge flow is laminar. Figure 3-1b depicts the mean picture of the same flow conditions. In the mean picture one can easily observe that most of the surroundings have a black colour, while the main streamline is very bright. Based on this observation, one can conclude that the jet concentration is low in the surrounding environment, in comparison to the streamwise direction of the jet. This is because the flow is laminar without any external disturbances that can disrupt the jet's original direction and, according to the theory (Brownell and Su, 2004), the diffusion rates in laminar flows are relatively small comparing to the turbulent ones.

a)  b) 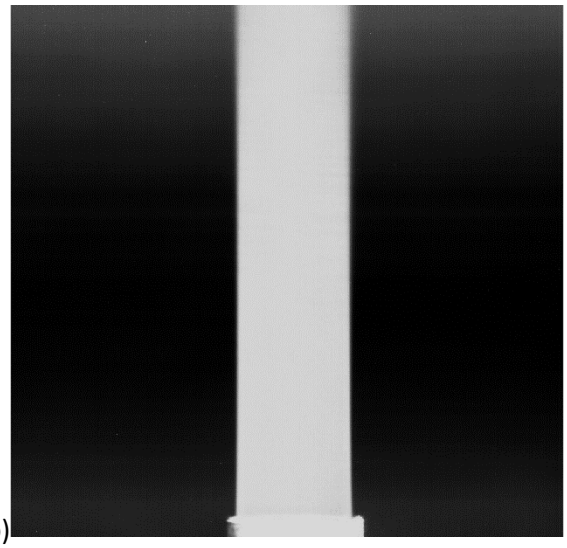

**Figure 3-1:** a) Sample image of the jet flow with $\mathbf{Re = 1400}$ in quiescent environment b) Mean picture

Next, the development of the jet flow in an isotropic turbulent (HIT) environment, as generated by all eight synthetic jets pointed at the orifice, is examined. Figure 3-2 depicts the sample and mean images of the plume in the HIT environment from the jet with a discharge rate of $Q$ = 10 l/min (Re = 1400). These images show that the jet's development is obstructed, apparently due to the external turbulence. The sample image indicates that the laminar discharge flow transitions to a turbulent flow near the jet exit. In the mean picture, one can observe that the brightness in the stream is intense only close to the orifice, and that the brightness in the surroundings is high compared to the previous case. This indicates that the jet diffuses faster in the HIT environment compared to the quiescent environment, presumably due to the increased entrainment rate caused by the external turbulence.

a)  b) 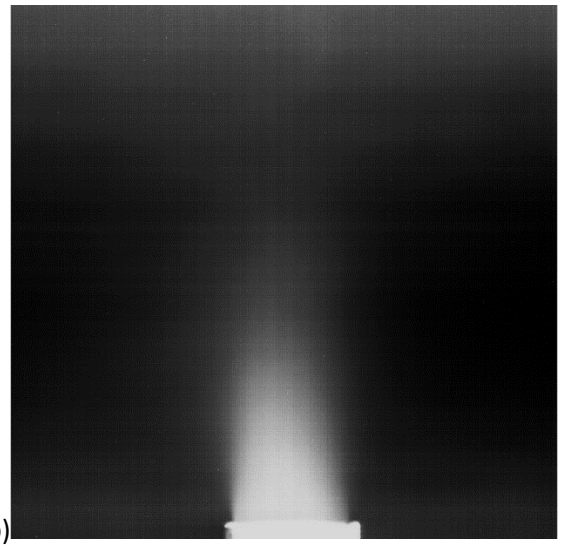

**Figure 3-2:** a) Sample image of the jet flow with $\mathbf{Re} = \mathbf{1400}$ in isotropic turbulent environment (HIT) b) Mean picture

Next, the pictures obtained in anisotropic turbulent environments are examined. These were created when only some of the loudspeakers (synthetic jets) were in operation for generating turbulence, as described previously. In Figure 3-3, the pictures obtained in the case where the turbulence was generated from the left-side loudspeakers, can be seen.

In the pictures presented in Figure 3-3, one can easily see that there is a preferred flow direction; the flow is directed to the right side since the left loudspeakers are the only ones in operation. At the exit of the orifice, one can assume laminar flow, although it quickly transitions to turbulent. The mean picture depicted on Figure 3-3b shows an increased brightness on the right side due to the direction of turbulence, meaning that the jet concentration is higher there.

a)  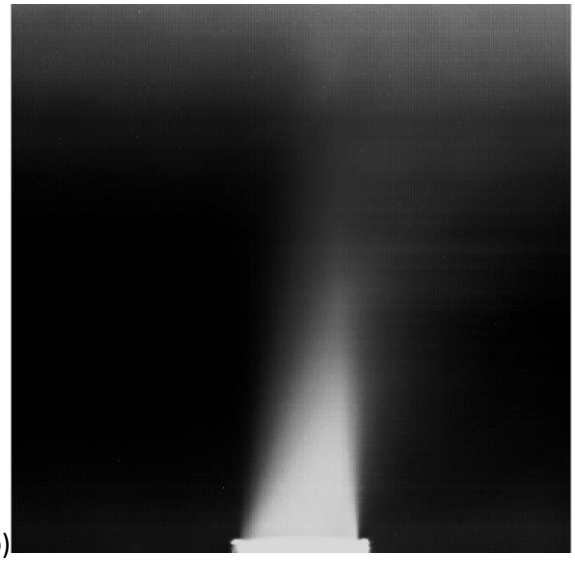 b)

**Figure 3-3:** a) Sample image of the jet flow with $\mathbf{Re} = \mathbf{1400}$ in anisotropic turbulent environment (Left-side loudspeakers) b) Mean picture

In Figure 3-4, the pictures regarding the case in which the turbulence was generated from the right-side loudspeakers can be seen. In this case, the direction of the jet flow is inclined towards the left side in accordance with the mean direction of the external turbulence. Accordingly, the mean picture (depicted in Figure 3-4b) shows an increased brightness on the left side, which means that the jet concentration is higher there. These pictures appear to be 'symmetrical' to the ones obtained in the previous case; this is reasonable as the left-side loudspeakers are placed 'symmetrically' to the right-side ones.

a)  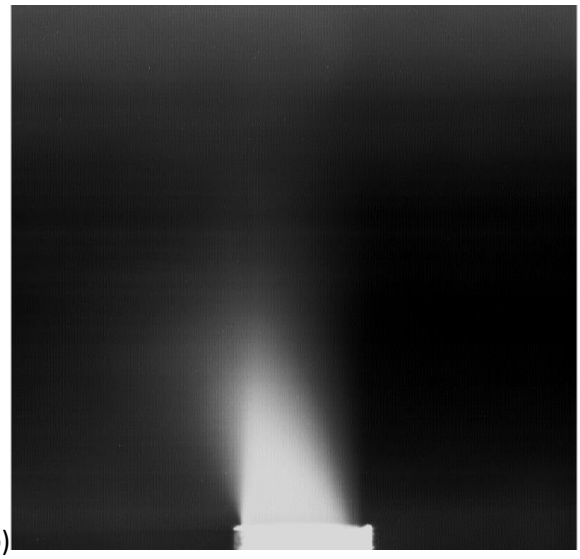 b)

**Figure 3-4:** a) Sample image of the jet flow with $\mathbf{Re} = \mathbf{1400}$ in anisotropic turbulent environment (Right-side loudspeakers) b) Mean picture

In Figure 3-5, the pictures regarding the case in which the external turbulence is generated from the upper side loudspeakers, are depicted. The jet flow development is strongly disrupted by the external turbulence, as evidenced from the suppressed shape of the flow. This is reasonable since the turbulent air flows in an opposite direction from that in which the jet flows. The flow is inhibited and assumes a random motion as soon as it exits the orifice, and, according to the mean picture, the jet is dispersing immediately in the surroundings while its core remains at a small height from the orifice. The jet flow has not a clear preferred direction; the observed small incline to the right is probably due to some of the environmental factors at the time of the experiment or, imperfections in the operation of the loudspeakers (unequal turbulence generation).

a)  b) 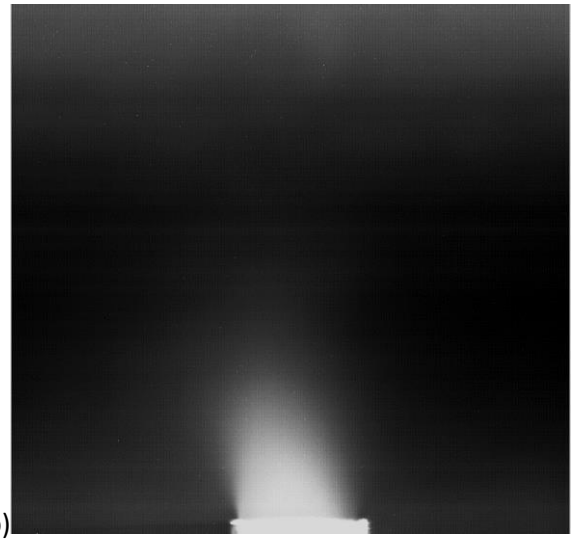

**Figure 3-5:** a) Sample image of the jet flow with $\mathbf{Re} = \mathbf{1400}$ in anisotropic turbulent environment (Upper-side loudspeakers) b) Mean picture

The last case regards the case in which the external turbulence is generated from the bottom side loudspeakers. The sample and mean images for the jet flow of 10 l/min (Re = 1400) are presented in Figure 3-6. Here, the turbulent air has similar direction with the jet flow and thus, the development of the jet flow proceeds unobstructed. As for the jet concentration, this is relatively high (bright pixels) in the direction of the flow and low (dark pixels) in the surrounding environment. The pictures show that, as the smoke ascends, the radius of the plume decreases, presumably due to increased entrainment of turbulent ambient air.

a) 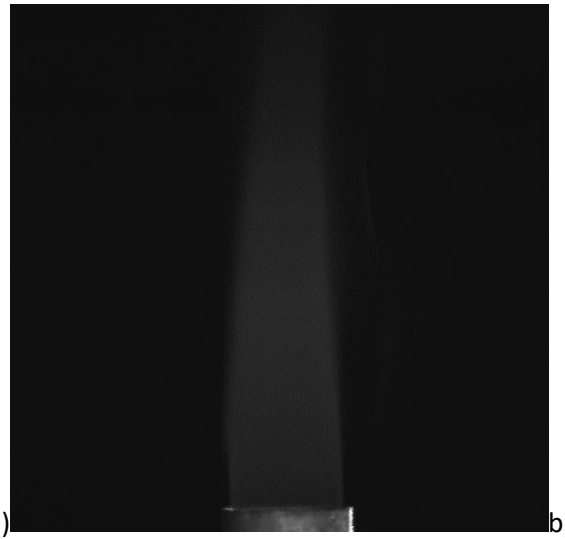 b) 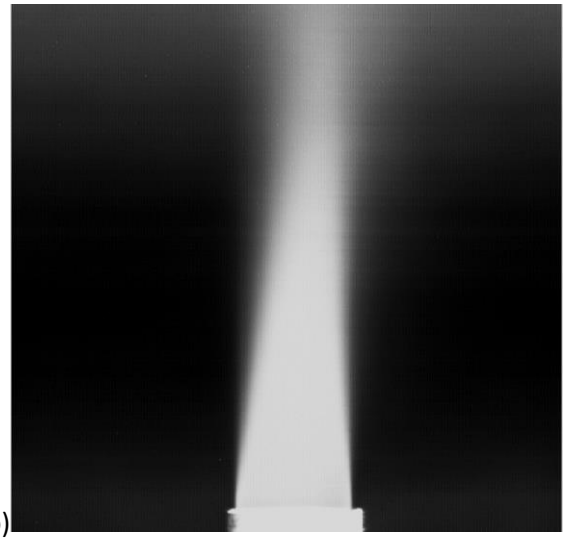

**Figure 3-6:** a) Sample image of the jet flow with $\mathbf{Re} = \mathbf{1400}$ in anisotropic turbulent environment (Bottom-side loudspeakers) b) Mean picture

### 3.1.2 Standard deviation pictures

The standard deviation is a measure of the magnitude of the variation or, dispersion (in a distribution) of a set of values. When a high standard deviation is given, the values are spread in a wider range and have increased unpredictability, in comparison with a low standard deviation, which means that the values are close with one another and tend to be closer to the mean (Bland and Altman, 1996). In this thesis, the standard deviation is depicted in a picture which shows the variation of the smoke concentration in each pixel of the picture. The darker pixels indicate a generally small variation in the value of the jet concentration in that pixel (e.g., a low jet diffusion rate), while the brighter pixels indicate a greater variation in the value of the jet concentration in that pixel (e.g., a high jet diffusion rate).

Following the same order as in the previous subsection, the standard deviation picture obtained for the jet flow of Q= 10 l/min in quiescent environment is analyzed first. This picture is presented in Figure 3-7. The dominant color in this picture is black, presumably due to the little to no disturbances caused by the lack of turbulence in this case. Some brighter pixels can be noticed in the shear layers of the flow with the ambient environment. This can be possibly attributed to the fact that the dissipation rate in these layers is greater and thus, the jet concentration is altering faster there.

a)  b) 

**Figure 3-7:** a) Sample image of the jet flow with $\mathbf{Re} = \mathbf{1400}$ in quiescent environment b) Standard deviation picture

Next, Figure 3-8 presents the pictures obtained in the case where the ambient turbulence was homogenous and isotropic (i.e., it was generated from all loudspeakers).

a)  b) 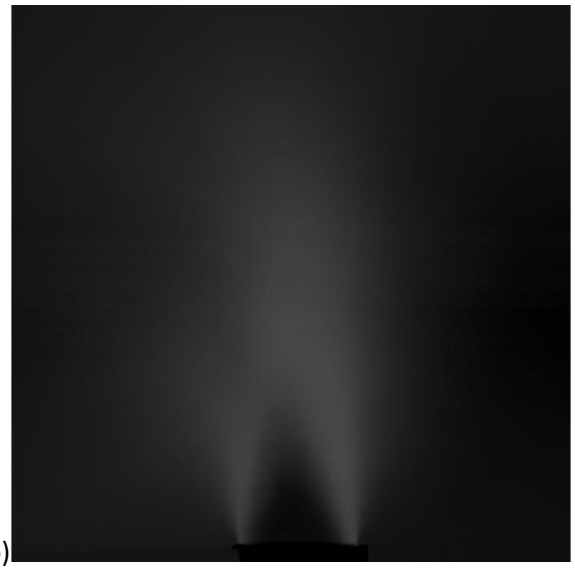

**Figure 3-8:** a) Sample image of the jet flow with $\mathbf{Re} = \mathbf{1400}$ in isotropic turbulent environment (HIT) b) Standard deviation picture

Here, as it can be seen in the mean picture, the dark pixels in the jet flow direction are not as dominant as in the case of quiescent environment. This occurs because the external turbulence significantly disrupts the development of the flow. The external turbulence causes the diffusion rate to increase, resulting in increased variability in the values of the jet concentration (regions with brighter pixels). The region that maintains dark color is the one close to the orifice (i.e., the core of the jet), where apparently the diffusion rate is lower. One can also observe that the pixels in the surroundings are brighter than the respective

pixels in the case of quiescent environment. This indicates that the concentration is changing with time there, due to the diffusion of the jet.

The cases where the ambient turbulence is anisotropic are examined next. Figure 3-9 presents the images obtained in the anisotropic turbulent environment generated from the left-side loudspeakers. Here, the color variation of the pixels follows a similar pattern with the previous case. In other words, the pixels are as follows: a) darker close to the orifice, where the variation of the jet concentration is small, b) brighter in the outer region of the flow, where the jet concentration changes rapidly due to the external turbulence, and c) somewhat bright in the surroundings, apparently due to the increasing jet concentration there. The only significant difference in this case comparing to the previous one, is that the external turbulence is generated from the left-side loudspeakers, which causes the flow to exhibit an incline to the right side.

a)  b) 

**Figure 3-9:** a) Sample image of the jet flow with $\mathbf{Re} = \mathbf{1400}$ in anisotropic turbulent environment (Left-side loudspeakers) b) Standard deviation picture

In Figure 3-10, the pictures obtained in the case where the turbulence is generated from the right-side loudspeakers can be seen. These images appear to be 'symmetrical' to the ones obtained in the previous case. Here, the flow exhibits an incline to the left side since the direction of the external turbulence is towards that side. The distribution of the colored pixels can be interpreted similarly to the previous case.

a)  b) 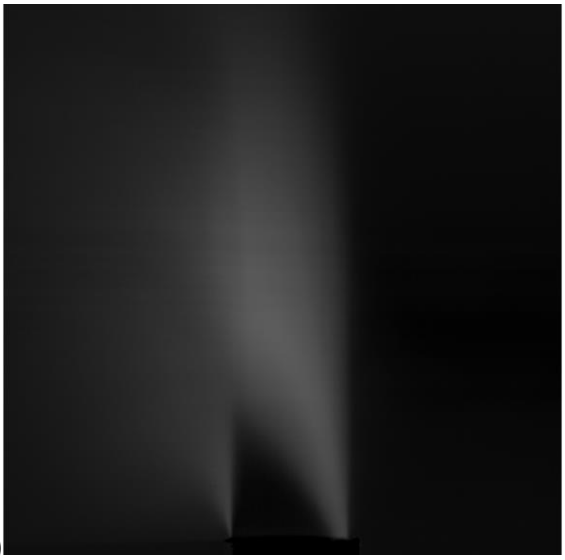

**Figure 3-10:** a) Sample image of the jet flow with $\mathbf{Re} = \mathbf{1400}$ in anisotropic turbulent environment (Right-side loudspeakers) b) Standard deviation picture

In Figure 3-11, the standard deviation picture for the case where the turbulence is generated from the upper-side loudspeakers is shown. One can observe that, the dark region near to the orifice, which corresponds to the core of the jet, is small compared to the previous cases. This indicates that the external turbulence greatly prevents the flow from further developing. Accordingly, one can observe that most of the pixels in the surrounding area have a black color, and the brighter pixels are situated close to the orifice.

a)  b) 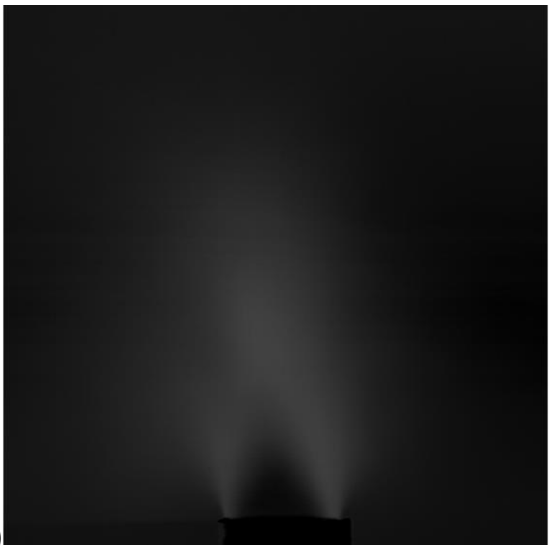

**Figure 3-11:** a) Sample image of the jet flow with $\mathbf{Re} = \mathbf{1400}$ in anisotropic turbulent environment (Upper-side loudspeakers) b) Standard deviation picture

The final case is the one in which the external turbulence is generated from the bottom-side loudspeakers. In Figure 3-12, the relevant images are depicted. Here, the turbulent air has a similar direction with the jet flow and thus, the development of the flow proceeds undisrupted. The deviation is higher (brighter pixels) at the boundaries of the flow with the surroundings, where the jet dissipates faster. The boundary region (brighter pixels) broadens as the jet flow is developing further downstream, presumably due to the increased entrainment of turbulent air. The effect of the external turbulence can be viewed by comparing the current picture with the corresponding one in quiescent environment.

a) 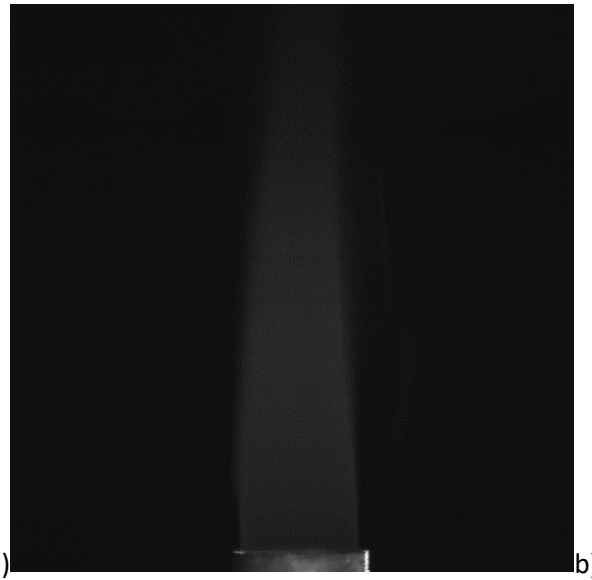 b) 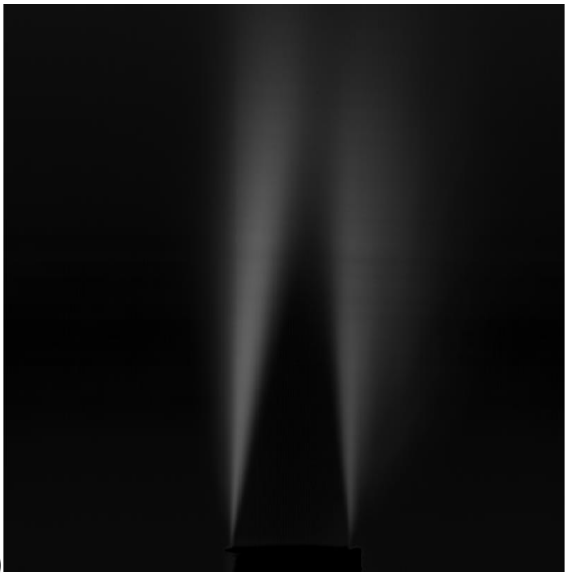

**Figure 3-12:** a) Sample image of the jet flow with $\mathbf{Re} = \mathbf{1400}$ in anisotropic turbulent environment (Bottom-side loudspeakers) b) Standard deviation picture

# 3.2 Mean radial concentration profiles

In this Section, the diagrams depicting the jet concentration distribution in the radial direction will be presented and discussed. The results were obtained in quiescent conditions, isotropic turbulent (HIT) environment and different anisotropic turbulent environments. In each case, the analysis included three types of jet discharge flow, that is, the laminar flow (i.e., $\mathrm{Re} = 1400$), the transitional flow (i.e., $\mathrm{Re} = 2800$), and turbulent flows with $\mathrm{Re} = 4200 - 9800$.

The radial concentration profiles were obtained at axial-downstream distances from the orifice equal to $1D_0$, $2D_0$ and $3D_0$, where $D_0$ is the diameter of the nozzle. The normalized intensity, which is representative of the normalized jet concentration, is presented on the vertical axis. The horizontal axis is the normalized radius $r/r_0$, where $r$ is the radial distance measured from the centre of the jet and $r_0$ is the nozzle radius. In the diagrams, the theoretical Gaussian profiles for turbulent jets in calm environment (see Section 1.3)

are also depicted for comparison; these are normalized with respect to the maximum concentration at the orifice.

### 3.2.1 Radial profiles in quiescent environment

In this Subsection, the radial concentration profiles obtained in quiescent environment are presented and discussed. The analysis starts with the quiescent environment to provide a point for reference and comparison in the subsequent study of the turbulent environments.

First, a laminar jet flow is examined. In Figure 3-13 the radial concentration profiles of the jet flow with $\mathrm{Re} = 1400$ (Q = 10 l/min) discharged into calm surroundings, are depicted. The three profiles, obtained at distances $1D_0$, $2D_0$ and $3D_0$, respectively, are shown with different colours.

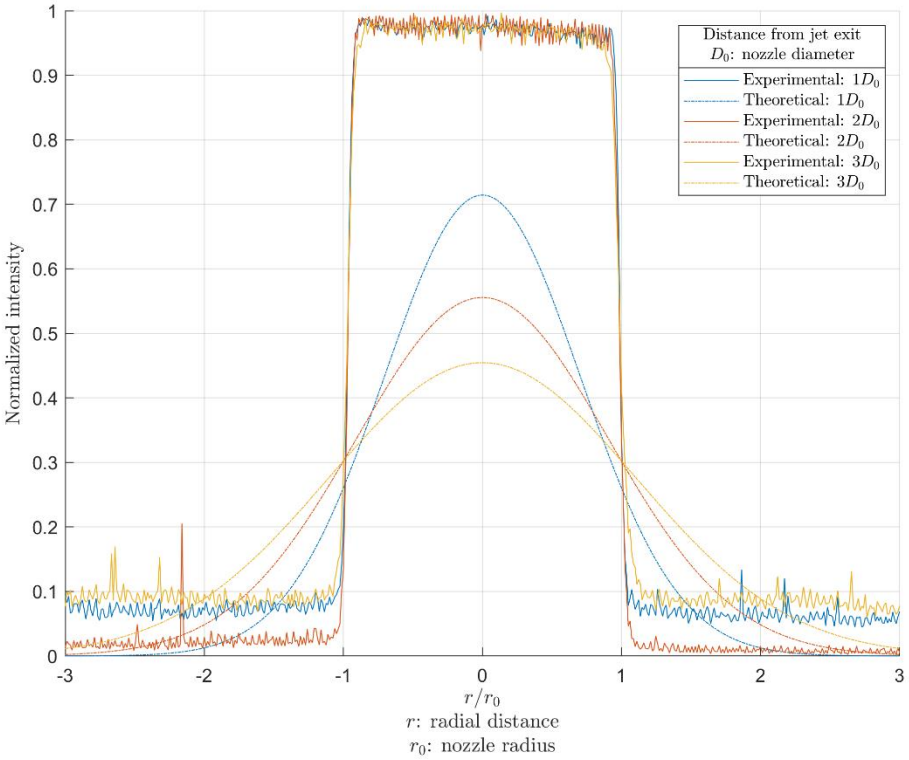


**Figure 3-13:** Radial concentration profile of the jet flow with $\mathbf{Re = 1400}$ in quiescent environment

In this diagram, it can be observed that the three experimental profiles show three identical rectangular-type distributions. Comparing them to the theoretical Gaussian curves, one can observe important differences. First, it can be observed that as the distance from the orifice increases, the peak of the theoretical curves strays further from the maximum value (e.g., the peak at the distance of $3D_0$ is approximately 0.64 of the peak at the distance of $1D_0$), while the peak of the experimental curves remains to the value of one. Furthermore, the experimental curves do not have the bell shape of the theoretical profiles. These differences can be explained by considering that the Gaussian profiles are predicted for

turbulent jets, whereas the experimental profiles were obtained with a laminar jet discharge flow. The laminar jet flow remains unaffected by the external environment till the distance of $3D_0$, presumably due to its low momentum and the low momentum of the calm air in the surroundings.

Next, a transitional jet flow is examined. The transitional flow had a Reynolds number of 2800 that is, a volumetric flow rate of 20 l/min. In Figure 3-14, the radial concentration profile is presented.

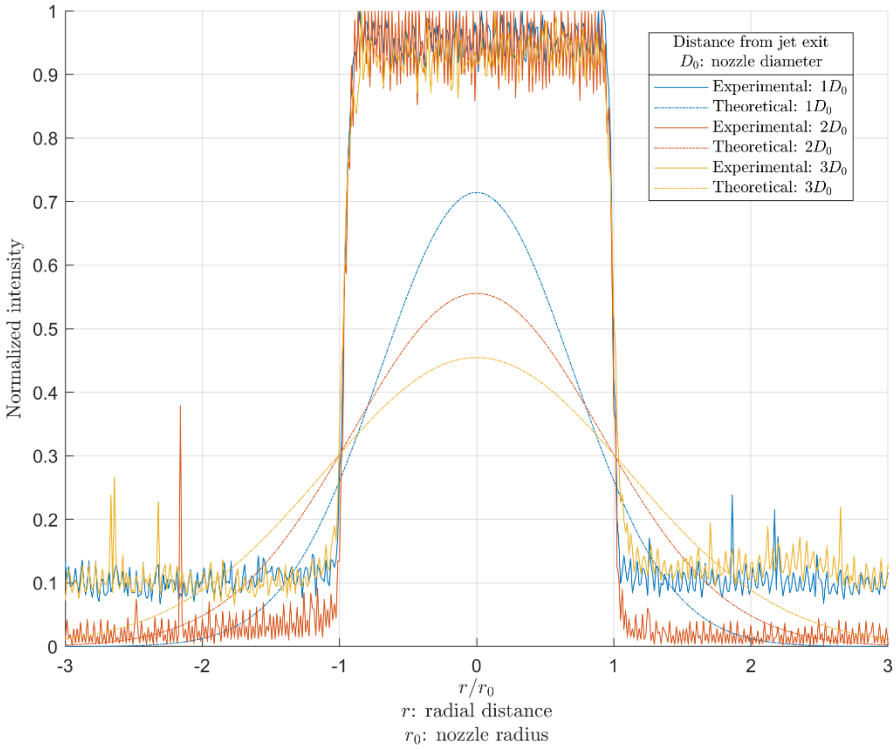


**Figure 3-14:** Radial concentration profile of the jet flow with $\mathbf{Re = 2800}$ in quiescent environment

Observing the previous diagram, one can see that in this case also, the experimental curves do not assume the bell shape of the theoretical profiles, and their peaks have approximately the same value in all three distances presented. This can be attributed to the relatively low momentum of the transitional jet flow in combination with the low momentum of the air in the surroundings (i.e., there are no external disturbances that can disrupt the flow). Therefore, a negligible amount of smoke particles is diffused in the environment, resulting in the jet concentration to maintain a high value for long distances in the streamwise direction.

The next measurement is obtained with an increased Reynolds number that corresponds to a turbulent jet discharge flow. In Figure 3-15 the radial concentration profiles of the jet flow with $\mathrm{Re} = 4200$ (volumetric flow rate of Q=30 l/min) are presented.

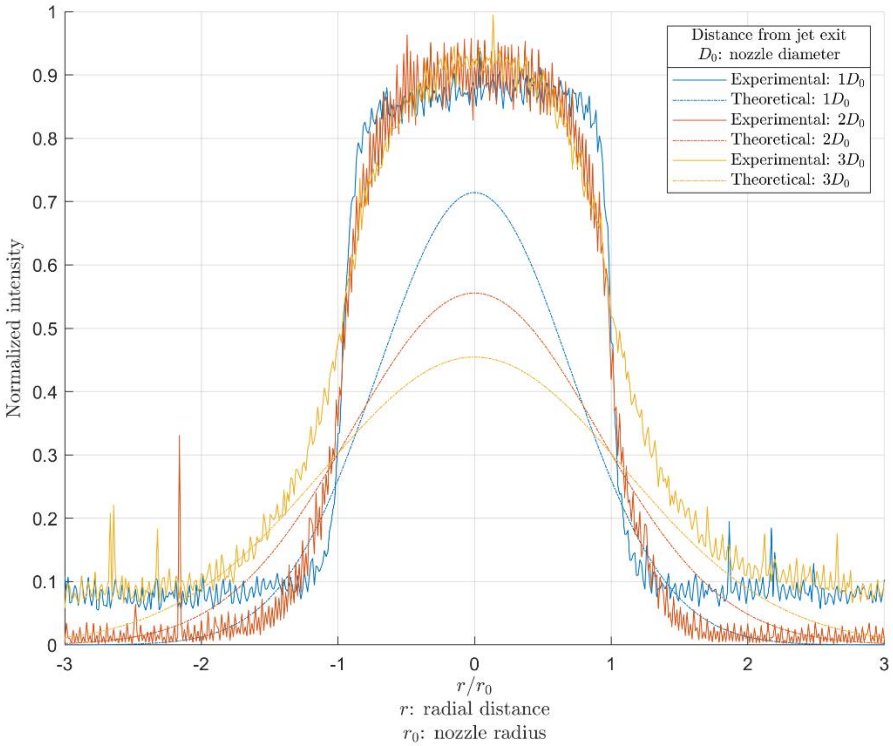


**Figure 3-15:** Radial concentration profile of the jet flow with $\mathbf{Re = 4200}$ in quiescent environment

Here, as it can be seen in the diagram, the experimental curves have taken the bell shape of the theoretical ones and have a similar appearance. This can be attributed to the turbulent nature of the flow, as indicated by the Reynolds number ($\mathrm{Re} = 4200 > 2900$). Importantly however, the three experimental profiles, obtained at the three downstream distances, exhibit slightly different width but practically the same peak, which indicates that the external (quiescent) environment does not affect the flow in the downstream direction.

The next measurement also regards a turbulent flow. Figure 3-16 depicts the radial concentration profiles for the jet discharged at a rate of 50 l/min ($\mathrm{Re} = 7000$) into the quiescent environment.

Here, the three experimental profiles are shown to exhibit bell-type distributions, with different slightly spread but practically the same peak. These appear to be similar with the profiles obtained for the jet flow with Q = 30 l/min ($\mathrm{Re} = 4200$). They are also similar with the radial profiles obtained for other jet flows in the range of 40 – 70 l/min ($\mathrm{Re} = 5600 - 9800$).

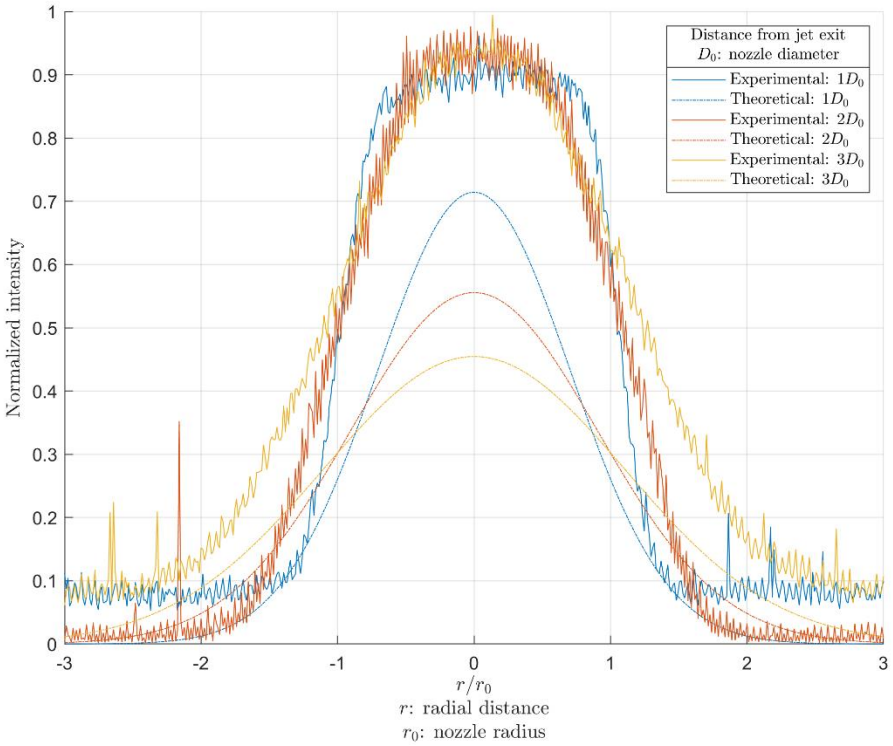


**Figure 3-16:** Radial concentration profile of the jet flow with $\mathbf{Re} = \mathbf{7000}$ in quiescent environment

The findings can be explained with the assistance of the Reynolds number and the relevant literature. When the Reynolds number is greater than 2900, the flow transitions to full turbulent. In turbulent flows the radial profile of mean concentration is closer to the bell shape of the theoretical Gaussian curves, since the flow widens and adopts a conical shape because of the jet turbulence.

In the profiles of the turbulent flows, it was observed that upon increasing the downstream distance from $1D_0$ to $3D_0$, the width of the curve increases but the peak remains practically the same. This may be explained by considering that: (a) the environment is quiescent; thus, the entrainment of the surrounding air and the diffusion of smoke particles have low rates; (b) the concentration of the plume is high and the downstream distance in the experimental procedure may be insufficient for the smoke's particles to be diffused. Furthermore, there could be experimental imperfections. It is noted that smoke could have been trapped on the top of the experimental structure from previous measurements, which might have interfered with the discharge flow and increased the observed jet concentration at the $3D_0$ distance in some measurements.

### 3.2.2 Radial profiles in isotropic turbulent (HIT) environment

In this Subsection, the radial profile diagrams obtained in a homogeneous and isotropic turbulent environment (HIT) are presented and discussed. The ambient turbulence is considered homogeneous and

isotropic (HIT) since it is generated from all eight loudspeakers (synthetic jets) being symmetrically pointed at the orifice.

First, the laminar flow is examined. In Figure 3-17 the radial profiles of mean concentration for the jet flow with $\mathrm{Re} = 1400$ projected into the HIT environment, are depicted.

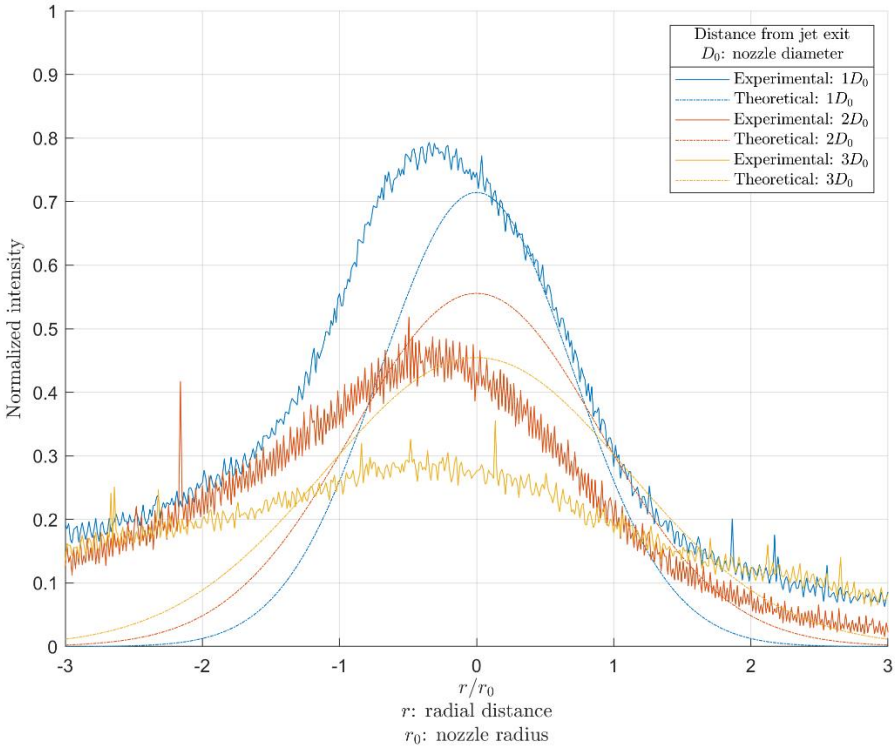


**Figure 3-17:** Radial concentration profile of the jet flow with $\mathbf{Re = 1400}$ in the HIT environment

These profiles differ from the corresponding ones in quiescent environment.The current three experimental profiles exhibit three different unimodal distributions, as opposed to the three identical rectangular-type distributions observed with the same jet flowrate in quiescent environment. The experimental curves have adapted a non-symmetrical bell like shape, that is, a shape closer to the Gaussian profile. This apparently occurs because the current environment is turbulent and thus, the jet's tracer diffusion rate is increased. Furthermore, the peaks of the present profiles are lower, which also indicates that the external turbulence increases the jet diffusion rate. Apparently, the momentum of the external turbulence is higher than the momentum of the laminar jet.

The ambient turbulence under study is assumed to be homogeneous and isotropic providing the same momentum in every direction and thus, a symmetrical shape of the curves is to be expected. The right and left sides of the diagram are however not symmetrical, possibly due to the 'non-steady' operation of some loudspeakers during the experiments. The loudspeakers intended to operate each with the same

power, however small deviations could have occurred during their operation, that is, they did not operate with the same power at all times. Here, the left-side loudspeakers presumably provided somewhat lower power then the right-side loudspeakers.

The next measurement regards the transitional jet flow with $\mathrm{Re} = 2800$ (Q = 20 l/min). Figure 3-18 depicts the radial profiles of mean concentration for this jet flow discharged into the HIT environment.

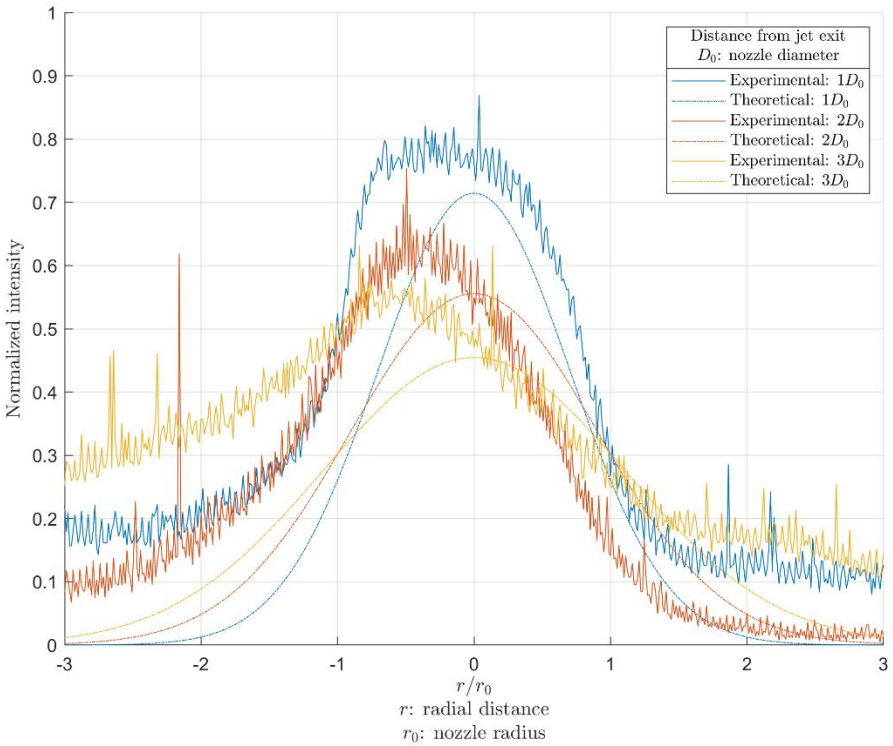


**Figure 3-18:** Radial profile of the jet flow with $\mathbf{Re = 2800}$ in the HIT environment

These radial profiles are similar to the previous laminar flow profiles i.e., the three experimental curves exhibit three unimodal ('asymmetric bell') distributions, apparently due to the external turbulence. The experimental peaks are, however, higher than the 'laminar flow' ones. This can be attributed to the increased flowrate and thus, the increased momentum of the jet. The left and the right side of this diagram are also not symmetrical, possibly also due to the non-steady operation of some loudspeakers, as it was previously explained.

Further analyzing the jet flow interaction with the turbulent surroundings (HIT), the next case is obtained when the flow of the jet is turbulent, in other words the Reynolds number value is greater than 2900. Figure 3-19 depicts the radial profiles of mean concentration for the jet flow with $\mathrm{Re} = 7000$ (Q = 50 l/min).

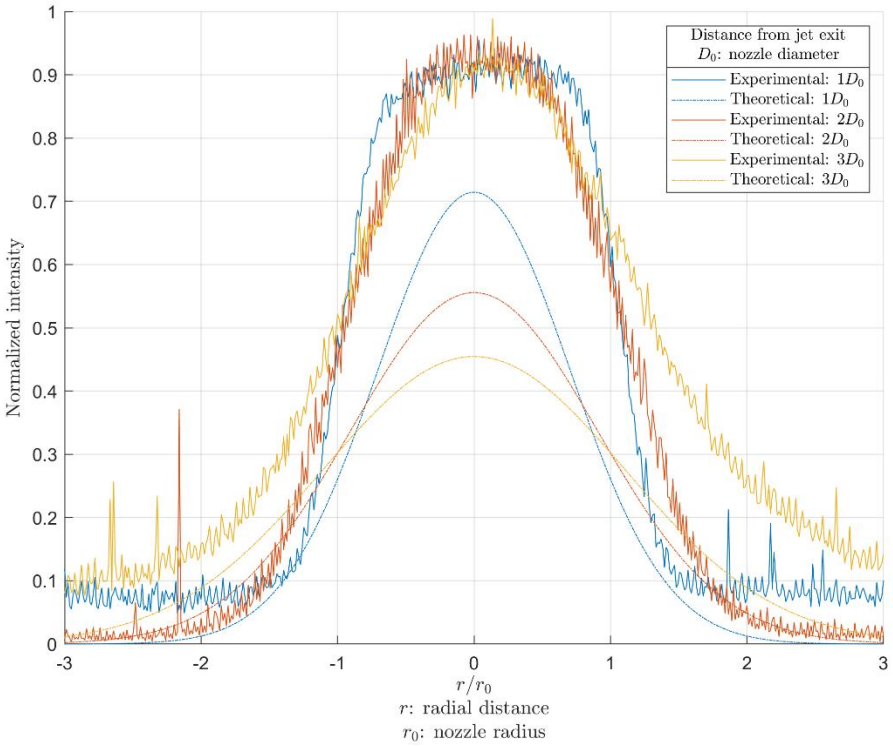


**Figure 3-19:** Radial profile of the jet flow with $\mathbf{Re} = \mathbf{7000}$ in the HIT environment

These profiles are qualitatively similar to the corresponding profiles (i.e., the ones obtained with turbulent jet flows) in quiescent environment, that is: (a) the experimental profiles show bell-type distribution; (b) the width of the curves increases with the downstream distance, but the peak remains the same. It therefore appears that the external turbulence does not affect the radial concentration profiles when the jet flow is turbulent. A turbulent jet flow has high momentum, which apparently cannot be affected by the momentum of the external turbulence. This can also explain the absence of the left-side incline, which it was observed in laminar and transitional flows.

The radial profiles obtained with other jet discharge flowrates in the range of Q = 30 - 70 l/min ($\mathrm{Re} = 4200 - 9800$) are similar to the ones presented in the previous diagram ($\mathrm{Re} = 7000$). This similarity can be attributed to the turbulent nature of these flows.

In brief, one can conclude that the external turbulence (HIT) has a significant effect on the laminar and transitional jet flows (Re ≤ 2800) but not on the turbulent jet flows (Re > 4200), in the range investigated. At low Reynolds numbers, the radial profiles in the HIT environment differ from the ones obtained in calm conditions, as they exhibit unimodal (asymmetric bell-like) and not rectangular distribution; this indicates that the external turbulence enhances the jet diffusion rate. At higher Reynolds numbers, the radial profiles in the HIT environment are qualitatively similar to the ones obtained in calm conditions, indicating that the jet turbulence is higher than the external turbulence.

### 3.2.3 Radial profiles in turbulent environment (Left/Right-side loudspeakers)

In this Subsection the radial concentration profiles obtained in two anisotropic turbulent environments are presented and discussed: (a) the turbulent environment generated from the left-side loudspeakers (b) the turbulent environment generated from the right-side loudspeakers.

Initiating the analysis, Figure 3-20 presents the radial concentration profiles for the laminar jet flow with Re = 1400 (flowrate Q = 10 l/min) discharged into the turbulent environment generated from the left-side loudspeakers.

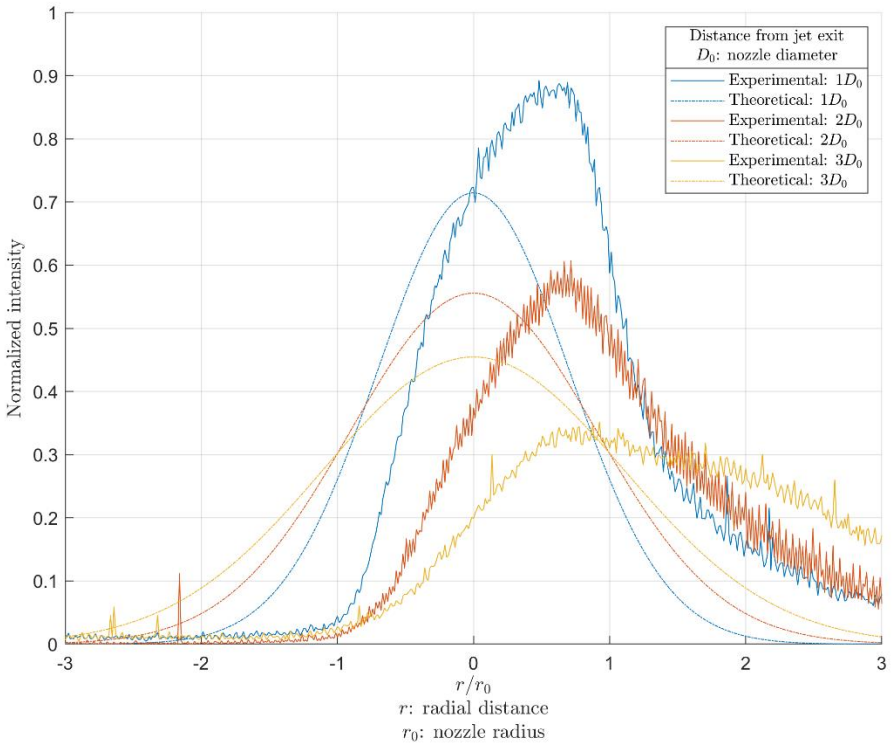


**Figure 3-20:** Radial profile of the jet flow with $\mathbf{Re} = \mathbf{1400}$ in anisotropic turbulent environment (Left-side loudspeakers)

In Figure 3-20, the three experimental profiles are shown to exhibit three unimodal ('asymmetric bell like') distributions, which are not symmetric to the vertical axis *r* = 0 nor other vertical axis, and their peaks are located to the right of the *r* = 0 axis. These profiles are of a type similar to the ones obtained in the HIT environment (Figure 3-17) and they can be interpreted in a similar manner. The external turbulence has higher momentum than the laminar jet and thus, causes the jet diffusion and air entrainment to increase, compared to the calm conditions (Figure 3-13), and accordingly, the profiles adopt a shape closer to the bell shape of the Gaussian profiles (depicted on the diagram).

The significant incline of the curves to the right is attributed to the direction of the external turbulence since this is generated from the left-side loudspeakers; the momentum of the ambient turbulent air is higher than the momentum of jet and alters the jet's original direction. Furthermore, the peaks of the experimental profiles are lower than their 'quiescent conditions' counterparts, presumably due to the external turbulence. These peaks are however higher than the peaks of the corresponding profiles obtained in the HIT environment, which may indicate that the turbulence under study has a less pronounced effect on the jet diffusion than the HIT environment.

Figure 3-21 presents the radial concentration profiles for the laminar jet flow of 10 l/min (Re = 1400) when discharged into the environment generated from the right-side loudspeakers.

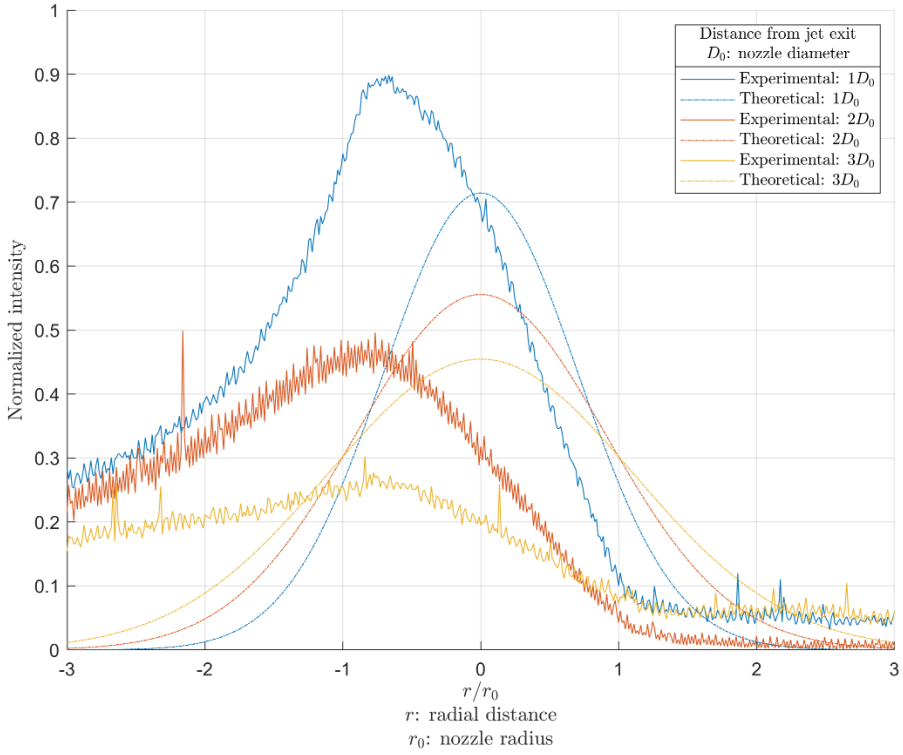


**Figure 3-21:** Radial profile of the jet flow with $\mathbf{Re = 1400}$ in anisotropic turbulent environment (Right-side loudspeakers)

Comparing this diagram with the previous one (Figure 3-20), one can observe that the main difference between them regards the direction of the external turbulence. The experimental curves in this diagram are inclined to the left since the external turbulence is generated from the right-side loudspeakers. These two diagrams appear to be 'symmetrical', which is reasonable as the left-side loudspeakers are placed 'symmetrically' to the right-side ones. Furthermore, these peaks are higher than the peaks of the corresponding profiles obtained in the HIT environment, which may indicate that the turbulence under study has a less pronounced effect on the jet diffusion than the HIT environment.

Continuing the analysis, Figure 3-22 presents the radial profiles of the transitional jet flow with Re = 2800 (discharge rate 20 l/min) discharged into the turbulent environment generated from the left-side loudspeakers.

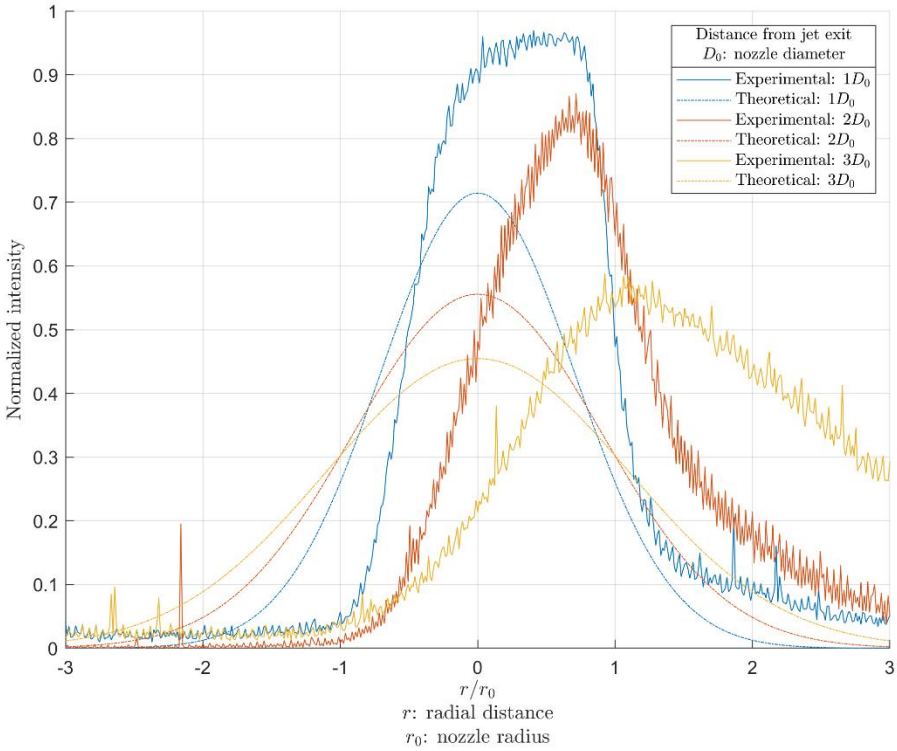


**Figure 3-22:** Radial profile of the jet flow with $\mathbf{Re = 2800}$ in anisotropic turbulent environment (Left-side loudspeakers)

In this plot, one can see that the shape of these experimental curves resembles that of the laminar flow's ($\mathrm{Re} = 1400$), i.e., they are of an 'asymmetric bell like' shape. Accordingly, this can be attributed to the external turbulence, which disrupts the development of the flow; it enhances the jet diffusion and air entrainment, and the curves adapt a shape closer to the bell shape of the Gaussian profiles. The experimental curves are inclined to the right since the turbulence is generated from the left-side loudspeakers. The main difference between this plot and the one of the laminar flow's, regards the peaks of the profiles. Here, the peaks of the experimental curves have comparatively ascended. This can be attributed to the increased momentum of the transitional flow compared to that of the laminar flow.

Continuing the analysis, Figure 3-23 presents the radial profiles for the jet flow with Re = 2800 (discharge rate 20 l/min) discharged into the turbulent environment generated from the right-side loudspeakers.

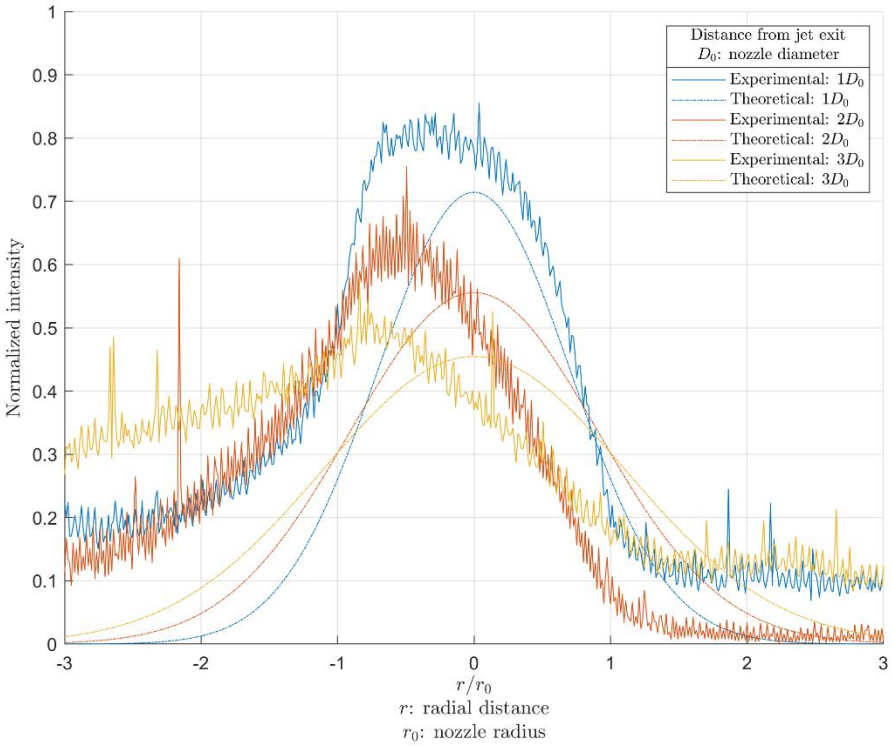


**Figure 3-23:** Radial profile of the jet flow with $\mathbf{Re} = \mathbf{2800}$ in anisotropic turbulent environment (Right-side loudspeakers)

This plot shows that the radial profiles obtained when the turbulence is generated from the right-side loudspeakers are nearly 'symmetrical' to the radial profiles obtained when the turbulence is generated from the left-side loudspeakers (for the same jet flowrate). Here, the curves are inclined to the left since the turbulence is generated from the right-side loudspeakers (whereas the corresponding curves were inclined to the right since the turbulence was generated from the left-side loudspeakers). However, one can observe that the peaks of the current experimental curves are lower, compared to their left-side counterparts. This effect can be attributed to the operational imperfections of the loudspeakers, i.e., the power provided by the right-side loudspeakers exceeded that of the left-side ones in these measurements.

Finally, a turbulent jet flow is examined. Figure 3-24 depicts the radial concentration profiles for the jet discharged with a rate of 60 l/min ($\mathrm{Re} = 8400$) into the turbulent environment generated from the left-side loudspeakers.

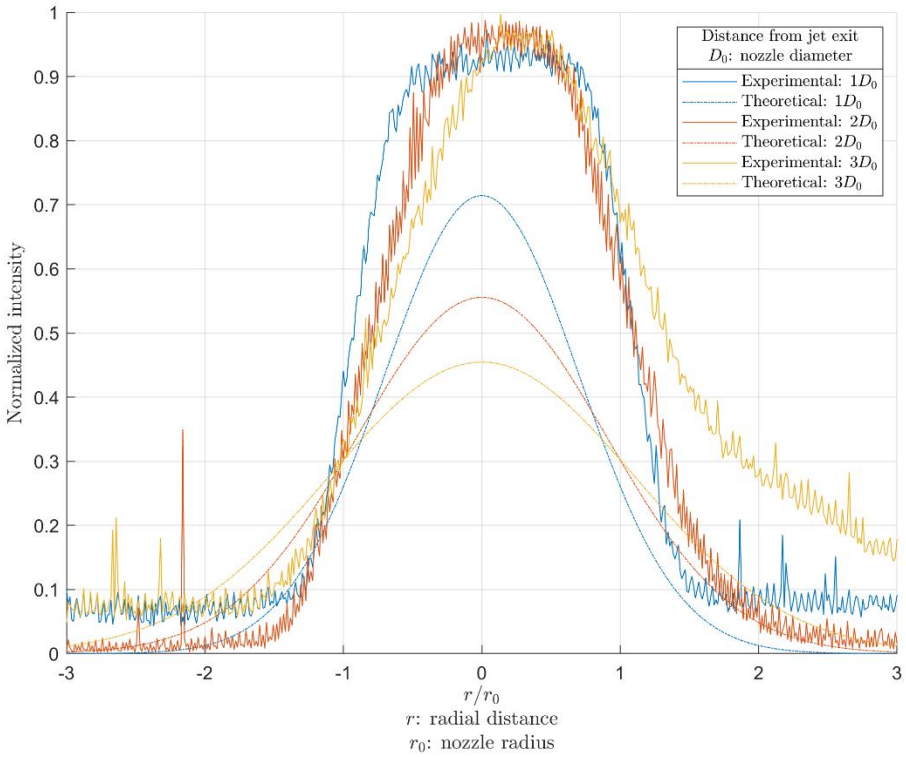


**Figure 3-24:** Radial profile of the jet flow with $\mathbf{Re} = \mathbf{8400}$ in anisotropic turbulent environment (Left-side loudspeakers)

In Figure 3-24, the experimental profiles are shown to exhibit bell-type distributions, in which the width may increase with the downstream distance, but the peak remains the same. These profiles are qualitatively similar to the ones obtained with turbulent jet flows in the quiescent environment (Figure 3-16). It therefore appears that the external turbulence does not affect the radial concentration profiles when the jet flow is turbulent. A turbulent jet flow has high momentum, which apparently cannot be affected by the momentum of the external turbulence. This can also explain the 'relative symmetry' of these profiles (in laminar and transitional flows the curves were leaning clearly to one side since their momentum is relatively low and it can be affected by the momentum of the external turbulence).

Figure 3-25 presents the radial concentration profiles for the above jet flowrate of 60 l/min (Re= 8400) when projected into the turbulent environment generated from the right-side loudspeakers.

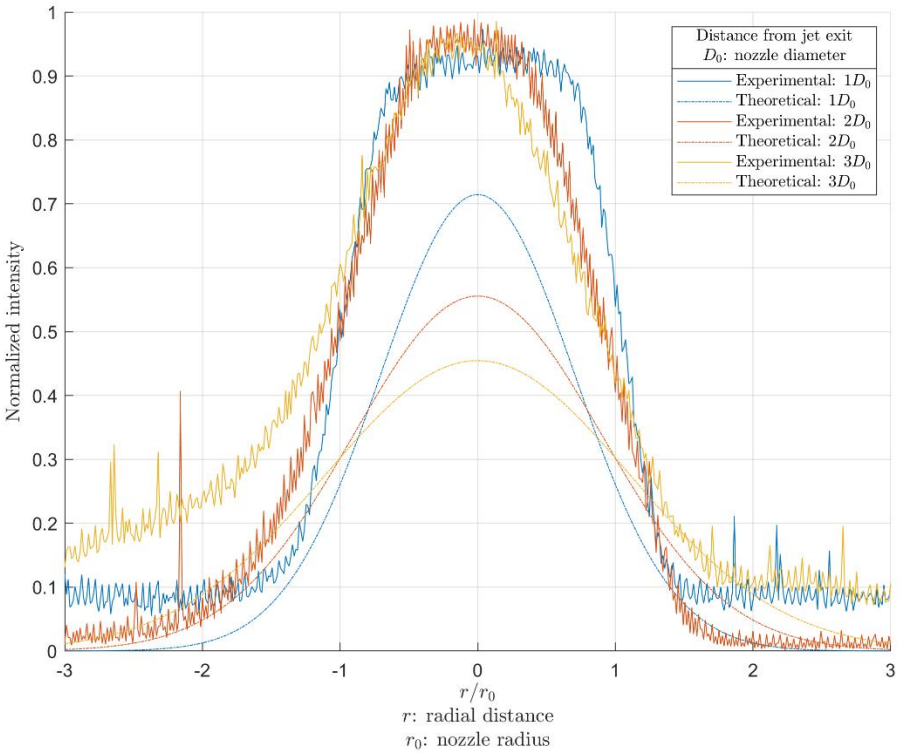


**Figure 3-25:** Radial profile of the jet flow with $\mathbf{Re = 8400}$ in anisotropic turbulent environment (Right-side loudspeakers)

Here, as far as the shape of the curves are concerned, the explanations are the same as with the case where the turbulence is generated from the left-side loudspeakers. The experimental curves are almost symmetrical and a possible small incline to the left side, can be explained by considering that the turbulence in this case is generated from the right-side loudspeakers.

The radial profiles obtained with other jet discharge flowrates in the range of Q = 30 – 70 l/min ($\mathrm{Re} = 4200 - 9800$) in the two anisotropic environments under study, are similar to the respective profiles presented in the previous two diagrams. This similarity is attributed to the turbulent nature of the flow.

### 3.2.4 Radial profiles in turbulent environment (Upper-side loudspeakers)

In this Subsection the radial concentration profiles obtained in a different anisotropic turbulent environment are presented and discussed. Here, the ambient turbulence is generated from the upper-side loudspeakers, as it was described in the experimental setup Subsection.

First, the laminar jet flow is examined. The laminar jet flow has a Reynolds number of $\mathrm{Re} = 1400$ and a volumetric flow rate of 10 l/min. Figure 3-26 depicts the radial concentration profile of this flow.

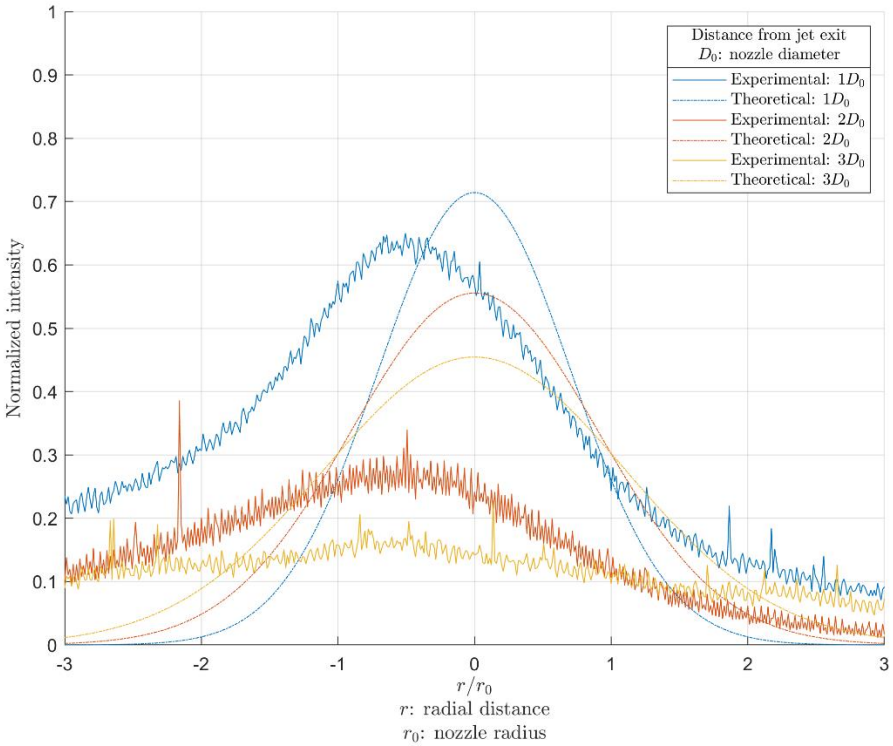


**Figure 3-26:** Radial profile of the jet flow with $\mathbf{Re} = \mathbf{1400}$ in anisotropic turbulent environment (Upper-side loudspeakers)

Examining the plot, one can see that the peaks of the experimental curves differ significantly from their 'quiescent conditions' counterparts, e.g., the peak of the normalized intensity is approximately 0.65 at the distance of $1D_0$ from the orifice. This can be attributed to the direction of the external turbulence, which is generated from the upper-side loudspeakers thus, it inhibits the flow exiting the orifice and disrupts its original course, resulting in the quickened diffusion of the plume's particles in the environment.

The experimental profiles are shown to exhibit asymmetric bell-like distributions. This shape is taken by the curves because of the external turbulence, which causes the jet diffusion to increase, as explained in the previous Subsections. The lack of symmetry between the two sides of the experimental curves can be attributed to the operational imperfections of the loudspeakers, as described previously. In this case, as it appears from the diagram, the two loudspeakers in the upper-right-side of the support structure operated with greater power than their upper-left-side counterparts

Next, the transitional jet flow with a Reynolds number of $\mathrm{Re} = 2800$ (discharge rate of 20 l/min) is examined. The following Figure 3-27 depicts the relevant radial profile of mean concentration.

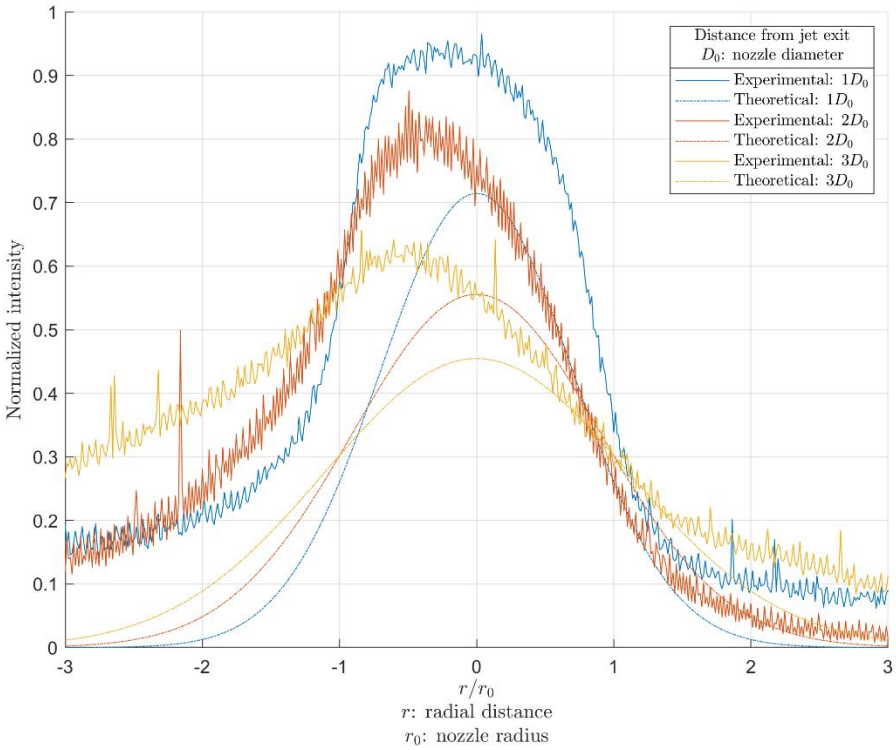


**Figure 3-27:** Radial profile of the jet flow with $\mathbf{Re = 2800}$ in anisotropic turbulent environment (Upper-side loudspeakers)

These radial profiles are also shown to exhibit unimodal 'asymmetric bell-like' distributions, as the laminar jet profiles. Here however, one can observe that the peaks of the experimental curves are higher, and the shape of the profiles appear to approach closer to the bell-shape of the Gaussian curves. This could be related to the increased momentum of this transitional jet compared to the momentum of the laminar jet, and thus the decreased impact of the external turbulence. The lack of symmetry of these curves may be also related to the operational imperfections of the loudspeakers, as it was previously explained with the laminar flow. The incline to the left is however less pronounced since the momentum of the transitional jet is higher than that of the laminar flow.

Next, a turbulent flow is examined. In Figure 3-28 the radial profiles of mean concentration for the turbulent flow with $\mathrm{Re} = 8400$ (Q = 60 l/min) can be seen. The radial profiles of the other turbulent flows ($\mathrm{Re} = 4200 - 9800$) were similar to the profiles presented in this diagram.

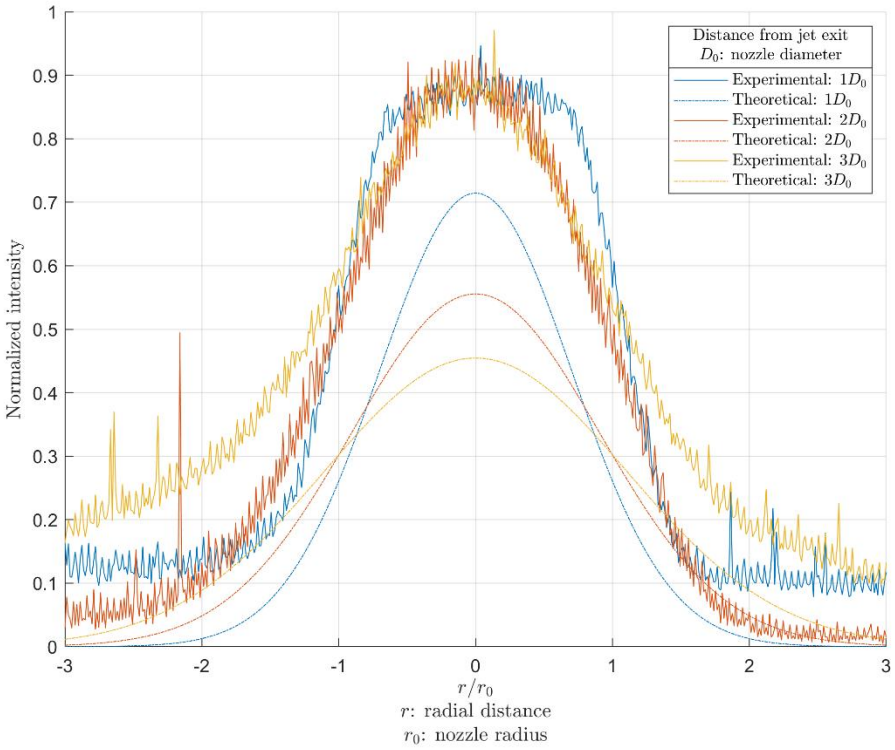


**Figure 3-28:** Radial profile of the jet flow with $\mathbf{Re = 8400}$ in anisotropic turbulent environment (Upper-side loudspeakers)

As far this diagram is concerned, the experimental curves have taken the bell shape; the width may increase with the downstream distance, but the peak remains the same. This is due to the turbulent nature of the flow, as explained in the previous Subsections. The turbulent jet flow has high momentum, compared to the laminar and transitional flows, which apparently cannot be affected by the inferior momentum of the external turbulence. Therefore, the curves adopt symmetrical bell shape profiles, in contrast to the asymmetric profiles obtained with the laminar and the transitional flows, and the jet concentration maintains high values for greater distances downstream.

### 3.2.5 Radial profiles in turbulent environment (Bottom-side loudspeakers)

In this Subsection the radial concentration profiles obtained in another anisotropic turbulent environment are presented and discussed. This anisotropic environment was generated by the bottom-side loudspeakers, as described in the experimental section.

First, the laminar jet flow with Reynolds number $\mathrm{Re} = 1400$ (volumetric flow rate Q=10 l/min) is examined. Figure 3-29 depicts the radial profile of mean concentration for the previous flow discharged into the anisotropic turbulent environment under study.

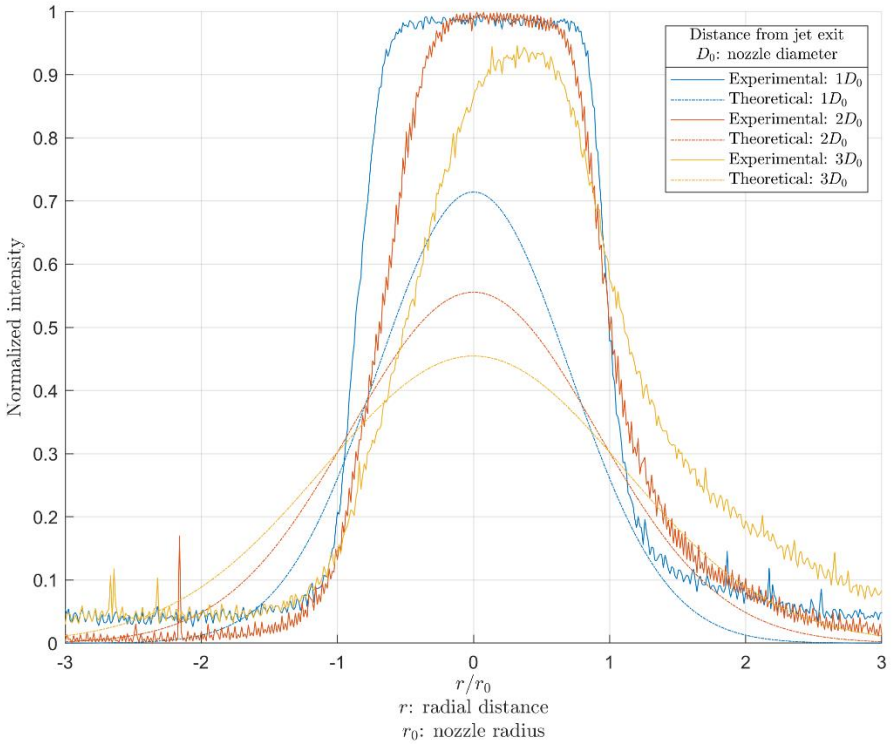


**Figure 3-29:** Radial profile of the jet flow with $\mathbf{Re} = \mathbf{1400}$ in anisotropic turbulent environment (Bottom-side loudspeakers)

This diagram shows that the profiles at distances of $1D_0$ and $2D_0$ resemble more the rectangular-type profiles obtained in quiescent environment (Figure 3-13) rather than the asymmetric bell-like profiles obtained in turbulent environments, with the same jet flowrate. The ambient turbulence under study appears not to significantly affect the jet diffusion. This takes place because of the location of the bottom loudspeakers compared to the upper loudspeakers. The external turbulence is not opposing the jet discharge flow, resulting in smaller obstructions in the flow's development. As the distance from the orifice increases, the flow becomes more susceptible to external disturbances; this could explain the bell shape of the curve representing the $3D_0$ distance.

Furthermore, the peaks of the experimental curves are high, which can also be attributed to the small diffusion rates of the smoke particles contained in the jet flow due to the small external disturbances. As it can be seen in the diagram, the normalized concentration is 1 at the distances of $1D_0$ and $2D_0$ and remains close to 1 at the distance of $3D_0$; a similar pattern was observed only in the case of the quiescent environment (Figure 3-13). The asymmetry of the curve representing the $3D_0$ distance can be attributed to the operational imperfections of the loudspeakers. The flow at this distance is more susceptible to external disturbances and thus, it shows an incline to the right. The non-perfectly steady operation of the loudspeakers has been discussed in detail previously. In this case the loudspeakers on the left part of the bottom side may have operated with increased power.

Next, the transitional jet flow with Reynolds number of $\mathrm{Re} = 2800$ and a discharge rate of Q= 20 l/min, is examined. Figure 3-30 depicts the relevant radial profile of mean concentration for this jet flow when discharged into the anisotropic turbulent environment under study.

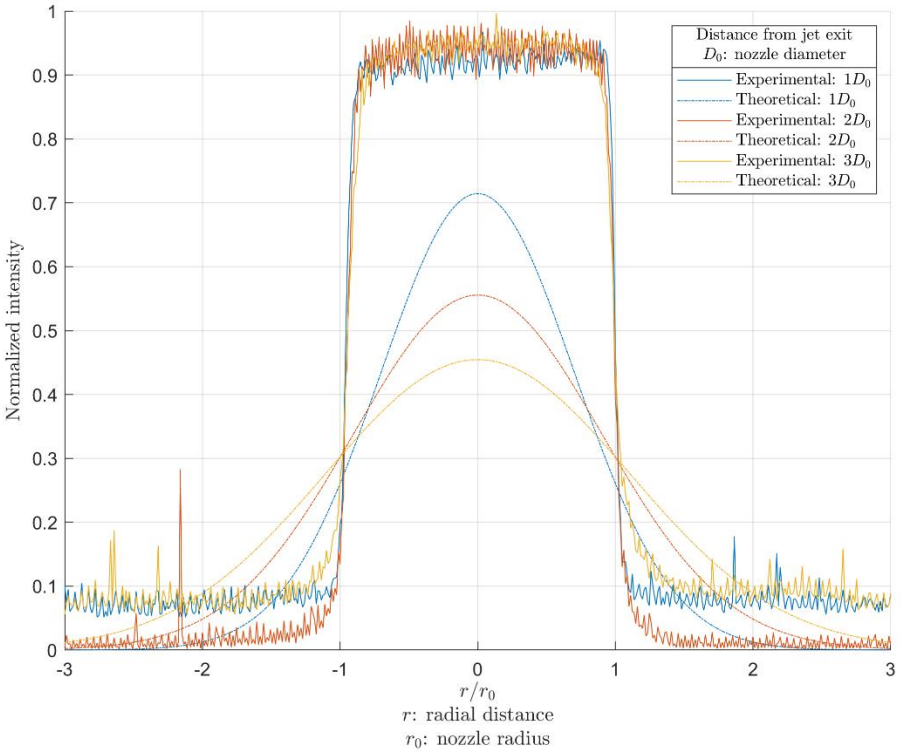


**Figure 3-30:** Radial profile of the jet flow with $\mathbf{Re = 2800}$ in anisotropic turbulent environment (Bottom-side loudspeakers)

This diagram shows that the three experimental profiles exhibit three identical rectangular-type distributions, i.e., the concentration along and across the jet is constant, up to the distance studied. These profiles are similar with the corresponding profiles in quiescent environment and different from the corresponding profiles in the other turbulent environments investigated. They indicate that the jet remains unaffected by the external turbulence under study, up to the 3-diameter distance from the orifice. This pattern is presumably related to (a) the location of the loudspeakers producing the ambient turbulence, i.e., they are pointed to a direction which does not interfere significantly with the jet discharge flow and its initial development (b) the increased momentum of the transitional flow compared to the laminar flow, which apparently exceeded the momentum of the external turbulence, thus making the external turbulence unable to disrupt the development of the jet flow.

Lastly, a turbulent flow is examined. Figure 3-31 shows the radial profile of mean concentration for the turbulent jet flow with $\mathrm{Re} = 8400$ (volumetric flow rate Q=60 l/min) discharged into the turbulent environment generated from the bottom loudspeakers. The profiles obtained with other turbulent jet

flows with Reynolds number in the range of Re = 4200 – 9800 (Q = 30-70 l/min) are similar to the profiles presented in the current diagram.

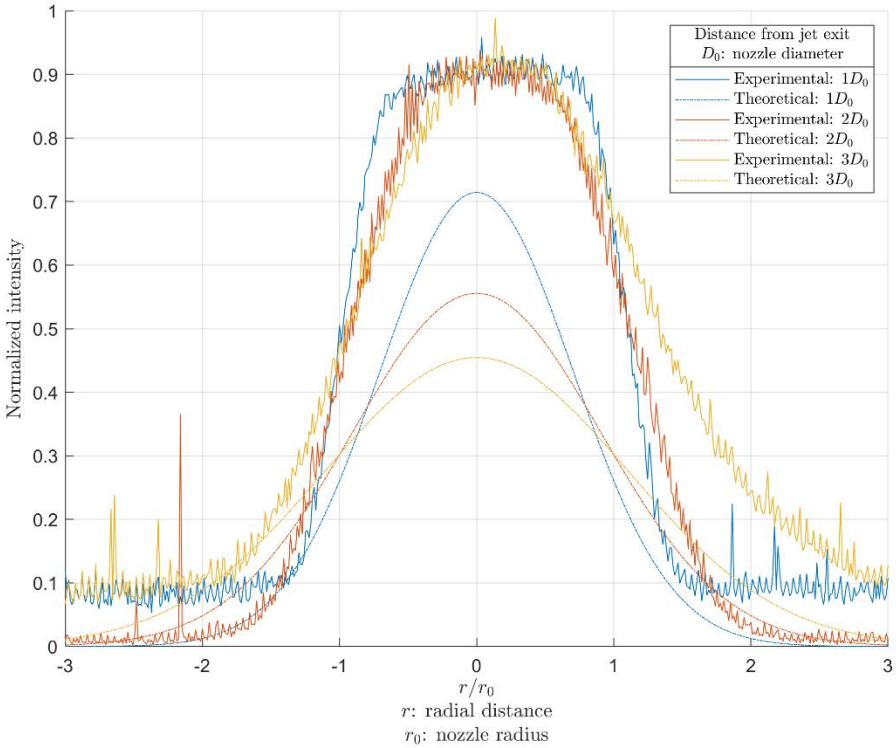


**Figure 3-31:** Radial profile of the jet flow with $\mathbf{Re = 8400}$ in anisotropic turbulent environment (Bottom-side loudspeakers)

This plot shows that the three profiles have adopted the bell-type distributions, in which the width may increase with the downstream distance, but the peak remains the same. These profiles are qualitatively similar to the profiles obtained with turbulent flows in calm conditions and the other turbulent environments examined. They can accordingly be explained by considering that turbulent flows have high momentum which cannot be affected by the momentum of the external turbulence in the conditions investigated.

## 3.3 Mean centerline concentration profiles

In this Section the diagrams depicting the evolution of the mean centerline concentration with the axial-downstream distance are presented and discussed. The results were obtained in quiescent environment and isotropic turbulent (HIT) ambient conditions. The cases of anisotropic turbulent environment are not examined here since, in most of them, the direction of the flow deviates significantly from the vertical axis. In each case, the analysis included three types of jet discharge flow, that is, the laminar flow (i.e., Re = 1400), the transitional flow (i.e., Re = 2800), and turbulent flows with Re = 4200 – 9800.

The mean centerline concentration profiles describe the evolution of the jet concentration along the centerline of the jet. In the diagrams presented in this section, the normalized intensity in the center of the jet (vertical axis) is plotted against the normalized axial-downstream distance (horizontal axis). The former is a measure of the smoke concentration as depicted in the mean pictures and described in the relevant section. The latter is given by the ratio $x/D_0$, where $x$ is the axial-downstream distance measured from the orifice, and $D_0$ is the nozzle diameter. In the diagrams, the theoretical profiles are also depicted for comparison; these are derived from the Gaussian model for turbulent jets in calm conditions (see Section 1.3).

### 3.3.1 Centerline profiles in quiescent environment

The analysis of the centerline concentration profiles initiates with the measurements obtained in quiescent environment. The flow's interaction with the quiescent environment is simpler to visualize.

The first type of flow to be examined is the laminar flow. The properties of the laminar flow used for the measurements are $\mathrm{Re} = 1400$ (Q =10 l/min). In Figure 3-32 the mean centerline concentration profile for this flow is depicted. This plot shows that the theoretical mean centerline concentration of the plume emitted from the jet in a quiescent environment is decreasing with the axial distance. However, the line derived from the experimental procedure seems to follow a different pattern. The experimental line has approximately the constant value of unity along the axial-downstream direction up to the 3-diameter distance examined. This difference can be attributed to the low momentum of the laminar flow in combination with the low momentum of the calm ambient air. First, the theoretical equations are derived for turbulent jets and thus, it is reasonable that they do not properly describe the present laminar jet. Furthermore, due to the quiescent environment, the laminar flow is being allowed to develop for further distances downstream uninterrupted, thus the smoke's particles contained in the flow are carried for longer distances too. The current profile is consistent with corresponding radial profile, which also suggests that the flow is not affected from the external environment up to the downstream distance examined.

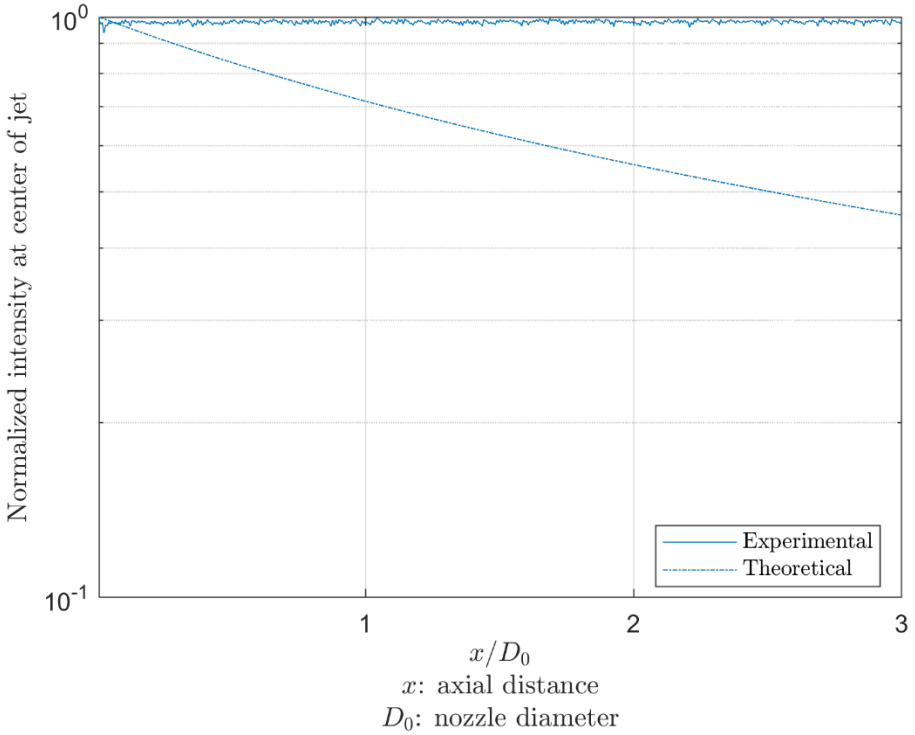


**Figure 3-32:** Mean centerline concentration profile of the jet flow with $\mathbf{Re = 1400}$ in quiescent environment

The next type of flow to be examined is the transitional flow. In the experimental procedure the transitional flow used had the properties of $\mathrm{Re} = 2800$ and Q=20 l/min. In Figure 3-33 this flow's centerline concentration profile is depicted. This plot portrays the jet concentration in the axial streamwise direction along with the theoretical line. The experimental line shows that the jet concentration decreases slightly at a very small distance close to the orifice, and then it remains constant at a value of about 0.93 up to the distance examined. The present experimental line has a strong resemblance to the experimental line of the laminar flow. This resemblance can be similarly attributed to the Reynolds number of the flow and the quiescent surrounding environment. The Reynolds number indicates a transitional flow, which does not provide sufficient momentum for the jet to be diffused in the ambient environment up to the distance examined. This is also enhanced by the quiescent surrounding environment, which does not provide any obstructions. Therefore, the flow is allowed to develop without any disruption from external factors.

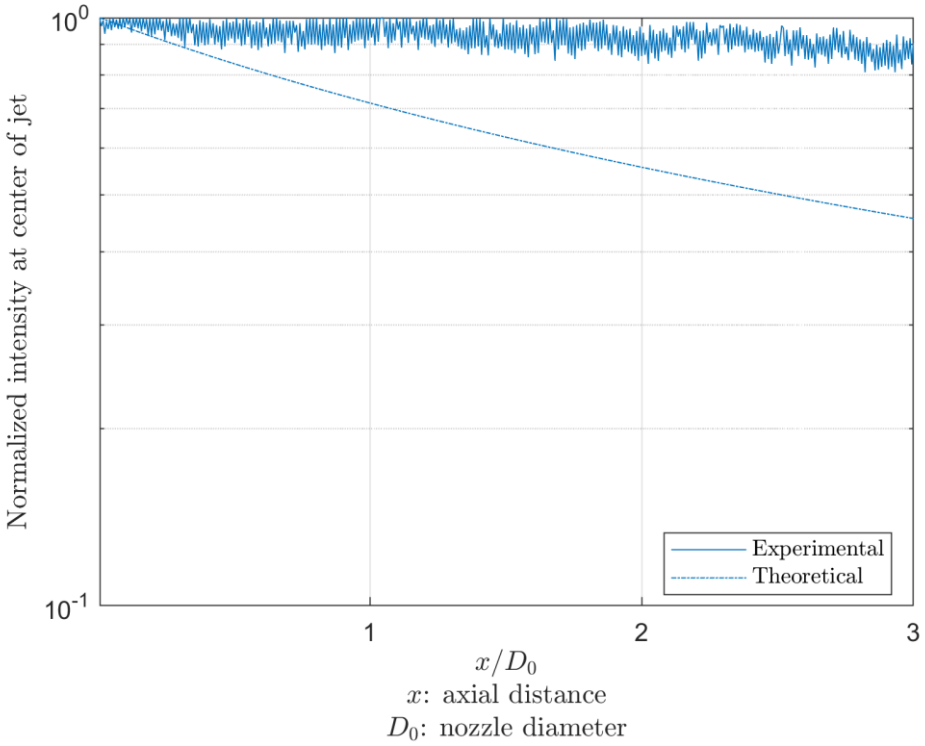


**Figure 3-33:** Mean centerline concentration profile of the jet flow with $\mathbf{Re = 2800}$ in quiescent environment

The next type of flow to be examined in this Subsection is the turbulent flow with $\mathrm{Re} = 7000$ and Q=50 l/min. In Figure 3-34 the jet concentration devolution in the streamwise direction is depicted. Examining this plot, one can clearly see that the experimental line differs from the theoretical line, in a way that resembles their counterparts in the laminar and transitional flows. In the current case, the normalized jet concentration starts with a value of unity and decreases at a very slow rate, till it reaches a value of approximately 0.9. This effect can be attributed to the quiescent ambient environment, which does not provide sufficient momentum to disrupt the development of the jet flow, thus keeping the jet concentration almost constant along the centerline up to the distance studied. Furthermore, one may notice that despite the flow's increased momentum due to its turbulent nature, the jet diffusion seems unchanged comparing to the case of the transitional flow.

It is noted that the axial profiles obtained with other turbulent flows in the range of 30-70 l/min ($\mathrm{Re} = 4200 - 9800$) are similar with the profile in the diagram presented here ($\mathrm{Re} = 7000$), presumably due the turbulent nature of the flow. Thus, the axial profiles indicate that there is no significant jet diffusion and air entrainment along the centerline up to the 3-diameter distance, in consistency with the corresponding radial profiles.

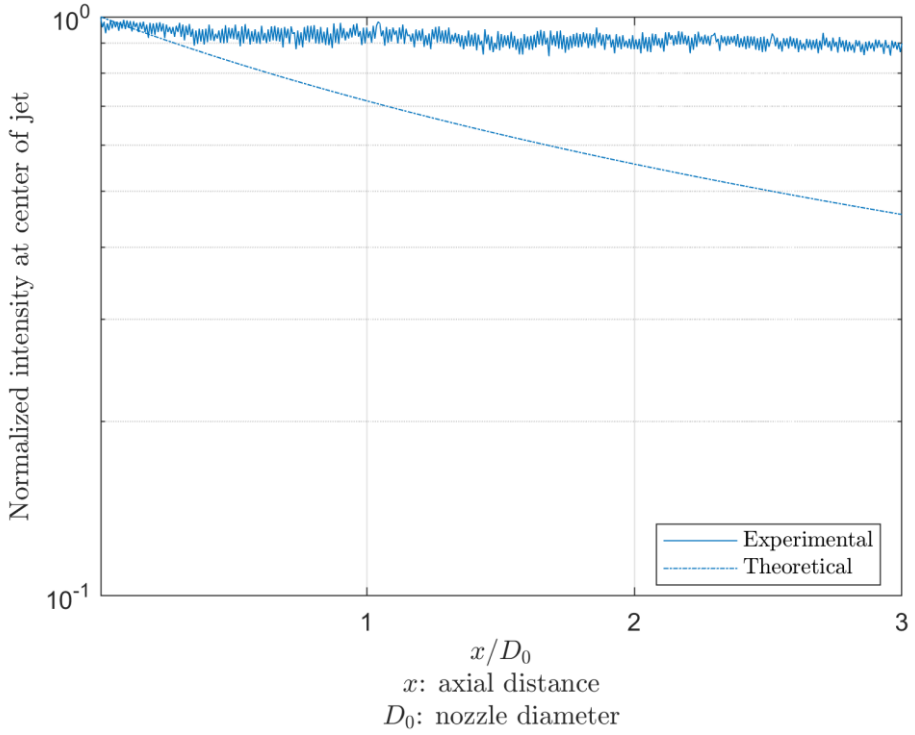


**Figure 3-34:** Mean centerline concentration profile of the jet flow with $\mathbf{Re = 7000}$ in quiescent environment

Finally, one can conclude that the axial profiles, in consistency with the radial profiles, indicate that there could be a central region of the flow that is not significantly affected by diffusion. The length of that region apparently exceeds the 3-diameter distance examined in this work. The examination of longer distances was not practically feasible due to the geometry of the support structure. Additionally, as it was previously mentioned, there was uncertainty regarding the amount of smoke that remained on the top of the structure and its potential interference with the measurements at the longer distances (the smoke was trapped in a piece of cloth placed to protect from external light).

### 3.3.2 Centerline profiles in isotropic turbulent environment (HIT)

In this Subsection, the axial-centerline profile diagrams obtained in the homogeneous and isotropic turbulent environment (HIT) are presented and discussed. The HIT environment was simulated by the operation of all eight loudspeakers, as it was previously described.

First, the laminar flow is examined. The properties of the laminar flow used during the experimental procedure were $\mathrm{Re} = 1400$ for Reynolds number and Q = 10 l/min for the volumetric flow rate. In Figure 3-35, the jet's centerline concentration (normalized intensity) is plotted against the normalized distance from the orifice ($x/D_0$). This diagram shows that the centerline concentration decreases significantly across the axial distance and reaches a value of 0.3 at the 3-diameter distance from the orifice. The decay rate is higher than the 'theoretical' rate (derived for turbulent jets in calm conditions), which predicts a value of about 0.5 at the 3-diameter distance. Comparing this diagram to the corresponding one in quiescent environment (Figure 3-32), one can deduce that the external turbulence significantly enhances the jet diffusion and air entrainment in the centerline direction.

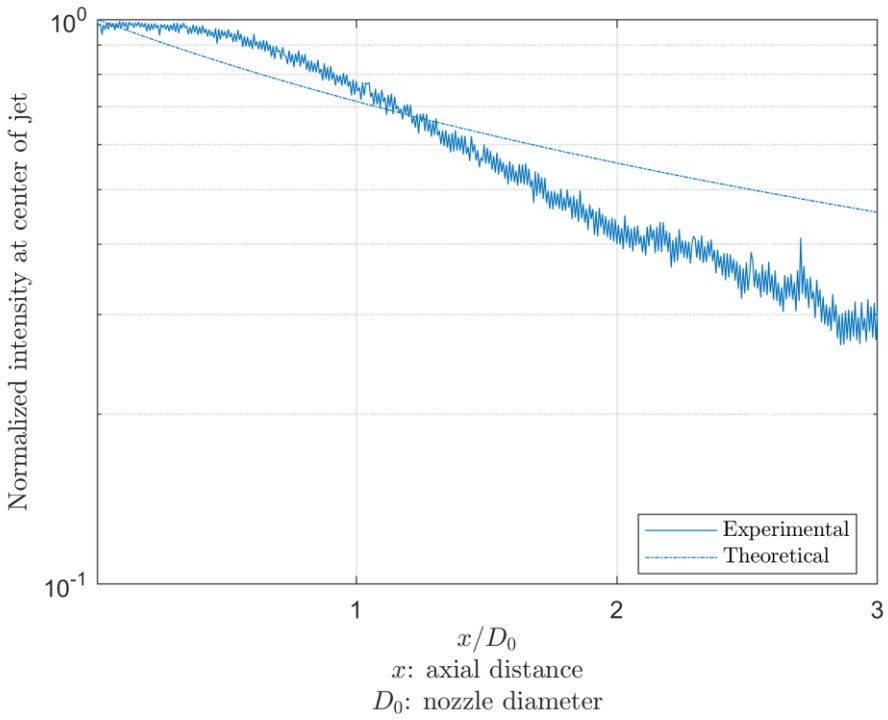


**Figure 3-35:** Mean centerline concentration profile of the jet flow with $\mathbf{Re = 1400}$ in the HIT environment

The next type of flow examined is the transitional flow. The transitional flow used for this experiment had the Reynolds number of $\mathrm{Re} = 2800$ and the volumetric flow rate of Q=20 l/min. In Figure 3-36 the mean centerline concentration profile of the jet concentration is depicted. This diagram indicates that the centerline concentration decreases significantly across the axial distance and reaches a value of 0.45 at the 3-diameter distance from the orifice. The decay rate appears to be similar to the 'theoretical' rate, and smaller than that of the laminar flow. Comparing this diagram to the corresponding one in quiescent environment, one can deduce that the external turbulence enhances appreciably the jet diffusion and air entrainment in the centerline direction. The enhancement may be less pronounced than with the laminar flow, possibly because the momentum of the transitional flow is higher, and thus the impact of the external turbulence is smaller.

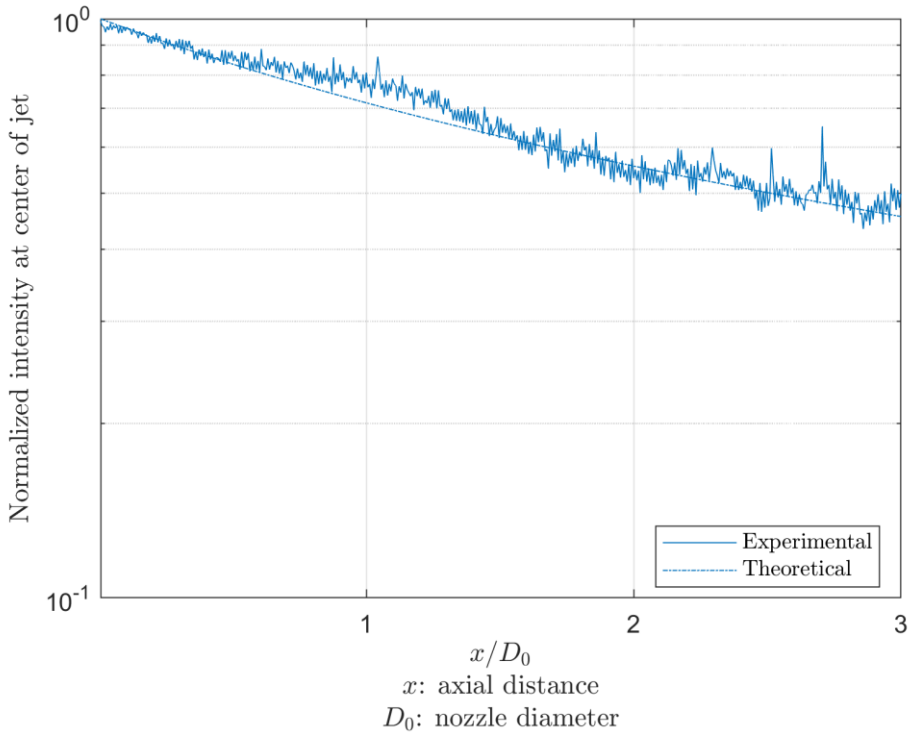


**Figure 3-36:** Mean centerline concentration profile of the jet flow with $\mathbf{Re = 2800}$ in HIT environment

The last type of flow examined is the turbulent flow. In Figure 3-37 the mean centerline concentration profile for the jet with Q=50 l/min and $\mathrm{Re} = 7000$ is depicted. The profiles obtained with other turbulent jet flowrates in the range of Q = 40 - 70 l/min (Re = 5600 – 9800) are similar to the one presented here (Re=7000).

Figure 3-37 indicates that the experimental line follows the same decay pattern with that in the quiescent environment. This translates to a very small decay rate. i.e., the normalized jet centerline concentration drops to a value of about 0.9 at the distance of $3D_0$ from the orifice. Comparing this diagram to the corresponding one in quiescent environment, one can deduce that, in this case, the external turbulence has practically no effect to the jet dissipation along the centerline. This can be attributed to the turbulent nature of the flow. The momentum of the current flow is significantly greater than the momentum of the external turbulence, thus the external disturbances have little to none effect on the development of the jet flow.

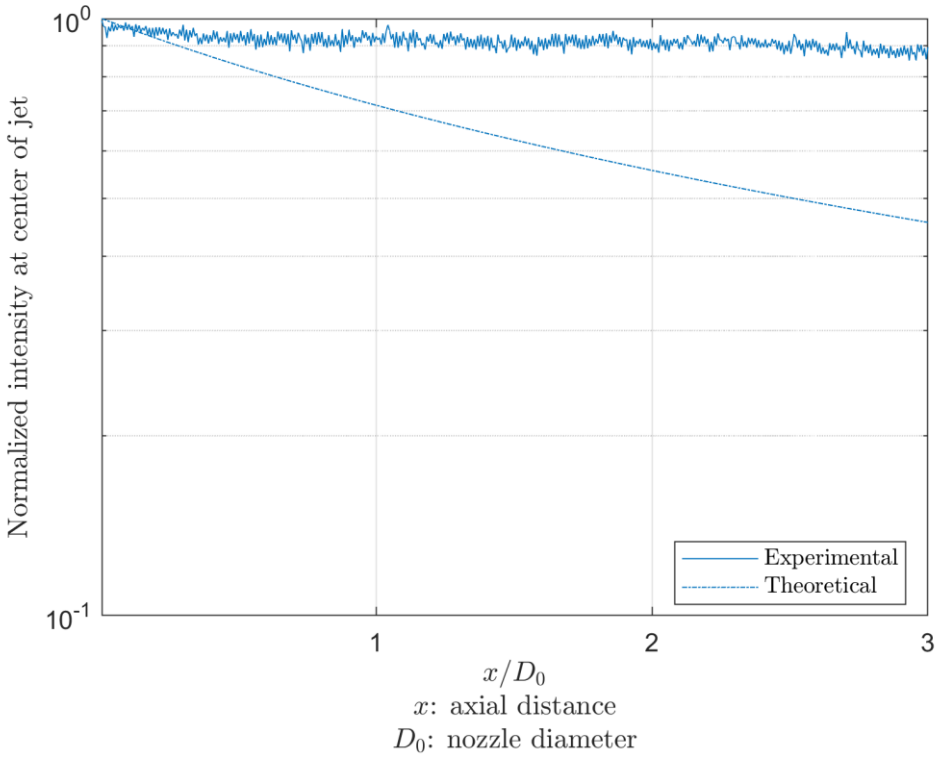


**Figure 3-37:** Mean centerline concentration profile of the jet flow with $\mathbf{Re} = \mathbf{7000}$ in HIT environment

## 3.4 Contour plots

In this Section, the jet flow and its interaction with the surrounding environment is studied with the aid of the concentration contour plots. The contour plots obtained in quiescent conditions, the isotropic turbulent (HIT) environment and the different anisotropic turbulent environments are presented and discussed. In each case, the analysis consists of three types of jet discharge flow: the laminar ($\mathrm{Re} = 1400$), the transitional ($\mathrm{Re} = 2800$) and turbulent flows ($\mathrm{Re} = 4200 - 9800$).

In general, a contour plot is consisted of several contour lines with a certain interval. A contour line (or, contour) is a curve along which the function or, the variable under study, has a constant value; the contour joins points of equal value (Courant, 1996). The distance between the contours indicates the magnitude of the gradient i.e., when the contour lines are closer together the gradient is higher. In the current study, the contour plots depict the geometry of the flow and the distribution of the tracer's concentration in the plane. A contour line represents the curve that joins the pixels of equal intensity in a mean picture. As it was discussed in the relevant Section, the intensity of the pixels stands for the value of the jet concentration in the flow (a higher intensity indicates a higher value of concentration). The contour plots 'resemble' the corresponding mean pictures albeit the geometry of the flow and the changes in concentration are clearly depicted by means of the contour lines.

In the contour plots, the vertical axis shows the normalized axial distance $x/D_0$, where $x$ is the axial-downstream distance measured from the orifice, and $D_0$ is the nozzle diameter. The horizontal axis shows the normalized radial distance $r/r_0$, where $r$ is the radial distance measured from the centre of the jet and $r_0$ is the nozzle radius. The contour lines present values of the normalized concentration with an interval of 0.1. The region inside the contour line of 0.9 is depicted with yellow colour, whereas the region between the contours of 0.9 and 0.8 is depicted with light brown colour. The 'yellow region' (c > 0.9) or, the 'yellow/brown region' (c > 0.8) can be regarded to represent the core of the flow, where the highest values of the jet concentration are observed. The blue colour indicates regions of low concentration (the darker the shade of blue, the lower is the concentration); the contour line of 0.2 may be considered to depict the boundary with the surroundings. The contour lines between the core of the flow and the surroundings depict the different levels of the jet concentration as it diffuses to the environment.

In the contour plots, the mean line of the jet flow is also depicted (by a red line). This is calculated by fitting a power law equation to the normalized $(r, x)$ data of the contour plot. The results are presented in the form $r/r_0 = a(x/D_0)^b$, where $a$ and $b$ are referred to as power-law coefficients (the power law coefficient $a$ and the exponent $b$). The aim of the mean line is to reveal the direction of the jet flow and possibly predict its further evolution. The coefficient $a$, indicates the value of the normalized radial

distance at an axial distance equal to the diameter of the nozzle. A positive value of $a$ indicates that the line is leaning to the right of the vertical axis ($r = 0$), whereas a negative value of $a$ indicates that the line is leaning to the left of the vertical axis ($r = 0$). The exponent $b$ provides an indication of the incline's gradient magnitude as the downstream distance increases.

### 3.4.1 Jet Angle

In this Subsection the jet angle created between the flow and the orifice is analyzed and discussed. The determination of the jet angle is important since it can be used to create a relation that describes how the flow radius evolves relevant to the distance in the streamwise direction of the flow. According to the theory of turbulent jets penetrating into quiescent fluid (Subsection 1.3.1), the theoretical (ideal) jet angle (ϕ) is $11.8^{o}$ and thus the radius R of the jet is varied with the downstream distance $X$ (measured from the virtual origin) in accordance to: $R(X) = \tan(\varphi)\, X$. This equation can be written in terms of the downstream distance $x$ (measured from the orifice) as $R(x) = \tan(\varphi)x + r_0$ or, in a dimensionless form as $R(x)/r_0 = 1 + 2\tan(\varphi)\,(x/D_0)$. In comparison to turbulent jets, laminar or transitional flow jets are expected to have narrower openings due to the decreased momentum of the flow. In this analysis, the calculation of the jet angle is made by setting a constant intensity (concentration) in the contour plot. The normalized concentration in the contour plot is set to the value of 0.2, which it is assumed to represent the boundary of the jet with the surroundings. The analysis regards the quiescent environment. Turbulent environments are not examined since the direction of the flow is disrupted.

The first flow examined is the laminar flow with Reynolds number of $\mathrm{Re} = 1400$ and volumetric flow rate of Q=10 l/min. Figure 3-38 depicts the contour line of 0.2 and concurrently the left and right-side fits in the vertical direction. As shown in the plot, the jet's angle on the left side is around 0.26°, while on the right side is approximately 0.45°. The deviation between the angles on the left and right side may be related to imperfections at the orifice. As far as the deviation between the experimental jet angles and the theoretical one ($11.8^{o}$), the large difference between them can be attributed to the fact that in this case the flow is laminar, resulting in a narrower expansion of the flow. For the creation of the relation between the expanding flow radius and the streamwise distance, the arithmetic mean is used. Here, this is equal to 0.35°. Therefore, the evolution of the flow is represented by the following equation, $R(X) = 0.0061X$.

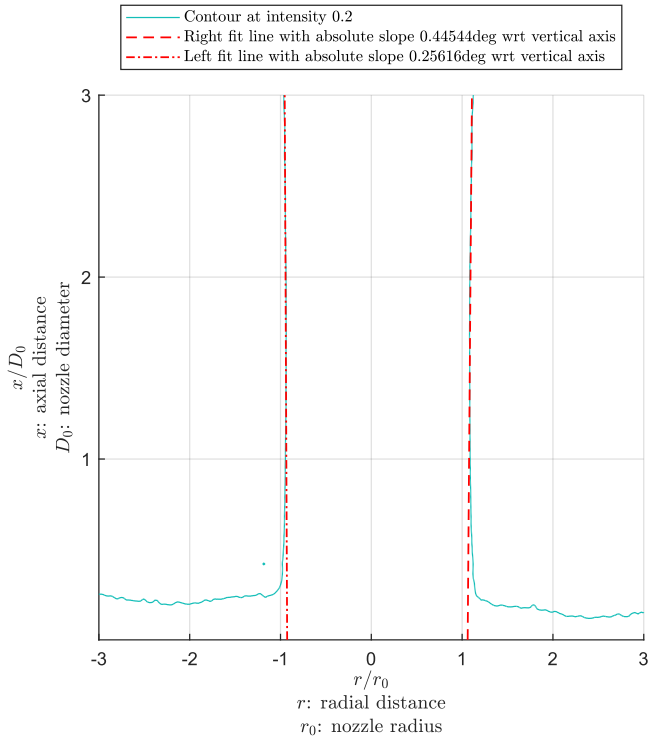


**Figure 3-38:** Jet's angle calculation for a jet flow with $\mathbf{Re} = \mathbf{1400}$ in quiescent environment

The next flow examined is the transitional flow with $\mathrm{Re} = 2800$ (volumetric flowrate Q=20 l/min). Figure 3-39 depicts the contour line of 0.2 and the left and right-side fits. As shown in this plot, the calculated angle of the left-side line is approximately 0.46°, while the calculated angle of the right-side line is around 0.73°. The difference between the two values may be related to imperfections at the orifice. As far as the deviation with the theoretical value of the angle is concerned, this divergence can be attributed to the different nature of the flows. A turbulent flow has a wider opening when it is emitted from the jet due to the increased momentum, comparing to a transitional flow where the opening is narrower. The arithmetic mean of the right and left angles is used to construct the relation between the flow expanding radius $R$ and the streamwise direction $X$. The arithmetic mean is approximately 0.59°; therefore, the expanding radius of the current flow can be calculated by the following relation: $R(X) = 0.0104X$.

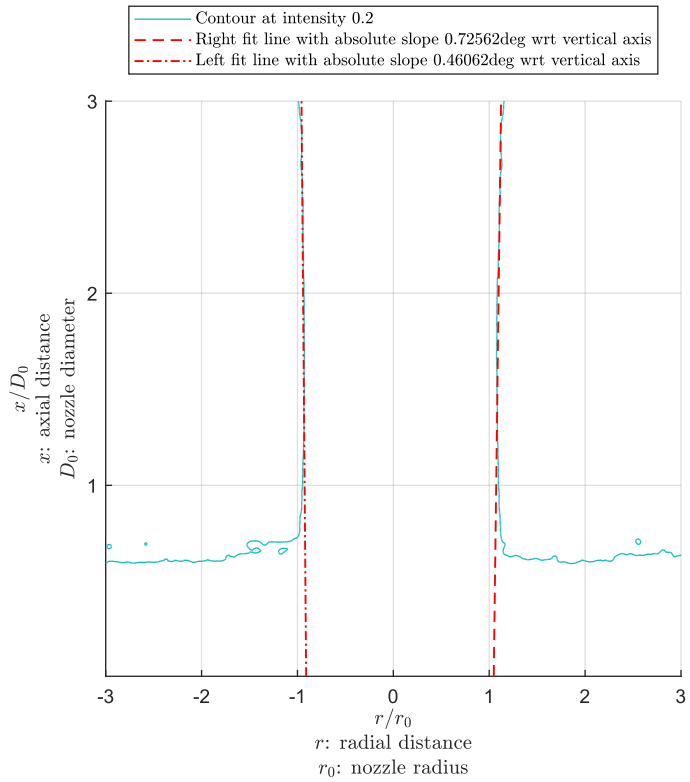


**Figure 3-39:** Jet's angle calculation for a jet flow with $\mathbf{Re} = \mathbf{2800}$ in quiescent environment

The next flow examined is the turbulent flow with $\mathrm{Re} = 5600$ (Q = 40 l/min). Figure 3-40 presents the contour line of 0.2 and the left and right-side fits for this turbulent flow. As shown in this plot, the calculated angle of the left side line is 8.22°, whereas the angle of the right-side line is approximately 9.45°. The difference between the two angles may be related to imperfections in the orifice. These angles are closer to the theoretical angle than the previous ones, which is reasonable since this flow is turbulent. This difference of roughly 3° to 4° between the experimental and theoretical angles can be attributed to experimental and processing uncertainty and, of course, the threshold of the contour line at intensity 0.2, which limits the opening of the angle. The arithmetic mean of the two experimental angles is 8.84 degrees, therefore the relation between the expanding flow radius $R$ and the streamwise direction $X$ of the flow can be written as $R(X) = 0.155X$.

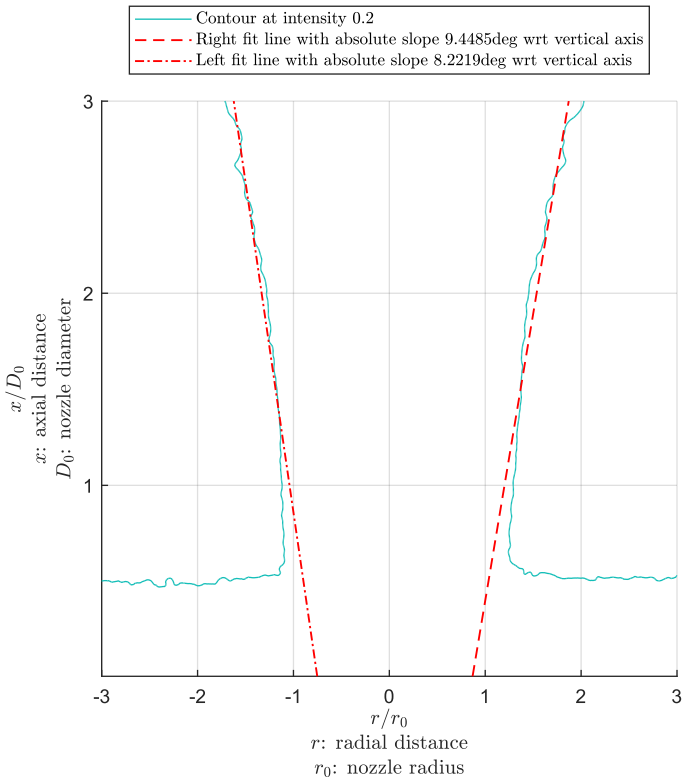


**Figure 3-40:** Jet's angle calculation for a jet flow with $\mathbf{Re = 5600}$ in quiescent environment

Next, the turbulent flow with Reynolds number $\mathrm{Re} = 9800$ (volumetric flowrate Q=70 l/min) is examined. Figure 3-41 depicts the contour of 0.2 and the left and right-side fits. As shown in this plot, the calculated angle in the left side is 8.43°, while the calculated angle in the right side is 8.95°. The mean value of the angle is 8.69° and the proportionality coefficient is 0.153. One can observe that the results of the previous two cases (Q = 40 and 70 l/min) are similar.

The results for all the jet flows examined, as shown in Table 6. The Table shows that the opening of the jet increases with the Reynolds number to reach a constant angle of about 8.8° at Re ≥ 5600, where a fully developed, turbulent flow is assumed to occur. This jet angle of 8.8° (proportionality coefficient of 0.155) is lower than the theoretical value of 11.8° (proportionality coefficient of 0.2), which can be mainly attributed to the concentration limit of 0.2 set to define the jet radius.

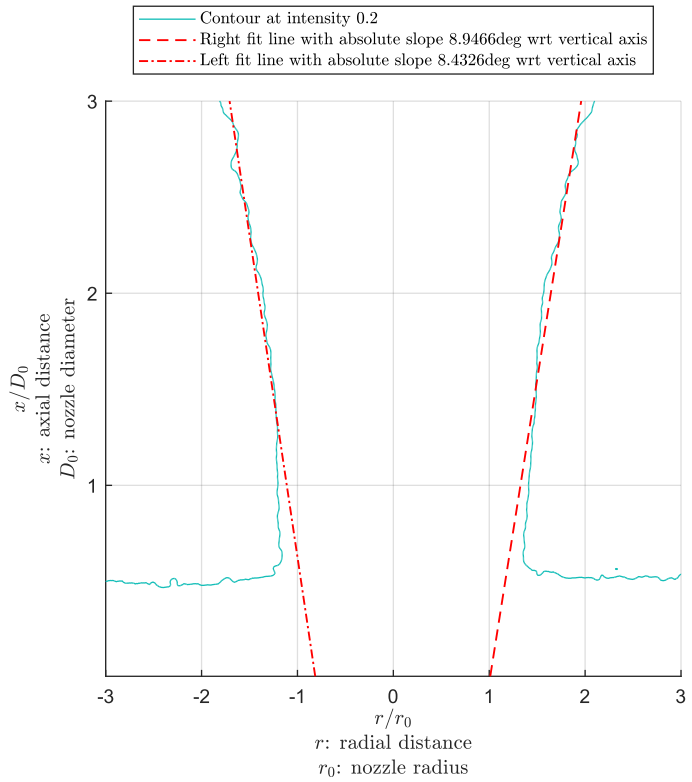


**Figure 3-41:** Jet's angle calculation for a jet flow with $\mathbf{Re} = \mathbf{9800}$ in quiescent environment

**Table 6:** Jet angle's evolution with the Reynolds number (Quiescent environment)

| Reynolds number | $Angle^o$ | $\tan(Angle^o)$ |
|---|---|---|
| **1400** | 0.351 ± 0.095 | 0.00612 ± 0.00165 |
| **2800** | 0.593 ± 0.133 | 0.0104 ± 0.0023 |
| **4200** | 7.134 ± 0.226 | 0.1252 ± 0.0040 |
| **5600** | 8.835 ± 0.613 | 0.1554 ± 0.0110 |
| **7000** | 9.015 ± 0.136 | 0.1586 ± 0.0024 |
| **8400** | 8.632 ± 0.117 | 0.1518 ± 0.0021 |
| **9800** | 8.690 ± 0.257 | 0.1528 ± 0.0046 |

### 3.4.2 Contour plots in quiescent environment

Initiating the analysis of the contour plots, the first case to be examined is the case of the quiescent surrounding environment. The case of quiescent surroundings is simpler than the other (turbulent) cases and provides the frame for the study of the contour plots.

The first type of discharge flow to be examined is the laminar flow. The laminar flow used in the current experimental procedure has the Reynolds number of $\mathrm{Re} = 1400$ and the volumetric flow rate of Q = 10 l/min. Figure 3-42 depicts the contour plot for this flow.

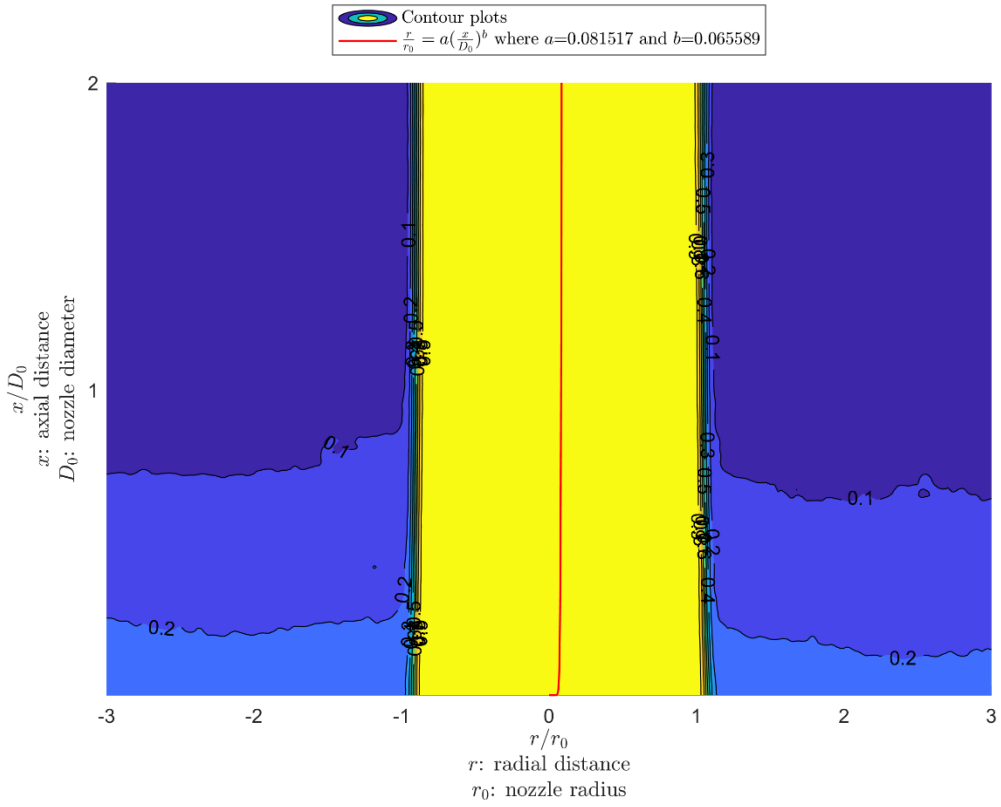


**Figure 3-42:** Contour plot of the jet flow with $\mathbf{Re} = \mathbf{1400}$ in quiescent environment

Firstly, one can notice that its shape strongly 'resembles' the corresponding mean picture (Figure 3-1). However, here the geometry of the flow is more distinctive and simultaneously the change in the values of the jet concentration is clearly depicted in the contour lines. The yellow color indicates the core of the flow (c > 0.9). The blue color indicates regions with low to no concentration. The darker shade of blue represents almost no concentration.

As it can be seen in the previous plot, the jet concentration in the flow direction is almost unaffected by the external environment and maintains the same value for all the downstream distance studied, thus, the yellow color region is kept unchanged. The normalized jet concentration values in this (yellow) region

of the flow are higher than the value of 0.9. Furthermore, the contour lines between 0.2 and 0.9 are really close with each other, in a way that they are not even distinguishable. This indicates a very large gradient's magnitude. Due to the unaffected flow, the jet concentration rapidly drops from a high value in the main region of the flow (yellow region, c > 0.9) to a low value in the surroundings (dark blue region, c < 0.2).

Finally, the direction of the flow is almost vertical. The calculated mean line of the flow, depicted by a red line that passes from the center of the orifice, is also shown to be an almost vertical line. The mean line is calculated by the power law equation, presented in the introductory part of this Section, with the coefficient $a = 0.0815$ and the exponent $b = 0.0656$.

Further analyzing the contour plots in quiescent surroundings, Figure 3-43 depicts the contour plot for the transitional flow with Reynolds number $\mathrm{Re} = 2800$ (flowrate Q=20 l/min).

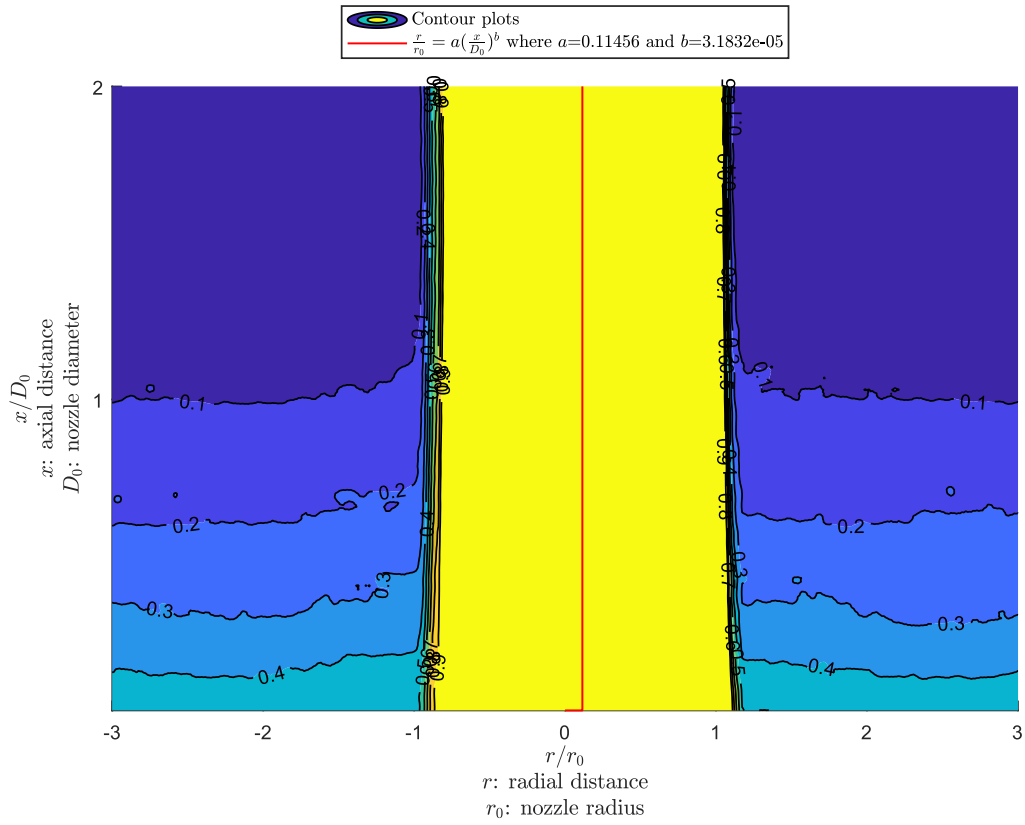


**Figure 3-43:** Contour plot of the jet flow with $\mathbf{Re = 2800}$ in quiescent environment

Examining the plot depicted in Figure 3-43, one can see that the jet concentration in the flow direction maintains the same value (yellow color region) along the downstream distance studied. This is like the case of the laminar flow.

The contour lines located at the boundary layer that separates the main region of the flow with the surrounding region are very close with one another, indicating a very large magnitude of the concentration gradient. This is also like the case of the laminar flow. It appears that the transitional flow doesn't have the sufficient momentum to diffuse the smoke particles contained in the jet flow into the surrounding environment. Also, the surrounding environment does not favor the diffusion of the smoke particles due to its quiescent state.

The flow appears to maintain its original course i.e., its direction is almost vertical. The mean line is also almost vertical in the range investigated. The mean line is calculated by the power law equation with the coefficient $a = 0.115$ and exponent the $b = 3.183 \cdot 10^{-5}$.

Completing the analysis of the flow's interaction with quiescent surroundings, the last type of flow to be examined is the turbulent flow. In Figure 3-44 the contour plot of the turbulent discharge flow with Reynolds number $\mathrm{Re} = 8400$ (flowrate Q = 60 l/min) is presented.

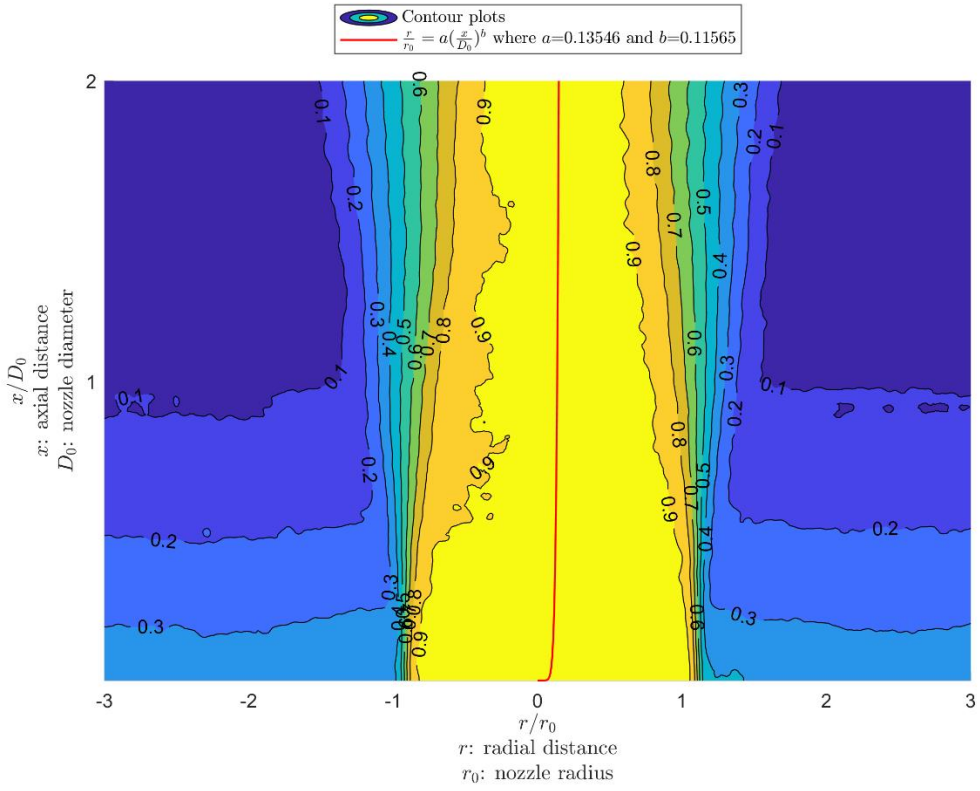


**Figure 3-44:** Contour plot of the jet flow with $\mathbf{Re = 8400}$ in quiescent environment

Observing this plot, one can see that the decay of the jet concentration is higher than the previous cases of the laminar and transitional flows. The flow appears to widen along the downstream direction and, the contour lines become more widely spaced across the jet, as the downstream distance increases. In other

words, the flow is adopting a conical shape, which should be due to the jet turbulence. The greater decay of the jet concentration can be accordingly attributed to the turbulent nature of the flow. In turbulent flows the jet flow momentum is greater, and therefore the mass transfer rate is increased, resulting in a higher quantity of smoke particles contained in the flow being diffused in the surrounding environment.

The diagram shows that the jet concentration remains high along the mean line of the flow (yellow/brown region), in agreement with the corresponding centreline profiles (Figure 3-34). Furthermore, in each cross section, the contour lines between the core of the flow and the surroundings are rather evenly spaced in both sides of the flow. This indicates that a gradual decay of the jet concentration is taking place crosswise upon diffusion into the surroundings, which is consistent with the bell-type distribution observed in the corresponding radial profiles (Figure 3-16).

The direction of the jet flow appears undisrupted, which can also be seen from the close to vertical mean line. This mean line is calculated by the power law equation with the coefficient $a = 0.135$ and the exponent $b = 0.116$.

The contour plots obtained with other turbulent flows in the range of $\mathrm{Re} = 4200 - 9800$ (Q = 30 - 70 l/min) are similar to the plot presented here ($\mathrm{Re} = 8400$), i.e., they exhibit a similar jet widening pattern with high concentrations along the axial-downstream direction, and a flow direction close to vertical. This similarity is apparently due to the turbulent nature of flow. In other words, when the flow becomes turbulent the contour lines are adopting a 'conical shape' pattern, which is different from the 'rectangular' pattern observed with the laminar and transitional flows. This 'conical shape' pattern appears to develop at $\mathrm{Re} = 4200$ and remains relative constant at $\mathrm{Re} = 5600 - 9800$.

**Table 7:** Power law coefficients for the mean line of the jet flows in quiescent environment

| **Reynolds number** | **Power law coefficients** | |
|---|---|---|
| | $a$ | $b$ |
| **1400** | 0.0815 | 0.0656 |
| **2800** | 0.115 | 3.18e-05 |
| **4200** | 0.108 | 0.155 |
| **5600** | 0.154 | 4.85e-08 |
| **7000** | 0.131 | 0.0723 |
| **8400** | 0.135 | 0.116 |
| **9800** | 0.151 | 0.149 |

Table 7 depicts the values of the $a$ and $b$ coefficients of the power law relation, presented in the introductory part of this Section, for all the jet flows examined in the quiescent environment. The values of the $a$ coefficient indicate that the mean lines are leaning slightly to the right; this small deviation from verticality is probably an 'offset' attributed to experimental and processing uncertainty.

### 3.4.3 Contour plots in turbulent environment (HIT)

In this Subsection, the contour plots depicting the jet flows in a homogeneous and isotropic turbulent (HIT) environment will be presented and discussed. This external turbulence was generated by all the eight loudspeakers, each located at each corner of the support structure, as it was described previously.

Commencing the examination of the contour plots, the laminar discharge flow with Reynolds number of $\mathrm{Re} = 1400$ and volumetric flowrate of Q=10 l/min is examined first. In Figure 3-45 the relevant contour plot is presented.

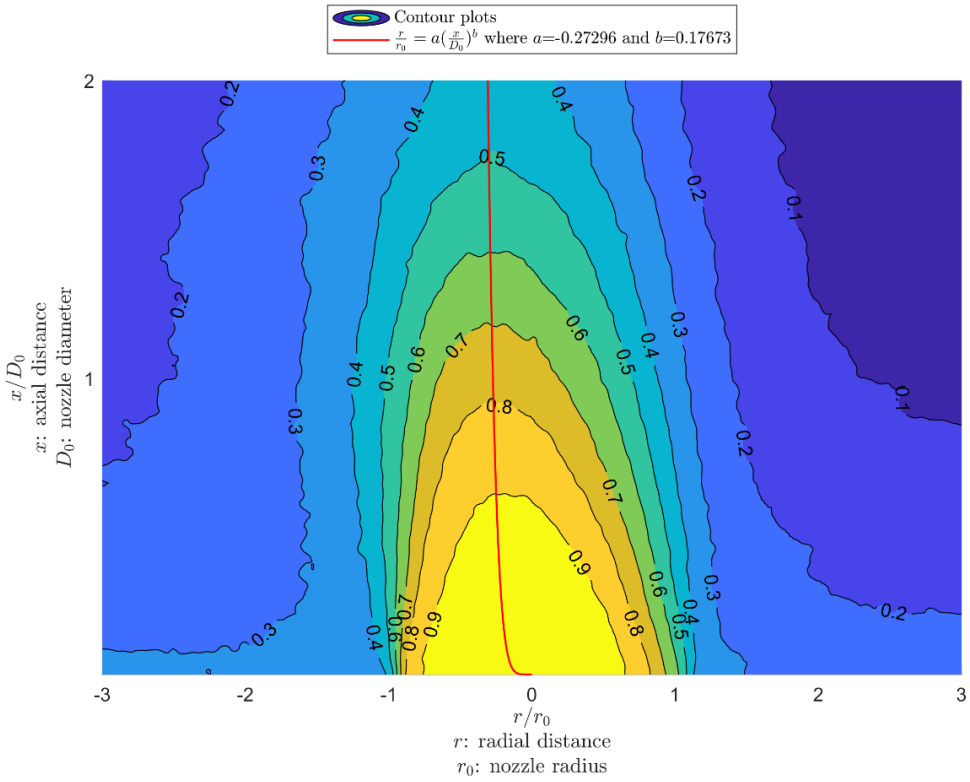


**Figure 3-45:** Contour plot of the jet flow with $\mathbf{Re = 1400}$ in turbulent environment (HIT)

Observing this contour plot, one can notice that the geometry of the flow is significantly altered in comparison to the corresponding plot in quiescent environment, e.g., the core of the flow (yellow/brown region) is small. This can be attributed to the external turbulence. The momentum of this laminar jet is small compared to the momentum of the external turbulence resulting in the suppression of the flow.

Furthermore, the contours between the core of the flow (c > 0.9/0.8) and the surroundings (c < 0.2) have a similar shape and they are gradually/distantly spaced compared to the quiescent environment, which indicates that the jet concentration decays gradually. The contours along the mean line of the flow appear to be rather widely spaced compared to the crosswise direction; this indicates that the rate of the jet diffusion in the downstream direction is low compared to the radial direction.

Interestingly, the direction of the flow is leaning to the left. If the generated turbulence was exactly homogeneous and isotropic, the direction of the flow should not have been altered because such external turbulence provides the same momentum from every direction. However, due to the non-steady operation of the loudspeakers, some of the loudspeakers operated with different power during the course of an experiment. In this case, the loudspeakers located in the right-side of the support structure operated with greater power, giving the jet flow the incline to the left. This can also be observed from the mean line due to its curvature at the left side. The mean line of the flow is described by the power law equation with the coefficient $a = -0.273$ and the exponent $b = 0.177$. The negative value of the $a$ coefficient indicates that the mean line is inclined to the left.

The next type of discharge flow examined is the transitional flow with a discharge rate of Q=20 l/min and Reynolds number $\mathrm{Re} = 2800$. In Figure 3-46 the relevant plot is depicted.

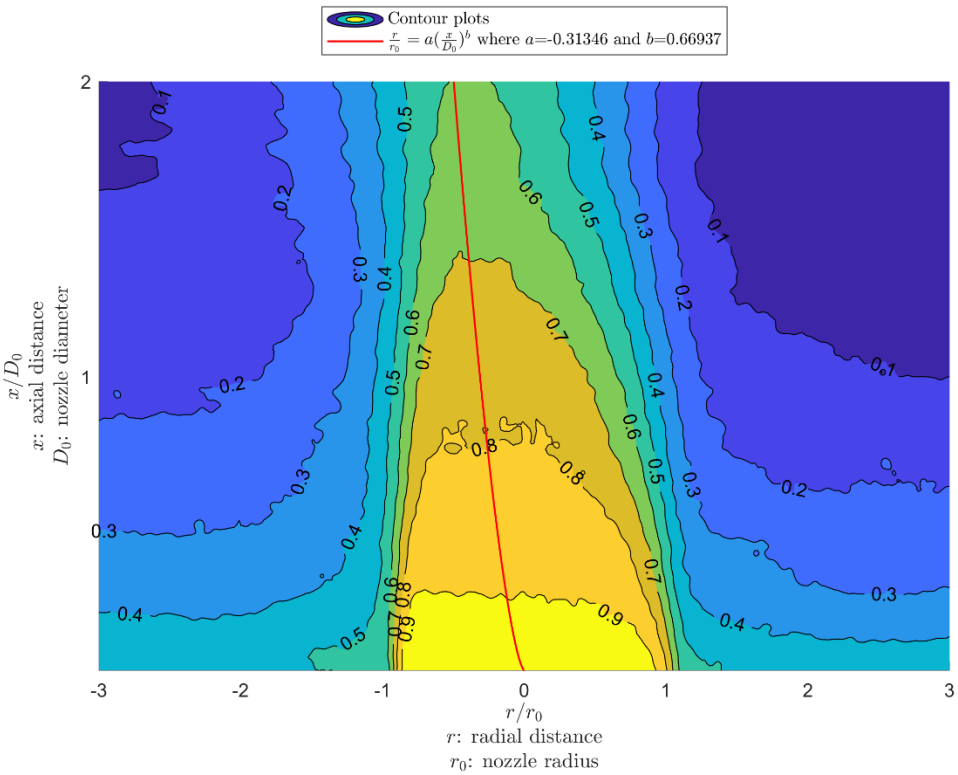


**Figure 3-46:** Contour plot of the jet flow with $\mathbf{Re = 2800}$ in turbulent environment (HIT)

In this contour plot, one can observe that the geometry of the transitional flow shares a strong resemblance with the geometry of the previously examined, laminar flow. Here, however the contour lines are more distorted than the same lines in the laminar flow plot. Also, some of them do not share the same shape, which was a common trait in the contour lines of the laminar flow plot. This can be attributed to the transitional nature of the flow. The flow's transformation from laminar to turbulent has begun and the first signs of chaotic movement have made their appearance.

Furthermore, one can notice that at the longer distances from the orifice, along the mean line, the jet concentration maintains a relatively high value comparing to the same distances in the contour plot of the laminar flow. This may indicate that the momentum of the transitional flow is higher than the laminar flow, and thus the impact of the external turbulence is comparatively smaller, resulting in smaller diffusion rate.

The direction of this transitional flow is inclined towards the left side, like the case of the laminar flow. This is presumably due to the non-steady operation of some loudspeakers, as it was previously explained. The flow's incline can also be seen in its mean line. The mean line of the flow is represented by the power law equation with a coefficient $a = -0.313$ and an exponent $b = 0.669$.

The last type of flow examined for the HIT environment is the turbulent flow. Figure 3-47 presents the contour plot for the jet discharged with a rate of 40 l/min ($\mathrm{Re} = 5600$).

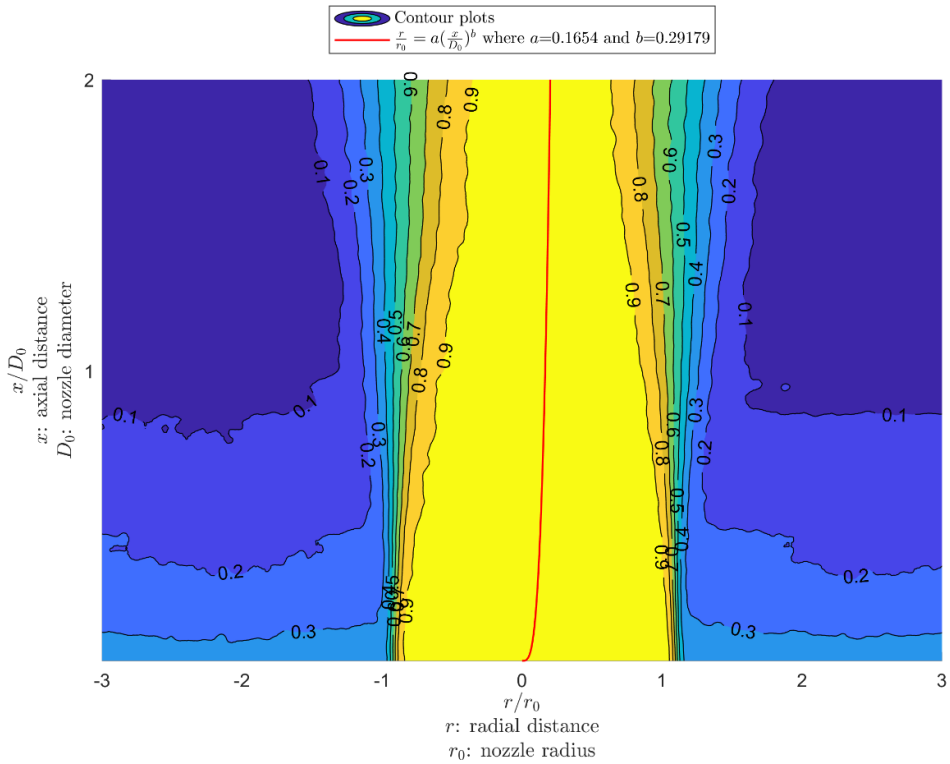


**Figure 3-47:** Contour plot of the jet flow with $\mathbf{Re} = \mathbf{5600}$ in turbulent environment (HIT)

In this plot, one can observe that the geometry of the flow and the spacing of the contour lines are qualitatively similar to the corresponding plot, i.e., the one obtained with a turbulent flow, in quiescent environment (Figure 3-44). The turbulent flow appears to retain the 'conical shape' pattern despite the turbulent environment. This indicates that the momentum of the turbulent jet is higher than the momentum of the ambient turbulence.

The former similarity is envisaged in both the concentration profile along the mean line and the flow widening pattern. The jet concentration maintains a high value (c > 0.9) along the flow direction, which is consistent with the relevant centreline concentration profiles (Figure 3-37). The jet flow in this direction appears to be unaffected by the external turbulence up to the distance studied. Furthermore, the jet widens along the downstream direction following a 'conical shape' pattern similar to the quiescent conditions i.e., the contour lines become more widely spaced across the jet, in both sides of the flow, as the flow progresses in the downstream distance. The spacing of the contours indicates a gradual decay of the jet concentration in the radial direction, in consistency with the bell-type distribution observed in the relevant radial profiles (Figure 3-19).

The direction of the flow is inclined towards the right-side. This incline is shown in the mean line, which is calculated by means of the power law equation with the coefficient $a = 0.165$ and the exponent $b =$

$0.292$. The observed deviation from the vertical line is however small (comparable to the offset observed in quiescent conditions) and it could be attributed to the experimental and processing uncertainty, as well as the operational imperfections of the loudspeakers.

The contour plots obtained with other turbulent jet flows in the range of $\mathrm{Re} = 4200 - 9800$ (Q = 30 – 70 l/min) are similar to the plot presented here ($\mathrm{Re} = 5600$) that is, they exhibit a similar jet widening pattern with high concentrations along the mean line, and a similar flow direction. This pattern appears to develop at $\mathrm{Re} = 4200$, and remains relative constant for $\mathrm{Re} = 5600 - 9800$, presumably due to the turbulent nature of the flow. Table 8 depicts the values of the coefficients of the power law equation, presented in the introductory part of this Section, for the mean lines of the jet flows examined in the HIT environment. Table 8 indicates that the laminar and transitional flows are inclined to the left ($a < 0$), whereas the turbulent flows are inclined to the right ($a > 0$). The latter incline ($a$) appears to be constant in the last four turbulent flows taking a small value i.e., a value similar to the 'offset' observed in quiescent conditions. In brief, the results indicate that the external turbulence (HIT) significantly enhances the diffusion of laminar and transitional jet flows ($\mathrm{Re} = 1400 - 2800$) but has a minor effect on the turbulent jet flows ($\mathrm{Re} = 4200 - 9800$).

**Table 8:** Power law coefficients for the mean line of the jet flows in the HIT environment

| **Reynolds numbers** | **Power law Coefficients** | |
|---|---|---|
| | $a$ | $b$ |
| **1400** | -0.273 | 0.177 |
| **2800** | -0.313 | 0.669 |
| **4200** | 0.274 | 0.433 |
| **5600** | 0.165 | 0.292 |
| **7000** | 0.178 | 0.302 |
| **8400** | 0.195 | 0.262 |
| **9800** | 0.165 | 0.207 |

### 3.4.4 Contour plots in turbulent environment (Left and right-side loudspeakers)

In this Subsection, the concentration contour plots obtained in two anisotropic turbulent environments are presented and discussed: (a) the turbulent environment generated from the left-side loudspeakers, and (b) the turbulent environment generated from the right-side loudspeakers. The analysis will be consisted of the three types of jet discharge flow: the laminar, the transitional and turbulent flows.

First, the laminar discharge flow with Reynolds number of $\mathrm{Re} = 1400$ (discharge rate Q=10 l/min) is examined. In Figure 3-48 the contour plot obtained in the turbulent environment generated from the right-side loudspeakers is depicted. In Figure 3-49 the plot obtained in the turbulent environment generated from the left-side loudspeakers is presented.

These contour plots differ from the corresponding plot in quiescent conditions, since the core of the flow is limited (yellow/brown region, c > 0.9/0.8) and the contour lines between the core and the surroundings (c < 0.2) are gradually distributed in the plane in an anisotropic manner. These plots can be interpreted in a way similar to the respective plot in the HIT environment. The momentum of the external turbulence is higher than the momentum of the laminar jet flow, and thus the flow is disrupted, and accordingly the jet diffusion is enhanced (compared to the calm conditions).

The (gradual) spacing of contours indicates that the jet diffuses gradually into the surroundings. The contours along the mean line appear to be widely spaced in comparison to the crosswise direction, indicating that the rate of the jet diffusion in the streamwise direction is lower than the radial direction. Such spacing was also observed with the same jet flowrate in the HIT environment.

The main trait of these plots is that the direction of the flow is shown to deviate significantly from the vertical axis. In Figure 3-48, the flow is inclined to the left since the external turbulence is from the right-side loudspeakers. The direction of the flow is depicted by the mean line of the flow; this is calculated by the power law equation with the coefficient $a = -0.756$ and the exponent $b = 0.154$. In Figure 3-49, the flow is inclined to the right since the external turbulence is from the left-side loudspeakers. The incline of the flow is also depicted by the mean line; this is calculated by the power law equation with the coefficient $a = 0.684$ and the exponent $b = 0.162$. These inclines are higher than the incline observed with the same jet flowrate in the HIT environment.

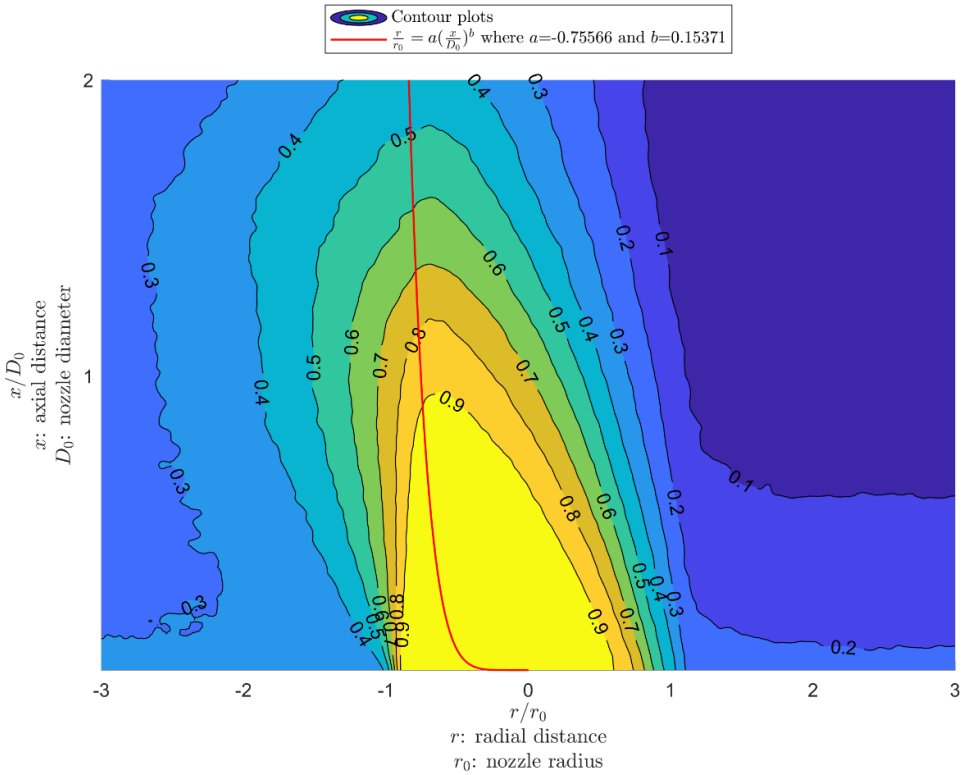


**Figure 3-48:** Contour plot of the jet flow with $\mathbf{Re} = \mathbf{1400}$ in anisotropic turbulent environment (Right-side loudspeakers)

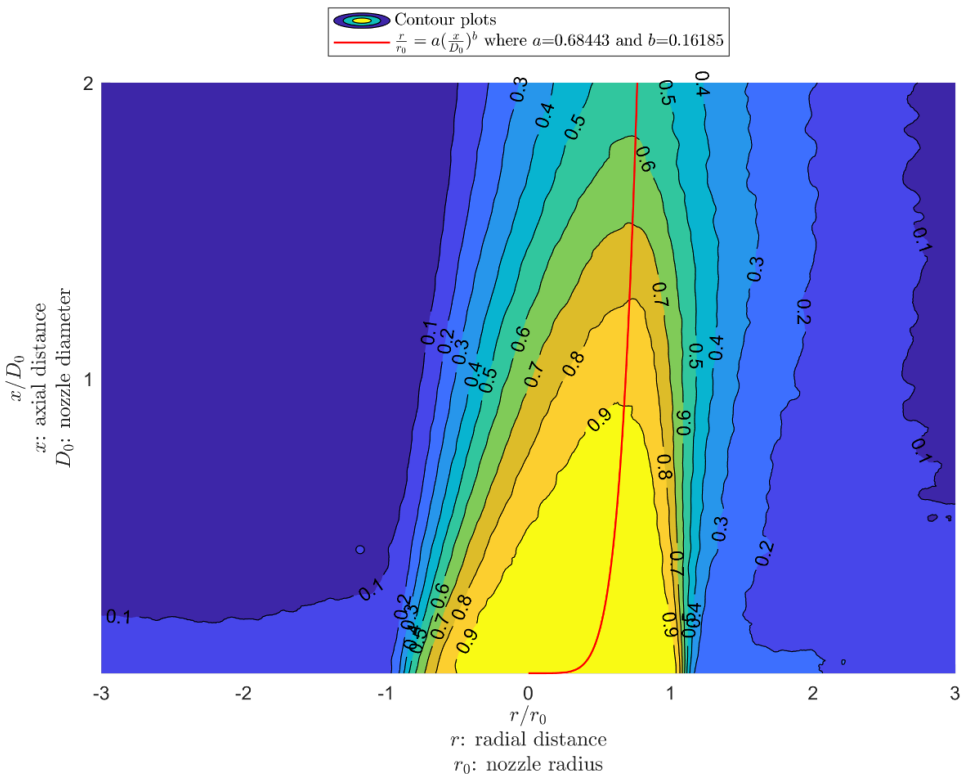


**Figure 3-49:** Contour plot of the jet flow with $\mathbf{Re} = \mathbf{1400}$ in anisotropic turbulent environment (Left-side loudspeakers)

Next, the transitional discharge flow with a flowrate of Q = 20 l/min and Reynolds number $\mathrm{Re} = 2800$ is examined. In Figure 3-50 the plot obtained for the turbulent environment generated from the right-side loudspeakers is presented. In Figure 3-51 the plot obtained for the turbulent environment generated from the left-side loudspeakers is presented.

Regarding the turbulence from the right-side loudspeakers, the contour plot in Figure 3-50 appears to resemble the plot of the laminar flow's, though here, the contour lines along the mean line are more widely spaced, and the incline to the left-side is smaller. These observations could be explained by considering that the momentum of the transitional discharge flow is higher than that of the laminar flow, and thus the impact of the external turbulence is comparatively smaller. The incline of the flow to the right can be seen in the mean line depicted on the former plot. This is calculated by the power law equation with the coefficient $a = -0.413$ and the exponent $b = 0.596$.

Regarding the turbulence from the left-side loudspeakers, Figure 3-51 indicates that the shape of the transitional flow is similar to that of the laminar flow, but the jet concentration is higher along the flow's direction (e.g. the length of the yellow region is higher). This is different from what it is observed with the right-side loudspeakers. This 'asymmetry' may be related to the operational imperfections of the loudspeakers, e.g., the left-side loudspeakers may have operated with power different than the nominal during the course of this experiment. The direction of the flow is significantly inclined to the right. The incline to the right can also be seen from the mean line of the flow depicted on the former plot. This is calculated by the power law equation with the coefficient $a = 0.754$ and the exponent $b = 0.553$. The plot suggests that the flow's incline is not accurately described in the mean line for the range investigated, which may be due to post processing error.

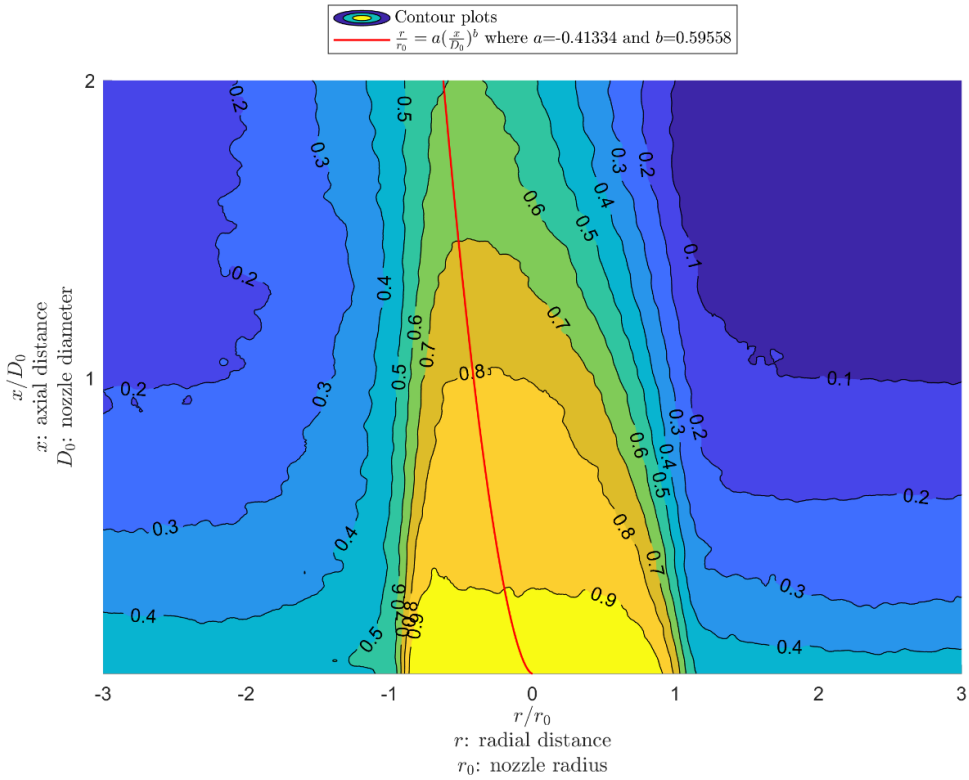


**Figure 3-50:** Contour plot of the jet flow with $\mathbf{Re} = \mathbf{2800}$ in anisotropic turbulent environment (Right-side loudspeakers)

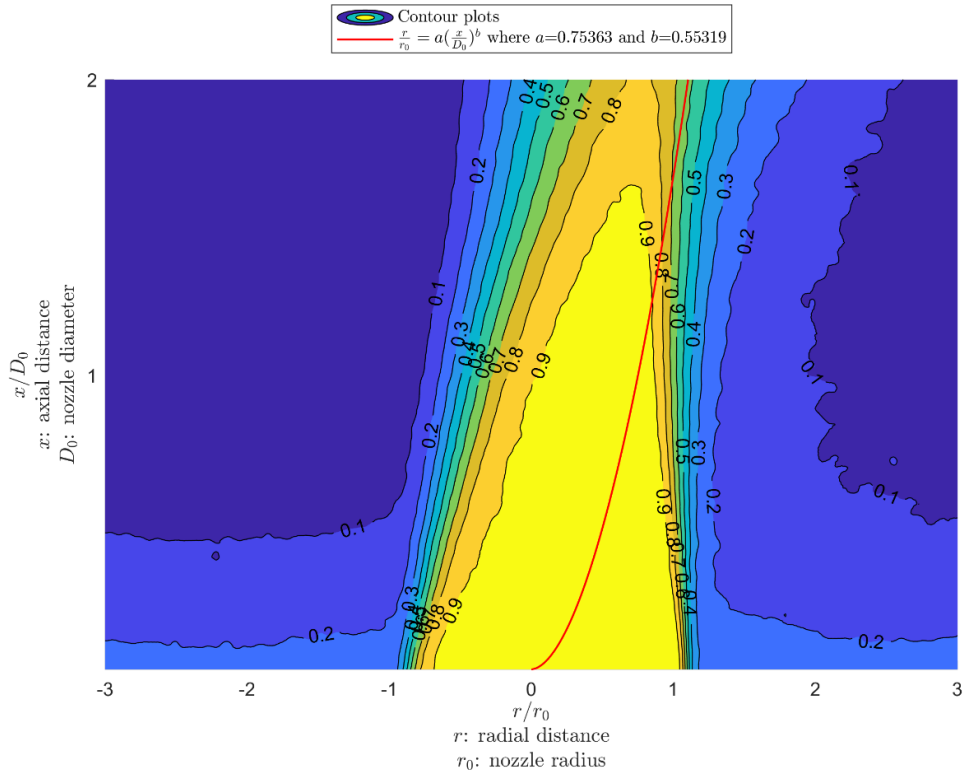


**Figure 3-51:** Contour plot of the jet flow with $\mathbf{Re} = \mathbf{2800}$ in anisotropic turbulent environment (Left-side loudspeakers)

Finally, the turbulent flow with a discharge rate of Q = 60 l/min and Reynolds number $\mathrm{Re} = 8400$ is examined. In Figure 3-52 the plot obtained for the turbulent environment generated from the right-side loudspeakers is presented. In Figure 3-53 the plot obtained for the turbulent environment generated from the left-side loudspeakers is presented.

In these contour plots, the geometry of the flow and the spacing of the contour lines are qualitatively similar to those obtained in the turbulent flow's plot in quiescent environment. This indicates that the effect of the external turbulence is small, presumably because its momentum is low compared to the momentum of the turbulent jet.

In both plots depicted in Figure 3-52 and Figure 3-53, the jet concentration maintains a high value along the mean line of the flow, as indicated by the shape of the yellow region (c > 0.9). The jet widens along the downstream direction following a pattern similar to the 'conical shape' pattern observed in quiescent conditions, which is consistent with the bell-type distribution observed in the corresponding radial profiles.

In Figure 3-52, the direction of the flow is almost vertical in agreement with the depicted mean line. The mean line is calculated by the power law equation with the coefficient $a = 0.0323$ and exponent $b = 2.608 \cdot 10^{-6}$. It is noted that there could be a small incline to the left consistent with the mean direction of the external turbulence which is generated from the right-side loudspeakers; this is not however depicted in the calculated mean line.

In Figure 3-53, the direction of the flow is inclined to the right apparently because of the external turbulence being generated from the left-side loudspeakers. This is also shown in the mean line, which is calculated by the power law equation with the coefficient $a = 0.263$, and the exponent $b = 0.422$. However, the incline of the flow may be overestimated in the calculated mean line.

The 'asymmetry' between the mean lines in the former and latter plots may be related to the non-equal power generated from the loudspeakers (e.g., the left-side loudspeakers may have operated with reduced power compared to the right-side ones) or, it may be related to post-processing uncertainty.

Tables 9 and 10, depict the values of the coefficients of the power law equation, presented in the introductory part of this Section, for the mean lines of all the jet flows examined in the anisotropic turbulent environments generated from the right and the left loudspeakers respectively.

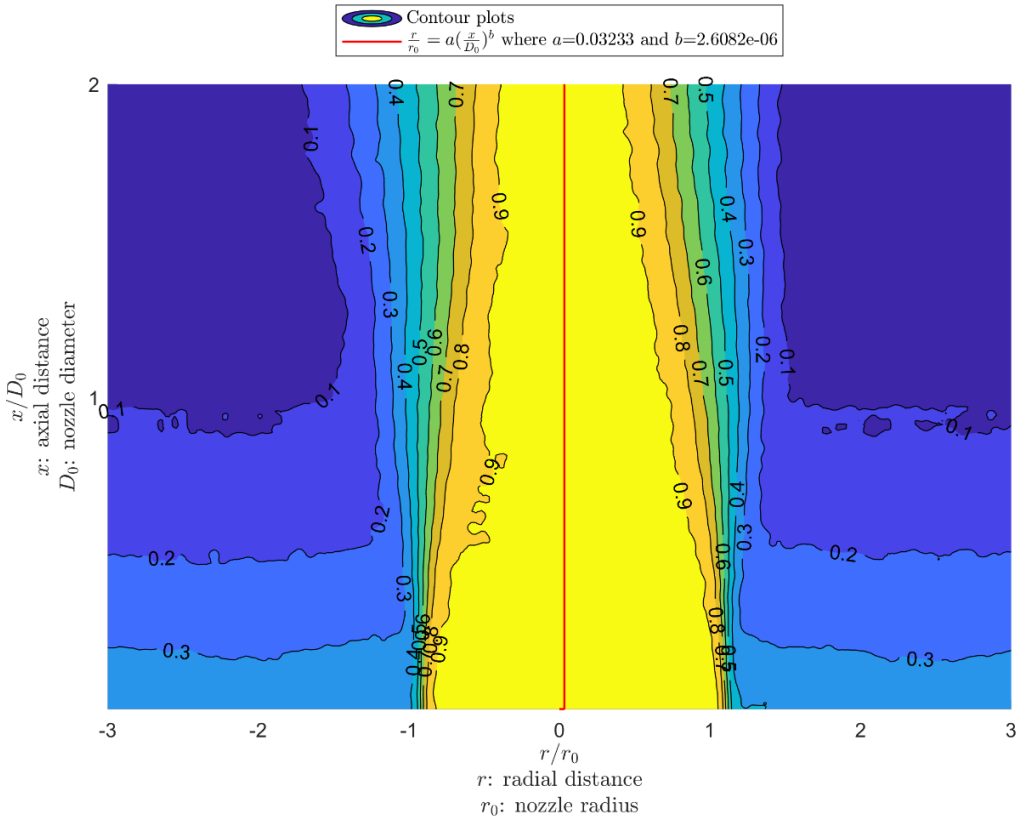


**Figure 3-52:** Contour plot of the jet flow with $\mathbf{Re} = \mathbf{8400}$ in anisotropic turbulent environment (Right-side loudspeakers)

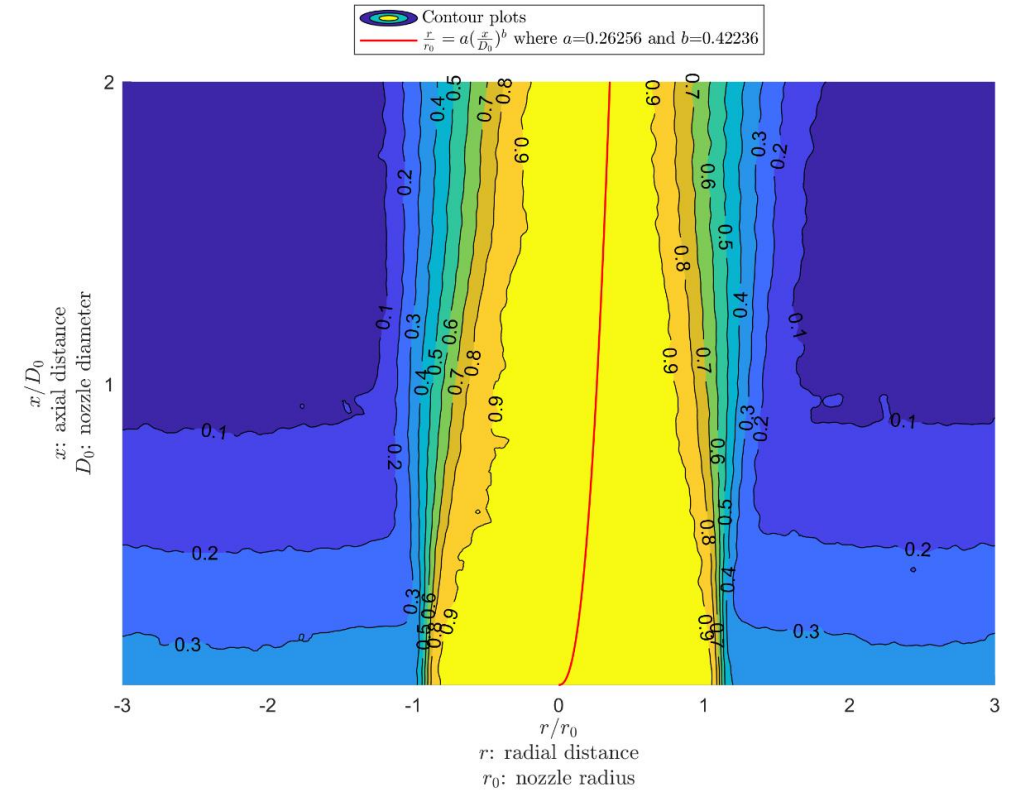


**Figure 3-53:** Contour plot of the jet flow with $\mathbf{Re} = \mathbf{8400}$ in anisotropic turbulent environment (Left-side loudspeakers)

The contour plots obtained for other turbulent jet flows in the range of $\mathrm{Re} = 4200 - 9800$ (Q = 30 - 70 l/min) in the ambient environments under study, are similar to the respective plot presented here ($\mathrm{Re} = 8400$) e.g., in both cases the plot obtained with $\mathrm{Re} = 4200$ had small differences, while the plot obtained with $\mathrm{Re} = 9800$ was almost identical. In each case, the plots appear to adopt a similar jet widening pattern with high concentrations along the downstream distance, whereas the differences in their direction can be deduced from Table 9 and 10. Table 9 (right-side loudspeakers) shows that increasing the Reynolds number causes the incline of the relevant mean lines to change from left ($a < 0$) to right ($a > 0$); in the last four turbulent flows, the $a$ is however small which indicates that their direction is close to vertical. Table 10 (left-side loudspeakers) indicates that the relevant mean lines are inclined to the right ($a > 0$). In both cases, the incline $a$ appears to approach a constant value with the increase of Re.

**Table 9:** Power law coefficients for the mean line of the jet flows in turbulent environment (Right-side loudspeakers)

| **Reynolds number** | **Power law Coefficients** | |
|---|---|---|
| | $a$ | $b$ |
| **1400** | -0.756 | 0.154 |
| **2800** | -0.413 | 0.596 |
| **4200** | -0.269 | 1.19 |
| **5600** | -0.0805 | 2.05 |
| **7000** | -0.0321 | 2.77 |
| **8400** | 0.0323 | 2.61e-06 |
| **9800** | 0.0519 | 1.95e-06 |

**Table 10:** Power law coefficients for the mean line of the jet flows in turbulent environment (Left-side loudspeakers)

| **Reynolds number** | **Power law Coefficients** | |
|---|---|---|
| | $a$ | $b$ |
| **1400** | 0.684 | 0.162 |
| **2800** | 0.754 | 0.553 |
| **4200** | 0.617 | 0.572 |
| **5600** | 0.346 | 0.686 |
| **7000** | 0.366 | 0.489 |
| **8400** | 0.263 | 0.422 |
| **9800** | 0.266 | 0.447 |

### 3.4.5 Contour plots in turbulent environment (Upper-side loudspeakers)

In this Subsection, the concentration contour plots obtained in another anisotropic turbulent environment are presented and discussed. This is the turbulent environment generated from the upper-side loudspeakers. Like in previous subsections, the current analysis will be consisted of the three types of jet discharge flow: the laminar, the transitional and turbulent flows.

Initiating the analysis, the laminar discharge flow with Reynolds number of $\mathrm{Re} = 1400$ and flowrate of Q = 10 l/min is examined. Figure 3-54 depicts the contour plot of this jet flow when discharged into the turbulent environment generated from the upper-side loudspeakers.

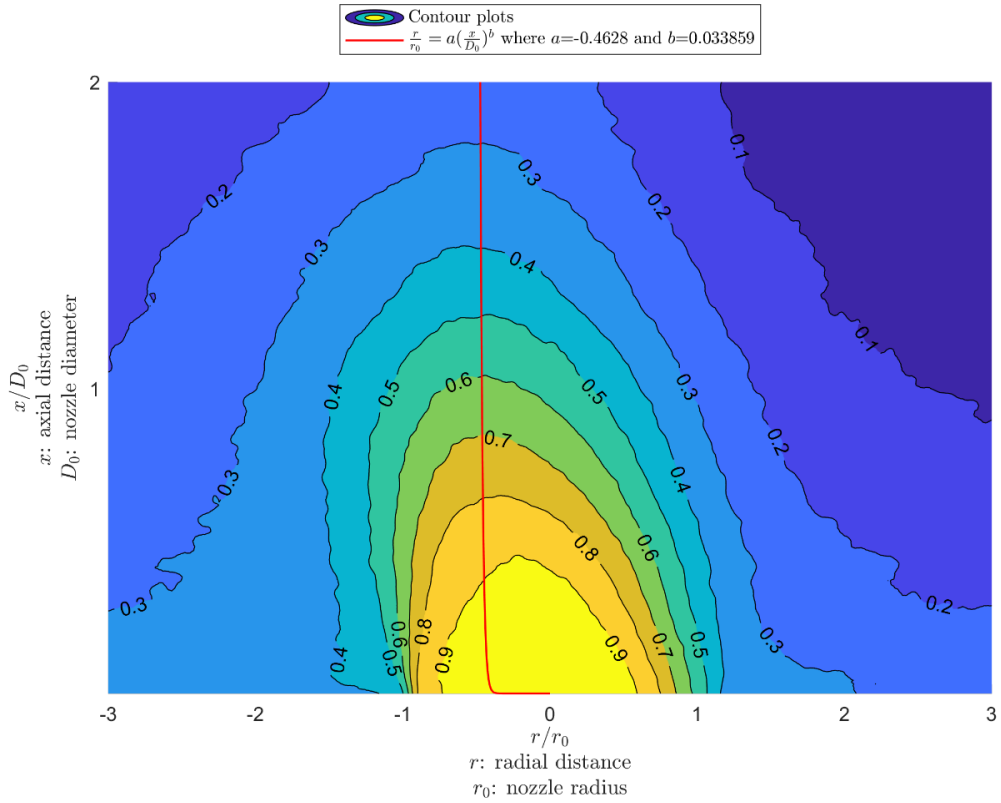


**Figure 3-54:** Contour plot of the jet flow with $\mathbf{Re} = \mathbf{1400}$ in anisotropic turbulent environment (Upper-side loudspeakers)

Firstly, one can observe the significant effect of the turbulent environment on the flow, that is, the obstruction of flow's development in the streamwise direction. This can be attributed to the small momentum that the laminar flow carries. The momentum of the external turbulence generated from the upper side loudspeakers is greater than the jet flow's momentum resulting in the obstruction of the jet flow's development, thus giving the flow a suppressed shape (e.g., the yellow/brown region representing the core of the flow is small and, the contour lines are gradually/distantly spaced in the plane).

Furthermore, the concentration along the mean line is shown to decrease. Observing the contour lines along the flow's direction, one can see that the space between them widens as the distance from the orifice increases; in other words, the higher concentration contours are equally spaced, while the lower value contours are gradually more widely spaced. This indicates that in the flow direction, the jet concentration decay rate is constant near the orifice and, as the distance from the orifice increases, the decay rate is gradually decreasing.

The direction of the flow shows a small incline towards the left-side. This is similar to what it was observed in the HIT environment with the same jet flowrate (Figure 3-45). The current incline can be accordingly explained by considering that the loudspeakers on the right part of the upper side operated with greater power than those on the left part of the upper side. The incline of the jet flow can also be seen in its mean line depicted on the plot. This is calculated by the power law equation with the coefficient $a = -0.463$ and the exponent $b = 0.0339$.

Continuing the analysis, the transitional discharge flow with Reynolds number $\mathrm{Re} = 2800$ (flowrate 20 l/min) is examined. Figure 3-55 depicts the contour plot of this jet flow discharged into the turbulent environment generated from the upper-side loudspeakers.

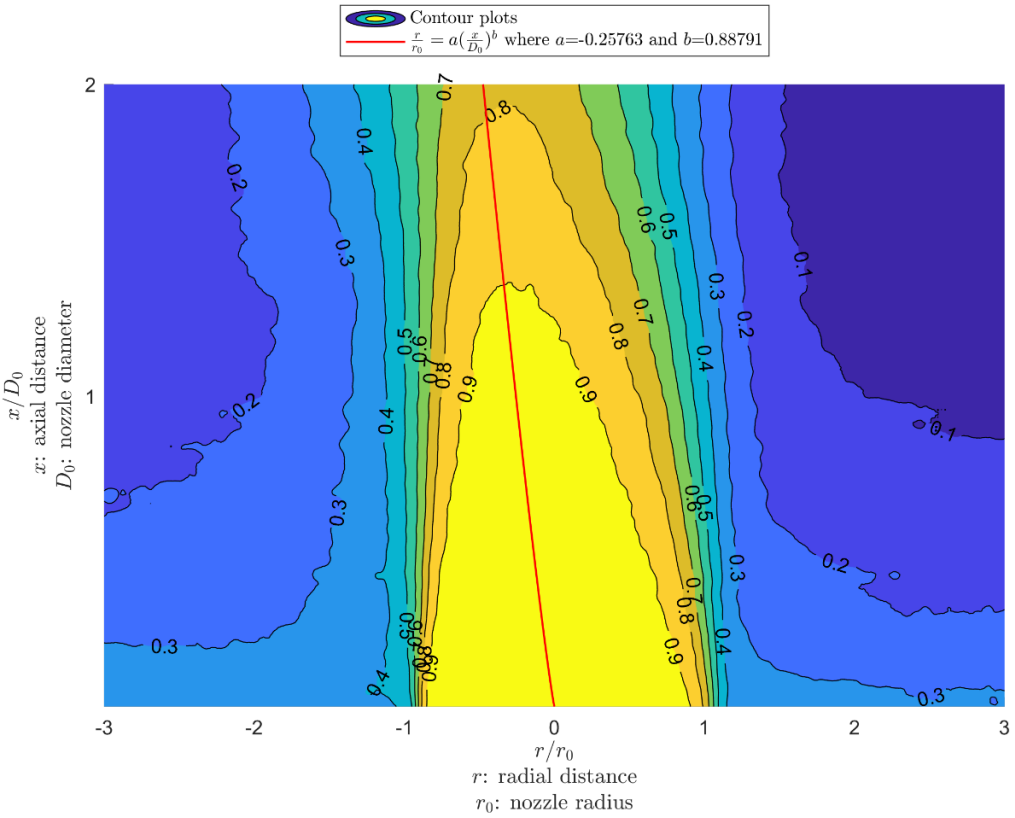


**Figure 3-55:** Contour plot of the jet flow with $\mathbf{Re = 2800}$ in anisotropic turbulent environment (Upper-side loudspeakers)

Firstly, one can observe that the geometry of the flow presented in the above plot, shares some resemblance with the geometry of the laminar flow in the current turbulent environment, which was presented earlier. However, it appears that the transitional flow is developed further, apparently because it has greater momentum than the laminar flow.

Furthermore, one can observe that the jet flow is inclined to the left-side. This presumably because the upper-right loudspeakers operated with greater power than the upper-left ones, as explained earlier. However, in this case, due to the increased momentum of the transitional flow comparing to the laminar flow's, the incline is smaller. The incline to the left can also be seen by the mean line depicted on the diagram. This is described by the power law equation with the coefficient $a = -0.258$ and the exponent $b = 0.888$.

Completing the study of the contour plots in this Subsection, the turbulent jet flow with a discharge rate of Q=70 l/min and a Reynolds number of $\mathrm{Re} = 9800$ is examined. In Figure 3-56 the relevant contour plot is depicted.

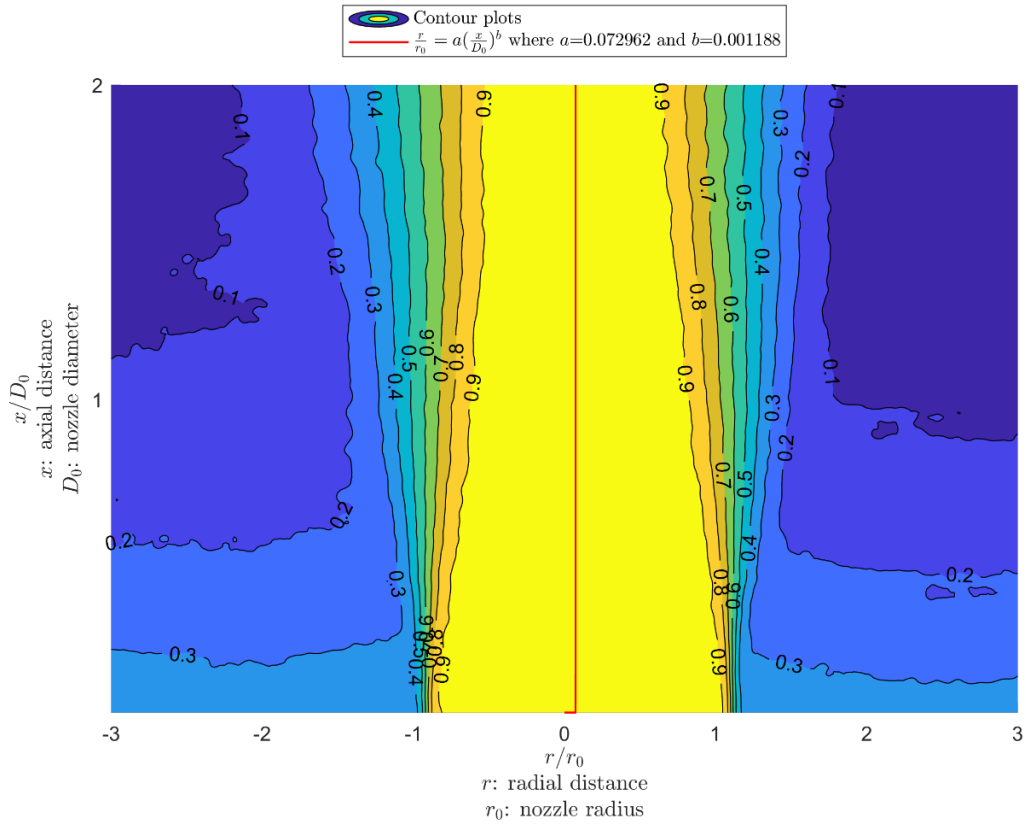


**Figure 3-56:** Contour plot of the jet flow with $\mathbf{Re = 9800}$ in anisotropic turbulent environment (Upper-side loudspeakers)

In this contour plot, the shape of the flow and the spacing of the contour lines are qualitatively similar to those in the turbulent flow's plot in quiescent environment. This observation indicates that the momentum of the turbulent jet flow is higher than the momentum of the turbulence generated from the upper-side loudspeakers, and thus the effect of the external turbulence on the jet flow is insignificant in the range investigated. The contour plot shows that the jet concentration maintains a high value along the mean line of the flow, as indicated by the shape of the yellow region (c > 0.9). The flow widens along the downstream direction, following a pattern similar to the 'conical shape' pattern observed in quiescent conditions, which is consistent with the bell type distribution of the corresponding radial profiles.

The contour plot shows that the direction of the flow is almost vertical, i.e., the flow maintains its original course remaining unaffected from the anisotropic external turbulence. The vertical direction of the flow is also depicted in the mean line presented on the plot. This mean line is calculated by means of the power law equation with the coefficient $a = 0.0730$ and the exponent $b = 0.00119$.

Table 11 depicts the coefficients of the power law equation, presented in the introductory part of this Section, for the mean lines of all jet flows examined in the current turbulent environment. The contour plots obtained with other turbulent flows in the range of $\mathrm{Re} = 4200 - 9800$ (Q = 30 - 70 l/min) are similar to the contour plot presented here ($\mathrm{Re} = 9800$), i.e., they exhibit a similar jet widening pattern with high concentrations along the downstream direction (c > 0.8). Table 11 indicates that the coefficient $a$ approaches a constant value with the increase of the Reynolds number, while the mean lines of the last four turbulent flows have a direction almost vertical.

**Table 11:** Power law coefficients for the mean line of the jet flows in turbulent environment (Upper-side loudspeakers)

| **Reynolds numbers** | **Power law Coefficients** | |
|---|---|---|
| | $a$ | $b$ |
| **1400** | -0.463 | 0.0339 |
| **2800** | -0.258 | 0.888 |
| **4200** | -0.178 | 1.01 |
| **5600** | -0.0204 | 2.69 |
| **7000** | -0.00495 | 3.77 |
| **8400** | 0.0555 | 0.0019 |
| **9800** | 0.073 | 0.00119 |

### 3.4.6 Contour plots in turbulent environment (Bottom-side loudspeakers)

The final part of the contour plot analysis regards, the case of turbulent surroundings with the external turbulence being generated from the loudspeakers located at the bottom of the support structure. As in previous subsections, the analysis will be consisted of the jet concentration interaction with the turbulent surroundings of the laminar, transitional and turbulent flows.

The first type of flow that is going to be presented is the laminar flow. The laminar flow used during the experimental procedure had the properties of $\mathrm{Re} = 1400$ for Reynolds number and Q=10 l/min for volumetric flow rate. In Figure 3-57 the contour plot of the current flow is depicted.

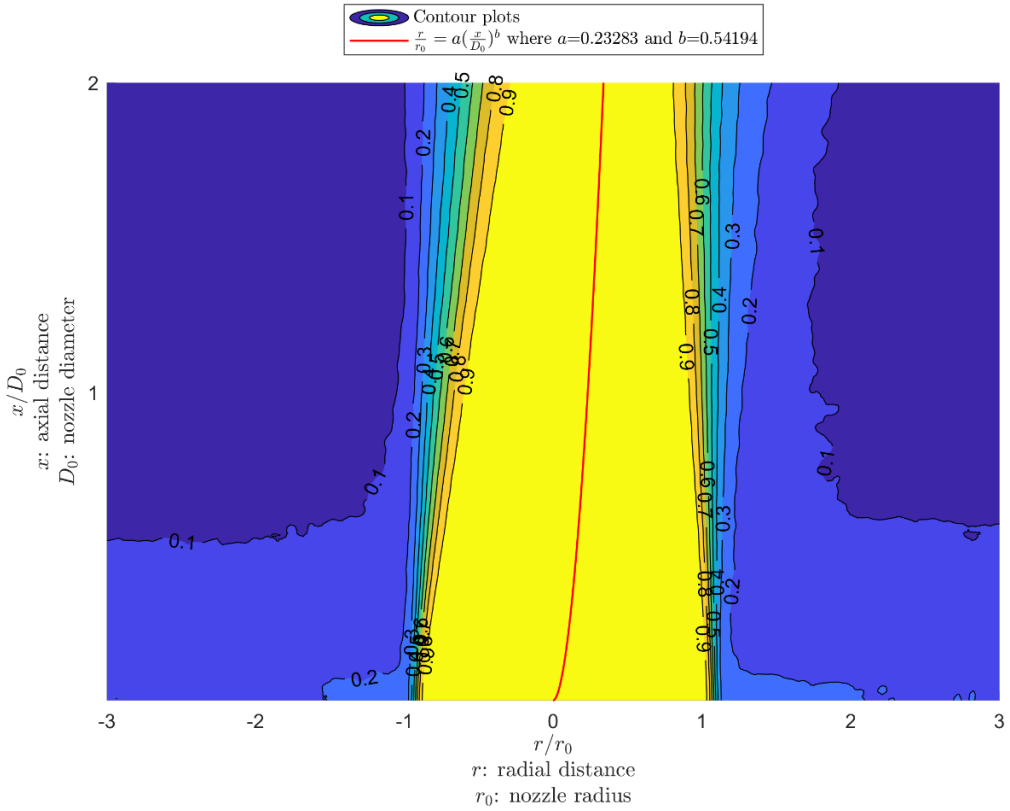


**Figure 3-57:** Concentration contour plot of the jet flow with $\mathbf{Re = 1400}$ in anisotropic turbulent environment (Bottom-side loudspeakers)

Examining the plot in Figure 3-57, one can observe that the jet flow is not adversely obstructed but it is allowed to develop further. This can be attributed to the direction where the loudspeakers are pointed with respect to the direction of the flow; therefore, the momentum of the external turbulence does not obstruct the development of the flow due to their similar direction. However, as the flow progresses further in the streamwise direction, the external turbulence has a visible effect on it. In contrast to the case of quiescent environment depicted in Figure 3-42, here with the increase of the axial direction, the jet widens due to increased air entrainment induced by the external turbulence.

The contour plot shows that the jet concentration maintains a high value along the mean line of the flow, as indicated by the shape of the yellow region (c > 0.9). The jet widens slightly along the downstream direction. The contour lines between the core of the flow (c > 0.9) and the surroundings (c < 0.2) are closely spaced but they become slightly more widely spaced across the jet, as the downstream distance increases.

Finally, a trait of the jet flow depicted in the current contour plot is its small incline to the right side, which it can also be seen in the depicted mean line. This incline can be attributed to the non-steady operation of the loudspeakers, as it was analyzed in previous subsections. The mean line is calculated by the power law equation with the coefficient $a = 0.233$ and the exponent $b = 0.542$.

The next type of flow examined in the current Subsection is the transitional flow. The transitional flow with a discharge rate of Q = 20 l/min and Reynolds number $\mathrm{Re} = 2800$ is examined. In Figure 3-58 the flow's contour plot is presented.

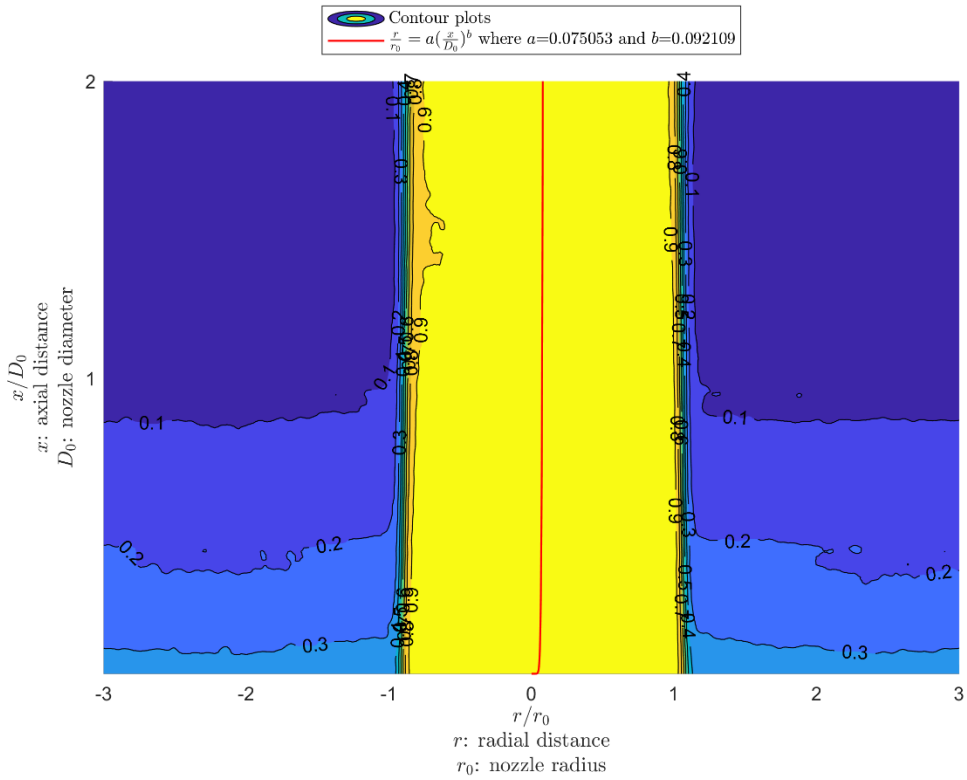


**Figure 3-58:** Contour plot of the jet flow with $\mathbf{Re = 2800}$ in anisotropic turbulent environment (Bottom-side loudspeakers)

Firstly, observing the current jet flow's geometry in the contour plot, one can assume that despite the external turbulence generated from the bottom-side loudspeakers, the flow remains unaffected. This can once more be attributed to the momentum of the flow and the direction in which the loudspeakers are pointed. As it was explained in the case of the laminar flow (Figure 3-57), the direction where the

loudspeakers are pointed is not opposed to the direction of the jet flow, thus the external turbulence has a reduced effect on the flow. However, in this case due to the transitional nature of the flow, the jet flow's momentum is greater than that of the laminar flow. Therefore, the direction of the external turbulence combined with the increased momentum of the transitional flow, provides a jet flow's geometry that seems to be unaffected.

Furthermore, the contour lines between the core of the flow and the surroundings are closely spaced to each other, in a way that they are hardly distinguishable. This indicates that the concentration gradient is very high. Due to the unaffected flow, the jet concentration rapidly drops from a high value in the main region of the flow (yellow region, c > 0.9) to a low value in the surroundings (dark blue region, c < 0.2). Additionally, the core of the flow (c > 0.9) appears to be unaffected from the external environment and the jet concentration remains high throughout the whole region of the jet flow.

Finally, the direction of the flow is almost vertical. This indicates that the effect of the anisotropic external turbulence on the flow is insignificant. The mean line of the flow is also shown to be almost vertical. This is calculated by the power law equation with the coefficient $a = 0.0751$ and the exponent $b = 0.0921$.

Concluding the analysis in this Subsection, the last type of flow to be examined is the turbulent flow. In Figure 3-59 the contour plot of the turbulent discharge flow with Reynolds $\mathrm{Re} = 7000$ (flow rate Q=50 l/min) is presented.

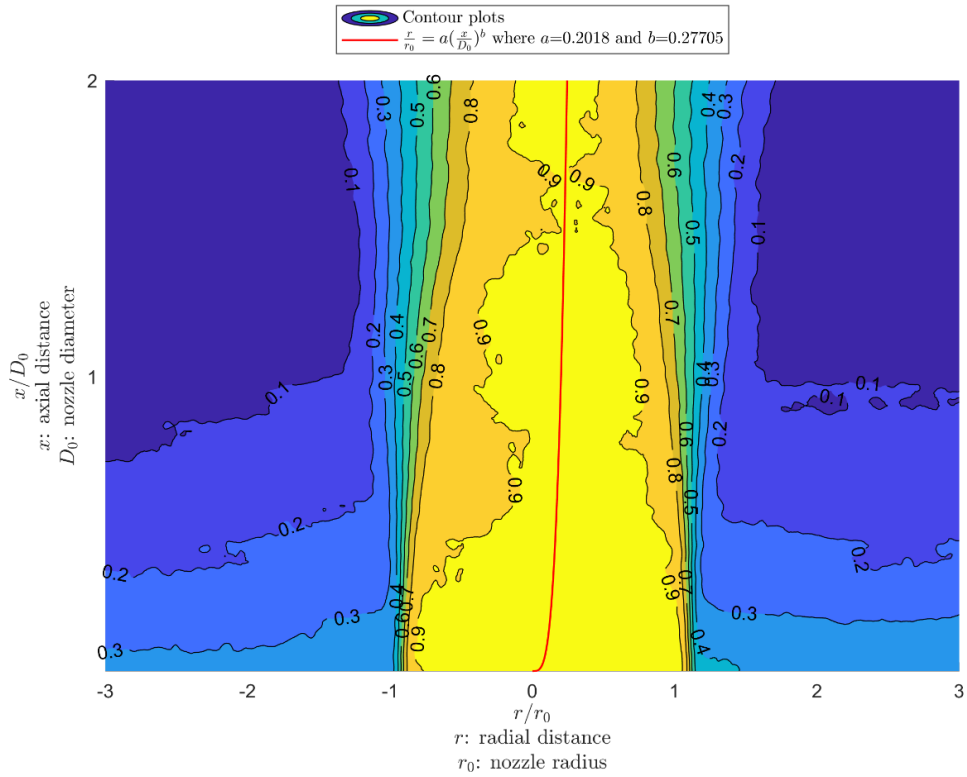


**Figure 3-59:** Contour plot of the jet flow with $\mathbf{Re} = \mathbf{7000}$ in anisotropic turbulent environment (Bottom-side loudspeakers)

In this contour plot, the shape of the flow and the spacing of the contour lines are qualitatively similar to those in the turbulent flow's plot in quiescent environment. This indicates that the effect of the anisotropic turbulent environment on the flow is small, and it can once again be attributed to the momentum of the turbulent flow. Turbulent flows have relatively great momentums; thus, the momentum of the external turbulence is not enough to interfere with the development of the flow.

As it is common in all turbulent flows that have been discussed so far, the jet concentration maintains a high value (c > 0.8) inside the main region of the jet flow. Furthermore, the jet widens along the streamwise direction, and the contour lines become more widely spaced in both sides of the plot as the flow progresses in the downstream distance. The direction of the flow shows a small incline to the right. This indicates that the external anisotropic turbulence has a small effect on the flow. The mean line also shows a small incline to the right; this is calculated by means of the power law equation with the coefficient $a = 0.202$ and exponent $b = 0.277$.

Table 12 depicts the coefficients of the power law equation, presented in the introductory part of this Section, for the mean line of each flow examined in the turbulent environment under study. The contour plots obtained for other turbulent jet flows in the range of $\mathrm{Re} = 4200 - 9800$ (Q = 30-70 l/min) are similar to the contour plot presented here ($\mathrm{Re} = 7000$) that is, they show similar jet widening pattern with high

concentrations along the downstream distance, and a similar flow direction as it can be deduced from Table 12. The (positive) values of the coefficient $a$ indicate that the mean of lines of the jet flows have a small incline to the right.

**Table 12:** Power law coefficients for the mean line of the jet flows in turbulent environment (Bottom-side loudspeakers)

| **Reynolds numbers** | **Power law Coefficients** | |
|---|---|---|
| | $a$ | $b$ |
| **1400** | 0.23283 | 0.54194 |
| **2800** | 0.075053 | 0.092109 |
| **4200** | 0.27167 | 0.57488 |
| **5600** | 0.23041 | 0.45262 |
| **7000** | 0.20180 | 0.27705 |
| **8400** | 0.21301 | 0.13659 |
| **9800** | 0.20346 | 0.14973 |

# 4. Conclusions

In this study, the concentration fields of jet flows ejected into quiescent and turbulent ambient environments, were examined with the aid of flow visualization method. Five different external turbulent fields were investigated, which were created by means of an experimental arrangement comprising of synthetic jets. In general, the results show that when a jet is discharged into a turbulent environment, the external turbulence disrupts the original geometry of the jet to a great extent when the jet flow is laminar or transitional (i.e. discharge flow's $\mathrm{Re} = 1400 - 2800$), and to a lesser extent when the jet flow is turbulent (i.e. discharge flow's $\mathrm{Re} = 4200 - 9800$), in the near-field region investigated. In other words, for laminar and transitional flows in turbulent surrounding environment, the structure of the jet becomes more variable, and the jet flow obtains a chaotic motion, as it evolves in the streamwise direction.

The effect of the ambient turbulence is derived from the analysis of the radial concentration profiles, the centreline concentration profiles and the contour plots of concentration. The effect is explained by considering the momentum of the jet flow in comparison with the momentum of the external turbulence. A lower Reynolds number corresponds to laminar or transitional jet flow regime, and lower jet momentum, resulting in the flow being more susceptible to disruptions caused by the turbulence in the surrounding environment. Furthermore, due to the low Reynolds number flow regime, the external turbulence is more capable to displace the jet, resulting in a meandering of the jet's flow main course. Conversely, when the Reynolds number is high, the flow becomes turbulent, the concentration profiles adopt a relative constant pattern, and the effect of the external turbulence is then minor in the near-field region investigated. Regarding the evolution of the jet flow, it can be concluded that the jet diffusion in the range investigated is enhanced when the surrounding environment is turbulent, and it is reduced when the jet flow is turbulent due to the greater momentum of the turbulent jet flow.

The radial mean concentration profiles followed 'bell' shape, including 'asymmetric bell shape'. Uniform concentration profiles were observed only in some measurements at low Reynolds numbers in quiescent environment, and the anisotropic turbulent field not opposing the flow direction. The 'bell' shape was most noticeable in turbulent jet flows in quiescent environment, and it was also maintained in all cases of turbulent ambient environment, even when the external turbulence was not homogeneous and isotropic. However, in laminar and transitional flows, as it was depicted in the relevant plots, the 'bell' shape was distorted due to the external turbulence being generated only from one direction. Distortion of the concentration profile had little occurrence when the jet flow was turbulent due to the flow's greater momentum. Finally, in laminar and transitional flows, the magnitude of the curve's peak was getting

progressively smaller with the increase of the distance from the nozzle exit along the streamwise direction, in cases where the surrounding environment was turbulent.

The diffusion of the jet concentration in the plane of the flow's direction is evidenced in the contour plots. The jet diffusion was observed in turbulent environments regardless of the jet Reynolds number, and for turbulent jets regardless of the environmental conditions. In the cases of laminar and transitional flows in most of the turbulent fields, the decay of the jet concentration was taking place along and across the jet and the mean flow's direction was distorted. In the cases of turbulent flows, the jet diffusion was evidenced by the jet widening pattern in the near-field region studied, while the mean flow direction approached closer to a vertical line. However, this pattern was not present in the laminar and transitional jet flows in quiescent environment. The lack of external momentum due to the quiescent ambient environment and the jet momentum provided by these flows was not sufficient to initiate the diffusion of the jet tracer particles into the surrounding environment.

Finally, it was found that for a jet penetrating a fluid at rest, the radius of the jet is proportional to the distance downstream from the jet's discharge location. The equation relating them is linear, but its slope is different for each type of flow. During this experimental investigation, it was observed that the increase of the Reynolds number causes this value to increase, the lowest value of about 0.0062 being observed at $\mathrm{Re} = 1400$ (laminar flow) and the highest value of about 0.155 being observed at $\mathrm{Re} = 5600 - 9800$ (Turbulent flows).

# 5. References


Abdel-Rahman, A. (2010). A review of effects of initial and boundary conditions on turbulent. In: *WSEAS Transactions on Fluid Mechanics* Vol. 5, Issue 4.

Abdel-Rahman, A. A.; Al-Fahed, S. F.; Chakroun, W. (1996). The near-field characteristics of circular jets at low Reynolds numbers. *Mechanics Research Communications*, *23*(3). https://doi.org/ 10.1016/0093-6413(96)00028-6.

Abramovich, G. N. (1963). The Theory of Turbulent Jets. In: *The Theory of Turbulent Jets*. https://doi.org/10.7551/mitpress/6781.001.0001.

Albertson, M. L.; Dai, Y. B.; Jensen, R. A.; Rouse, H. (1950). Diffusion of Submerged Jets. *Transactions of the American Society of Civil Engineers*, *115*(1). https://doi.org/10.1061/taceat.0006302.

Alnahhal, M. H. (2010). Turbulent Rectangular Jets, PhD Thesis, Dept. of Mechanical Engineering and Aeronautics, University of Patras

Bernard P.S. and Wallace J.M.: 2002, Turbulent flow, John Wiley and Sons, New Jersey

Birouk, M.; Chauveau, C.; Sarh, B.; Quilgars, A.; Gökalp, I. (1996). Turbulence effects on the vaporization of monocomponent single droplets. *Combustion Science and Technology*, *113–114*. https://doi.org/10.1080/00102209608935506.

Bland, J. M.; Altman, D. G. (1996). Statistics Notes: Measurement error. *BMJ*, *313*(7059). https://doi.org/10.1136/bmj.313.7059.744.

Brownell, C. J.; Su, L. K. (2004). Planar measurement of differential diffusion in turbulent jets. In: *34th AIAA Fluid Dynamics Conference and Exhibit*. https://doi.org/10.2514/6.2004-2335.

Cheng, N.-S.; Law, A. W.-K. (2001). Measurements of Turbulence Generated by Oscillating Grid. *Journal of Hydraulic Engineering*, *127*(3).https://doi.org/10.1061/(asce)0733-9429(2001)127:3(201).

Comte-Bellot, G.; Corrsin, S. (1966). The use of a contraction to improve the isotropy of grid-generated turbulence. *Journal of Fluid Mechanics, 25*(4), 657-682.

Comte-Bellot, G.; Corrsin, S. (1971). Simple Eulerian time correlation of full-and narrow-band velocity signals in grid-generated, 'isotropic' turbulence. *Journal of Fluid Mechanics, 48*(2), 273-337.

Courant, R.; Robbins, H.; Stewart, I. (1996). What is mathematics?: an elementary approach to ideas and methods. In: *American Mathematical Monthly*.

Cushman-Roisin, B. (2019). Environmental Fluid Mechanics, John Wiley & Sons, Inc. (Thayer School of Engineering, Dartmouth College https://cushman.host.dartmouth.edu/books/EFM/).

Goepfert, C.; Marié, J. L.; Chareyron, D.; Lance, M. (2010). Characterization of a system generating a homogeneous isotropic turbulence field by free synthetic jets. *Experiments in Fluids*, *48*(5). https://doi.org/10.1007/s00348-009-0768-5.

Hideharu, M. (1991). *Realization of a large-scale turbulence field in a small wind tunnel*. *8*(1–4), 53–64. https://doi.org/10.1016/0169-5983(91)90030-m.

Hinze, J. O. (1959). Turbulence: An Introduction to its Mechanism and Theory. *McGraw-Hill Series in Mechanical Engineering*.

Holman, J. P. (2002). Heat transfer 9th Edition. New York, Boston, McGraw-Hill, Inc.

Hwang, W.; Eaton, J. K. (2004). Creating homogeneous and isotropic turbulence without a mean flow. *Experiments in Fluids*, *36*(3), 444–454. https://doi.org/10.1007/s00348-003-0742-6.

Lewis, J. S. (2003). Encyclopedia of Physical Science and Technology (Third Edition). In: *Academic Press* (Issue 293).

Lorenz, E. N. (1963). Deterministic Nonperiodic Flow. *Journal of the Atmospheric Sciences*, *20*(2). https://doi.org/10.1175/1520-0469(1963)020<0130:dnf>2.0.co;2.

Luo, C., Guo, L., Zeng, S., & Long, T. (2021). Effects of turbulence fluctuation intensity in bioreactor of sewage treatment on physical and chemical properties of biofilms. *Bioprocess and Biosystems Engineering*, *44*(9). https://doi.org/10.1007/s00449-021-02566-y

McCorquodale, M. W.; Munro, R. J. (2018). A method for reducing mean flow in oscillating-grid turbulence. *Experiments in Fluids*, *59*(12). https://doi.org/10.1007/s00348-018-2636-7.

Monin, A. S.; Yaglom, A. M. (2013). Statistical Fluid Mechanics, Volume II. In: *Mechanics of Turbulence*.

Obligado, M.; Puy, M.; Bourgoin, M. (2013). Bi-stability of a pendular disk in laminar and turbulent flows. *Journal of Fluid Mechanics*, *728*. https://doi.org/10.1017/jfm.2013.312

Obot, N. T.; Graska, M. L.; Trabold, T. A. (1984). The near field behavior of round jets at moderate reynolds numbers. *The Canadian Journal of Chemical Engineering*, *62*(5). https://doi.org/10.1002/cjce.5450620503.

Pope, S. B. (2000), Turbulent Flows, Cambridge University Press, UK, p. 771.

Quinn, D. B., Watts, A., Nagle, T., & Lentink, D. (2017). A new low-turbulence wind tunnel for animal and small vehicle flight experiments. *Royal Society Open Science*, *4*(3). https://doi.org/10.1098/rsos.160960

Rajaratnam, N.; Flint-Petersen, L. (1989). Low Reynolds number circular turbulent jets. In: *Proceedings - Institution of Civil Engineers. Part 2. Research and Theory*, *87*.

Ricou, F.; Spalding, D. (1961). Measurements of entrainment by axisymmetrical turbulent jets. *Journal of Fluid Mechanics, 11*(1), 21-32.

Taylor, G. I. (1935). Statistical theory of turbulence-II. *Proceedings of the Royal Society of London. Series A - Mathematical and Physical Sciences*, *151*(873). https://doi.org/10.1098/rspa.1935.0159.

Thomas, D. G. (1972). A First Course in Turbulence. *Nuclear Science and Engineering*, *49*(2). https://doi.org/10.13182/nse72-a35514.

University of Sydney (2005): Classification of Flows, Laminar and Turbulent Flows. http://wwwmdp.eng.cam.ac.uk/web/library/enginfo/aerothermal_dvd_only/aero/fprops/pipeflow/node8.ht ml

Variano, E. A.; Cowen, E. A. (2008). A random-jet-stirred turbulence tank. *Journal of Fluid Mechanics*, *604*. https://doi.org/10.1017/S0022112008000645.

Vassilicos, J. C. (2015). Dissipation in turbulent flows. In *Annual Review of Fluid Mechanics* (Vol. 47, pp. 95–114). Annual Reviews Inc. https://doi.org/10.1146/annurev-fluid-010814-014637.

Xie, S., Jiang, G., Ye, B., & Shentu, B. (2020). Particle Image Velocimetry (PIV) investigation of the turbulent airflow in slot-die melt blowing. *Polymers*, *12*(2). https://doi.org/10.3390/polym12020279